Analysis of the Ies6 subunit of the INO80 chromatin remodelling complex.

Submitted for the degree of Doctor of Philosophy.

Sarah Elizabeth Lee Phelps

The Genome Damage and Stability Centre

University of Sussex

July 2015

Declaration

This thesis has been produced as a result of my own work at the Genome Damage and Stability Centre, the University of Sussex between October 2011 and July 2015. The data within it has been collected and analysed by me, and only where expressly stated has work been conducted in collaboration with others. I declare that work presented within this thesis, in the same or different form will not be submitted to another university for the award of any other degree.

……..

Sarah Phelps

UNIVERSITY OF SUSSEX

Sarah Phelps - Biochemistry

Analysis of the Ies6 subunit of the INO80 chromatin remodelling complex.

Summary

The INO80 complex is a large ATPase chromatin remodeller which contains 15 accessory subunits in *S. cerevisiae*. Its subunits include the highly conserved ATPases Ruvb1 and Ruvb2, the actin-related proteins Arp5, Arp8, Act1 and Arp4, Actin, and a number of IES (InoEighty Specific) subunits Ies1, Ies2, Ies3, Ies4, Ies5 and Ies6, in addition to subunits Nhp10 and Taf14. All 15 of the accessory subunits are assembled around a catalytic core component known as Ino80.

The INO80 complex has roles in transcription, DNA repair, replication, and chromosome segregation. These roles are in addition to its traditional nucleosome remodelling activities and the displacement of H2A.Z from chromatin. Recent studies in *S. cerevisiae* have identified the subunit Ies6 as a critical component of the INO80 complex. Deletion of *IES6,* which encodes the small accessory subunit, clearly mimics the deletion of the gene encoding the catalytic subunit, *INO80*. Surprisingly, only one domain within Ies6 has been formally identified based on sequence analysis. This domain belongs to the YL1_C class of domains. Such domains are commonly associated with DNA binding activity and transcription factors.

This study has further characterised the Ies6 subunit both genetically and biochemically. Genetically, it has demonstrated that single point mutations at regions of proposed subunit-subunit interaction between the Arp5 or Rvb2 subunits, or within the YL1_C are not sufficient to disrupt Ies6 function. However, expression of a double point mutation, *ies6(K114E/Y125A)*, in combination with *rad50* deletion, caused a sensitivity to replication inhibition, but not chromosome segregation inhibition, indicating a potential separation of function in this mutant due to the loss due of only one of the biological functions of Ies6.

Biochemically, we have confirmed that DNA binding capacity of Ies6 resides within the YL1_C domain. In addition, although it has been demonstrated that the removal of H2A.Z acetylation exacerbates the increase in cellular ploidy observed in *ies6* null cells, we found that overall levels of H2A.Z acetylation were not influenced by the loss of Ies6. This indicates that the role of H2A.Z acetylation in chromosome segregation may only affect ploidy status upon the loss of Ies6.

In addition, work on the R2TP complex (which contains the INO80 ATPases Ruvb1/Ruvb2, and subunits Tah1 and Phi1) has revealed the recruitment mechanism for the molecular chaperone, Hsp90, and the telomere length regulation protein, Tel2. Together, the R2TP complex, Hsp90 and Tel2 promote the stabilisation and maturation of multi-protein complexes. These include Phosphatidylinositol 3-kinase-related kinases (PIKKs, a family of kinases involved in Serine and Threonine phosphorylation), subunits of the INO80 complex and subunits of the SWR1 chromatin remodelling complex (a partner complex to INO80 that incorporates H2A.Z into chromatin).

Acknowledgements

Overall I would like to thank my supervisor, Professor Jessica Downs, for being supportive, approachable and fun to work with. Thank you for helping me through the tough times and the being there to share the good ones, and for having tissues in the office! Also to my second supervisor, Professor Penny Jeggo, for her advise and support. Special thanks to all my friends in the Downs lab, past and present, especially Dr Anna Chambers, who was there to help in any crisis. Finally, thanks to my friends, both in and out of the GDSC. As well as my family for their continuing help and support over the years, especially my partner Mark being there when I was at my most stressed.

I also wish to thank those that contributed to this work: Melinda Ductor Peters for allowing me to present her data on *ies6(K114E, Y125A)* sensitivity, Alžběta Kalendová for allowing me to use her constructs containing the truncated forms of Ies6, and Dr. Catherine Millar for kindly providing her plasmids of *htz1(K-R)* and *htz1(K-Q)* for these experiments. Furthermore, thanks to my collaborators on the R2TP chapter, especially Dr Marc Morgan for his constant chirpiness and guidance throughout the project.

Table of Contents

1 Introduction

1.1 Chromatin

Packaging of the eukaryotic DNA into chromatin provides a means of organisation and storage of the genome. Chromatin, in its basic state, stores DNA wound around protein octomers known as nucleosomes. Nucleosomes are composed of the basic core histone proteins, H2A, H2B, H3, and H4. The histone proteins were identified in early studies of the cell nucleus and chromosomes (Darlington, 1942).

Today, the regulation, structure and function of the core histone proteins is well defined. In eukaryotes, core histone genes are expressed exclusively in S-phase and are coupled with DNA replication (Robbins and Borun, 1967). Unlike other eukaryotic mRNAs, core histone mRNAs do not contain a polyadenylated tail at their 3' termini (Krieg & Melton 1984), and contain a highly conserved 26-base pair sequence, which includes a stem-loop (Dominski and Marzluff, 1999). The altered structure of the 3' termini results in a unique, single step, mRNA cleavage by the U7 small nuclear ribonucleoprotein (snRNP) (Gick et al., 1986) and the stem-loop binding protein (SLBP) (Wang et al., 1996).

The stem-loop regulates conical histone expression throughout the cell cycle, with transcription of core histones increasing upon entry into S-phase, then being rapidly degraded on S-phase completion (Harris et al., 1991). In addition, core histone genes contain few introns (Pandey et al., 1990) and are found in gene clusters within the genome (Marzluff et al., 2002), both of these factors contribute to the accelerated nature of histone transcription.

Structurally, each core histone contains a histone fold domain (HFD), important for heterodimeric histone interactions within the nucleosome (Arents and Moudrianakis, 1995). In addition, all core histones contain N-terminal tail domains, with H2A and H2B having both C-terminal and N-terminal tails that are important for higher-order chromatin structure. Early crystal structures of whole nucleosomes revealed each histone is bound to its histone partner (H2A-H2B and H3-H4) (Arents et al., 1991). This interaction is governed by the HFD, which consists of 3 α-helices (α1, α2, α3), separated by two loops (L1 and L2) (Luger et al., 1997). Joined at the HFD, histones arrange head to tail, crossing at α2, forming a 'handshake' motif, with the two loops exposed on the outside that act as important nucleosome-DNA interfaces (Luger et al., 1997). Two H3-H4 pairs are joined to form a tetramer and create a stable nucleosome core by interacting with the α-helices of H3 (Luger et al., 1997). Two H2A-H2B 'handshake' pairs assemble on either side of H4, thus leaving H2A-H2B pairs outside of the stable H3-H4 tetramer and accessible for histone exchange (Kulaeva et al., 2010). This basic arrangement of histones into a nucleosome is known as the nucleosome core particle (NCP), in eukaryotes, 147 bp of DNA is wound around each NCP, with approximately 20 bp of linker DNA between each nucleosome (Luger et al., 1997). This arrangement results in a nucleosome-DNA structure traditionally termed 'beads on a string' (Olins and Olins, 1974).

Furthermore, each histone within the NCP assembles with its N-terminal tail region extruding from the nucleosome (Luger et al., 1997), and a fifth histone, H1, which binds to the NCP and the linker DNA between each nucleosome (Richmond et al. 1997). Both these features are important for the compaction of chromatin by enabling the formation of higher order chromatin structures.

The idea that proteins could bind chromatin linker DNA, and subsequently affect its structure, was pioneered by the idea of 'chromodomains'. This term was first used to describe a short stretch of sequence homology between *Drosophila* proteins HP1 (heterochromatin-protein1) and polycomb group (PcG) (Paro and Hogness, 1991). Traditionally, chromatin has been categorised as either heterochromatin or euchromatin, depending on the level of compaction, and its staining pattern under light microscopy (Heitz, 1928). Today, the terms heterochromatin and eurchromatin are still used, but refer to the relative levels of transcription within chromatin. Tightly packed heterochromatin is often protein poor and associated with untranscribed regions, while euchromatin is commonly loosely packaged, protein rich, and associated with actively transcribed genes. In addition to the higher order structures formed by protein binding to linker DNA, the incorporation of histone variants, and the post-translational modification of histone N-terminal tails (both to be discussed in depth later) significantly impact chromatin structure.

Recent technical advances have allowed chromatin to be categorised according to its bound protein content and histone post-translational modifications, expanding the traditional definitions of heterochromatin and euchromatin. In one study, *D. melanogaster* chromatin is divided into five major classes, defined by the colours: green, blue, yellow, red, and black (Filion et al., 2010). Consequently, large areas of HP1 associated chromatin, termed 'green', and polycomb associated chromatin, termed 'blue', were both identified as the traditional heterochromatin. Euchromatin was divided into two different colours of 'yellow' and 'red', with high levels of proteins associated with active transcription and large quantities of mRNA being found. However, 'red' was

distinct due to the presence of the Brahma chromatin remodeller (RSC in *S. cerevisiae*), and 'yellow', showed increased levels of trimethylated H3K36 (Filion et al. 2010), a post-translational modification associated with transcriptional elongation. In addition to the expansion of heterchromatin and euchromatin characteristics, the study identified 'black' regions of chromatin as the most abundant, these were typically gene poor regions with little transcriptional activity. The insertion of reporter gene constructs into stretches of 'black' chromatin resulted in low levels of reporter gene expression, suggesting it functions to suppress transcription (Filion et al. 2010).

Given the influence of histones on chromatin structure, specifically, the insertion of variant histones, or histone PTMs, they are regarded as the determinants of chromatin function. The combinations found at specific chromatin types frequently correlate, giving rise to the idea that histones and their modifications provide a 'histone code' that ultimately governs chromatin states.

Histone variants and histone post-translational modifications will now be discussed in terms of their influence and importance in chromatin higher-order structure, and how these changes effect cellular processes.

1.1.1 Post-translational modifications

Core histones, and their variant counterparts, can undergo post-translational modifications to further specialise their roles. This provides a signalling mechanism to mark and define specific areas of chromatin. Post-translational modification of histone proteins can occur in the form of phosphorylation,

methylation, acetylation, ubiquitylation, sumoylation, ADP ribosylation, demination, and proline isomerisation. One way these modifications function is to disrupt the nucleosome and alter chromatin structure. For instance, the acetylation of histone tails removes their positive charge, which is known to prevent the formation of higher order structures. A good example of this is H4 K16 acetylation, acetylation is common modification on the H4 tail (Smith et al., 2003). This acetylation mark has been shown to influence both nucleosome and higher order chromatin structure (Shogren-Knaak et al., 2006), and is thought to govern protein interactions in both heterochromatin and euchromatin (Millar et al., 2004). Overall, euchromatin is known to contain high levels of acetylation, leading to relaxation of the chromatin and increased rates of transcription (Kuo et al., 1998; Kurdistani et al., 2004; Tse et al., 1998).

Alternatively, PTMs serve to recruit non-histone proteins, for example, in the H2A family, the conical histone, H2A, is phosphorylated on S129 in *S. cerevisiae* (Downs et al., 2000), S139 of H2A.X in *Homo sapiens* (also known as γ-H2A.X). This phosphorylation event signals the presence of a double strand break (DSB), and initiates the DNA damage response (DDR). This response includes activation of the DNA damage checkpoint, a process which delays cell cycle progression to allow time for DSB repair. In *H. sapiens*, phosphorylation of H2A.X is known to directly recruit MDC1 (mediator of DNA-damage checkpoint 1), which binds γ-H2A.X via its BRCT (BRAC1 C-terminal) motifs (Stucki et al., 2005). In this way, post-translational modifications serve as important regulators of various cellular processes, making them interesting targets for epigenetic studies.

Alterations to histones by PTM are now being highlighted as early indicators of human diseases. For example, the loss of PTM on histone H4 has been

identified as an early indicator of many cancers, with monoacetylation at K16 and trimethylation at K20 being predominantly lost, first in the early stages, then accumulating during cancer progression (Fraga et al., 2005). In addition, genome wide histone post-translational modifications associated with prostate cancer have now been classified (Seligson et al., 2005). In both cases, analysis of patient PTMs has the potential to provide a biological readout of cancer status or progression.

1.1.2 Histone variants

Histone variants are distinguished from their core histone counterparts by a few notable characteristics. Firstly, unlike core histones, most histone variant mRNAs do not contain a stem-loop and are polyadenylated at their 3' termini. However, there are a few exceptions to this, for example, the variant H2A.X is expressed in S-phase without polyadenalation, but during G0 and G1 phase expression, the 3' termini exhibits a polyadenalated tail (Mannironi et al., 1989). Secondly, histone variants are constitutively expressed throughout the cell cycle rather than being limited to S-phase. For instance, mRNA levels of the H2A.Z variant, unlike conical H2A, are unaffected by inhibition of DNA replication (Hatch et al., 1990). Thirdly, the genes encoding histone variants are distributed throughout the genome and are not found in gene clusters.

In *H. sapiens* multiple genes encode for a single variant, resulting in many different isoforms that are alternatively spliced to produce further diverging isoforms. These changes ultimately govern the histone fold, function and post-translational modifications, putting variants at the forefront of cellular signalling

pathways. Given this, variants are highly conserved, and many have been implicated in human disease. For example, a histone variant of H3 found in mammals, H3.3, is commonly mutated in brain cancer patients (Schwartzentruber et al., 2012), and a H1.5 variant expression is commonly elevated in prostate tumours (Khachaturov et al., 2014). Though, the numbers of known histone variants, and their isoforms, is vastly different for each of the core histones. For example, H4 only has one known isoform, while H3 is far less diverse than H2A or H2B, this is thought to be due to the structural significance of H3 and H4 within the nucleosome. For the purposes of this thesis, I will now focus on H2A, its histone variants, their specific functions and subsequent post-translational modification.

H2A is widely accepted as the most diverse of all the histone variants, containing four known variants in *H. sapiens*, mH2A, H2A.B, H2A.X, and H2A.Z, with a total of eight different isoforms between them, of these, H2A.X and H2A.Z are the most widely studied. H2A.X is transcribed by the H2A.X gene, which has a single isoform. This isoform is highly expressed within the genome and is found at telomeric heterochromatin, the XY body, sites of DNA damage, tRNA genes, replication origins, rDNA, and certain transposons. The deletion of the H2A.X gene results in male sterilisation in mice and genomic instability in human cells. In *S. cerevisiae* H2A.X is orthologous to the post-translational modification of the conical histone H2A by phosphorylation on S129 (Downs et al., 2000).

For H2A.Z, two genes, H2A.Z.1 and H2A.Z.2, encode the variant in *H. sapiens*, with H2A.Z.1 producing only a single isoform, and H2A.Z.2 producing two splice variants, H2A.Z.2.1 and H2A.Z.2.2. The H2A.Z.2 gene isoforms are the most poorly characterised, with H2A.Z.2.1 being known to have a widespread expression pattern within the genome, but little known about its localisation or phenotype,

and H2A.Z.2.2 is known to be expressed in the brain and skeletal muscle tissues, but nothing is known about its functions. In contrast, H2A.Z.1, commonly referred to as H2A.Z, has been highly studied and characterised from yeast to humans. It has a widespread expression profile within the genome, being found localised to gene promoters, tRNA genes, enhancers, transposons, and regions of silent heterochromatin.

1.1.2.1 The H2A.Z histone variant

The histone H2A.Z is highly conserved throughout evolution, and around 90% of its sequence is conserved from *P. falciparum* to *H. sapiens* (Louzalen et al., 1996). Sequence conservation with conical H2A is around 60% (Figure 1 A and B), and the main identifier of H2A.Z is the alteration of the C-terminal 'docking domain' responsible for contact with H3 within the nucleosome (Wratting et al., 2012; Figure 1 B). This domain physically alters the shape of the H2A.Z-containing nucleosome, and destabilises its interaction with the H3-H4 tetramer (Suto et al., 2000). In addition, nucleosomes containing one H2A-H2B, and one H2A.Z-H2B, are unstable due to changes in the structure of loop L1, which causes steric hindrance (Suto et al. 2000), it is thought that this change in conformation is what gives H2A.Z its flexibility for transcription.

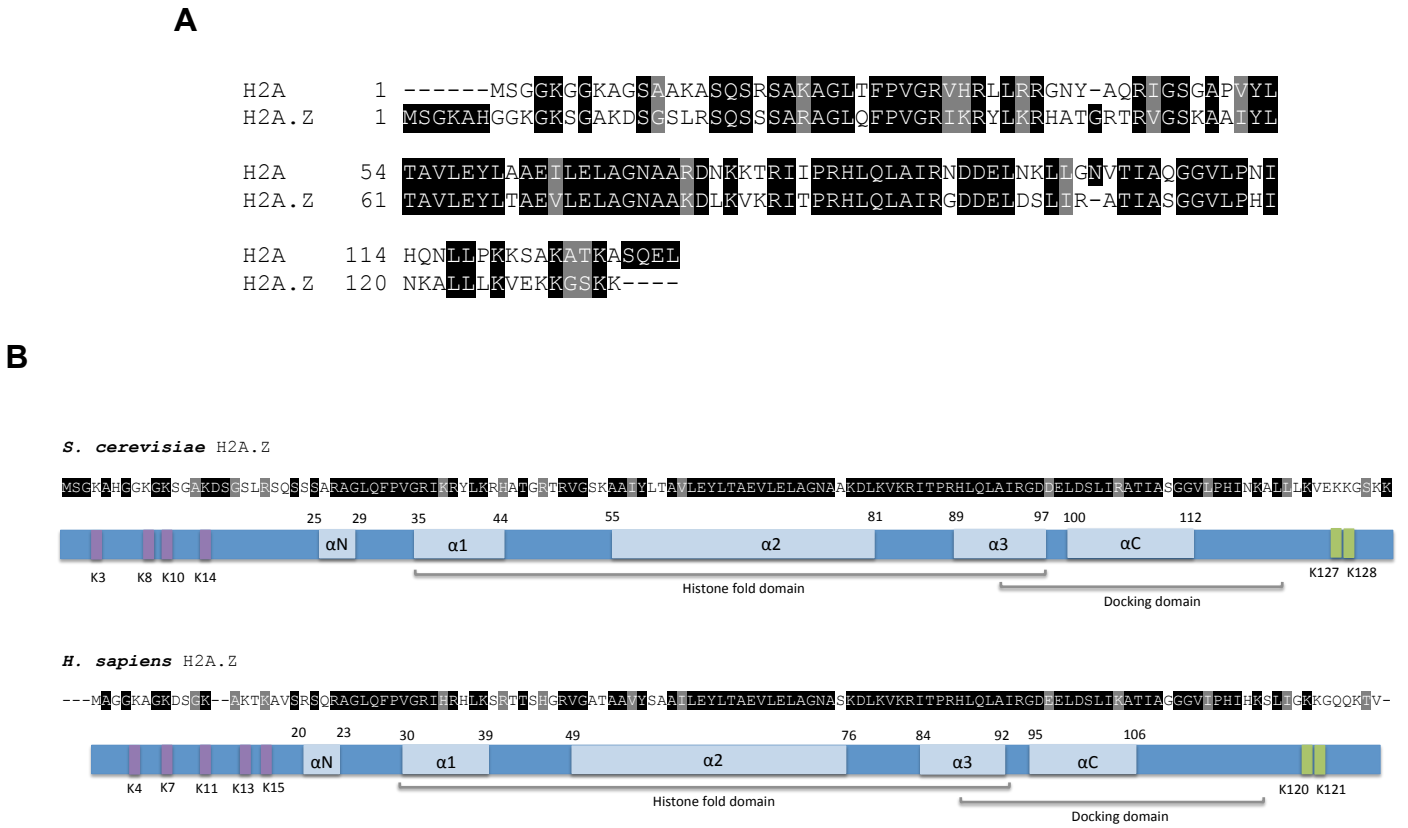

Figure 1: H2A and its variant H2A.Z share sequence homology, which is conserved from yeast to humans.

A. Alignment showing sequence variation between conical histone, H2A, and variant, H2A.Z, from *S. cerevisiae*. Alignment produced using ClustalW and BoxShade. Consensus residues are highlighted in black, similar in grey.

B. Alignments showing the sequence conservation between variant histone H2A.Z from *S. cerevisiae* and *H. sapiens*. Alignment produced using ClustalW and BoxShade. Consensus residues are highlighted in black, similar in grey. Schematics bellow the sequences indicate the relative positions of acetylated lysine residues (purple boxes), the histone fold domain, the docking domain and ubiquitinated lysine residues (green boxes). Adapted from: (Zlatanova and Thakar, 2008) and (Talbert and Henikoff, 2010).

Deletion of H2A.Z is lethal in many higher eukaryotes, including *D. melanogaster* (Clarkson et al., 1999; Daal and Elgin, 1992), *X. Leavis* (Louzalen et al., 1996) and *mus musculus* (Faast et al., 2001), and lethal in combination with genes required for development in *C. elegans* (Shibata and Nishiwaki, 2014). In mice, homozygous deletion of H2A.Z ($H2A.Z^{-/-}$) causes embryonic lethality at a developmental stage characterised by accelerated, complex differentiation (Faast et al., 2001). This defect would likely extend to *H. sapiens* due to the evolutionary conserved nature of H2A.Z, however, H2A.Z is not essential for viability in simple eukaryotes. Given the ability to produce viable null mutants in yeast, including, *S. pombe* and *S. cerevisiae*, H2A.Z has been widely studied in these organisms.

An early study in *S. pombe* indicated H2A.Z, encoded by the *PTH1* gene, was important for maintenance of chromosomal stability, suggesting a role in segregation or transmission during mitosis (Carr et al., 1994). Studies have since built on this, suggesting H2A.Z is important for the regulation of cohesion (Tapia-Alveal et al., 2014). Furthermore, deletion of the gene encoding H2A.Z in *S. cerevisiae, HTZ1*, causes sensitivity to benomyl, camptothesisn (CPT), and hydroxyurea (HU) (Mehta et al. 2010), in addition to inhibited growth and reduced plasmid maintenance (Daniel et al., 2006). Such phenotypes suggest H2A.Z is important for DNA damage and chromosome segregation. Indeed, recent studies in *S. cerevisiae* suggest roles similar to the *S. pombe* homolog, where cohesin regulation is mediated by H2A.Z (Sharma et al., 2013).

In contrast, early studies in *S. cerevisiae* focused on its roles in transcriptional regulation meaning this role is highly characterised. The quantification of *HTZ1*-activated genes revealed 214 genes were activated, and 107 were repressed in the presence of the *HTZ1* gene (Santisteban et al., 2000). In

addition, H2A.Z occupancy is high in euchromatic regions, and inhibits the Sir1-dependent transition of euchromatin into a silent heterchromatic state (Meneghini et al., 2003; Santisteban et al., 2000). H2A.Z occupancy correlates with transcriptional start sites (TTS) of inactive genes (Li et al., 2005; Zhang et al., 2005), where it acts as a primer for transcription, and is subsequently lost upon the initiation of gene expression (Adam et al., 2001).

Given the direct influence of H2A.Z-mediated chromatin structure on transcription, it could be an important indicator for human diseases where genes influenced by H2A.Z occupancy have been misregulated. Indeed, altered expression patterns of H2A.Z have been confirmed in breast, prostate, bladder, and colorectal cancer. In breast cancer, misregulation of estrogen receptors (ERα and ERβ), known ligand-dependant transcription factors, cause increased proliferation of mammary cells and elevated levels of replication. In addition, DNA damage caused by estrogen metabolites, results in a higher mutation frequency, and greater risk of cancer development. Interestingly, H2A.Z incorporation is high in ERα regulated gene promoters, and depletion of H2A.Z in human fibroblasts causes defects in estrogen signalling and loss of estrogen mediated cell proliferation (Hua et al., 2008; Laflamme et al., 2009). This suggests H2A.Z may mark areas of the genome for ERα recruitment.

In estrogen responsive breast cancers, tamoxifen is used to inhibit estrogen binding to the ERs. Overexpression of H2A.Z in breast cancer cells with low estrogen levels causes increased cell proliferation, even in the presence of tamoxifen, suggesting expression of H2A.Z can overcome ER inhibition (Svotelis et al., 2014). This may provide mechanism for the occurrence of hormone resistant breast cancers. Furthermore, bladder cancer cell lines, known to overexpress

H2A.Z, have high rates of cell proliferation, correlating with increased H2A.Z incorporation at the transcriptional start site (TSS) of genes regulating cell proliferation (Kim et al., 2013). Similar effects on transcription have been discovered in prostate cancer cell lines (Baptista et al., 2013). However, it is without doubt that the mechanisms behind H2A.Z incorporation and removal are equally vital to the regulation of H2A.Z effects on transcription.

In *S. cerevisiae,* incorporation of H2A.Z-H2B dimers into chromatin is achieved by the SWR1 chromatin remodelling complex (Krogan et al., 2003; Mizuguchi et al., 2004; Figure 2 A), homologous to SRCAP in *H. sapiens*. Deletion of *SWR1*, in *S. cerevisiae*, results in the loss of H2A.Z on chromatin, specifically at promoters known for H2A.Z enrichment (Kobor et al., 2004). In *H. sapiens*, in addition to SRCAP, the histone acetyltransferase Tip60 (Yamamoto, 1997), is a second human homologue of Swr1, which is part of the TIP60 complex (Cai et al., 2003). It has been shown to incorporate H2A.Z into nucleosomes at *p21* promoter regions (Gévry et al., 2007).

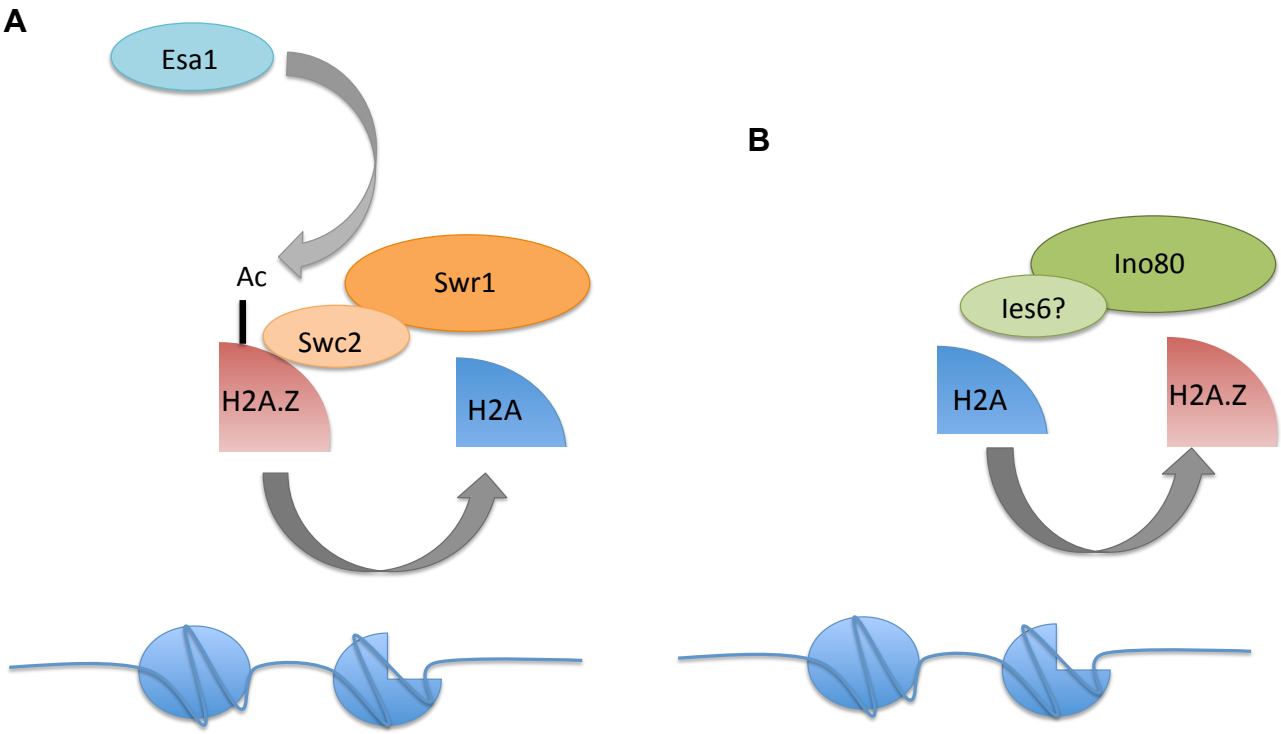

Figure 2: In *S. cerevisiae,* SWR1 complex incorporates acetylated H2A.Z and the INO80 complex evicts it.

A. Schematic showing the acetylation of H2A.Z by Esa1, then subsequent incorporation of H2A.Z into chromatin via interaction with the Swc2 subunit of SWR1.

B. Schematic showing the role of Ino80 in H2A.Z eviction and incorporation of H2A, a function where contributing accessory subunits have yet to be identified.

In terms of H2A.Z removal, in *S. cerevisiae*, the INO80 chromatin remodelling complex has been identified as the mechanism of H2A.Z eviction (van Attikum et al., 2007; Papamichos-Chronakis et al., 2011; Figure 2 B). In one study, deletion of *INO80* caused aberrant, unregulated incorporation of H2A.Z at gene promoters, and increased levels of H2A.Z in whole cell lysates (Papamichos-Chronakis et al., 2011). Furthermore, deletion of *INO80* or the INO80 subunit, *IES6*, increases the levels of H2A.Z at the centromere, which alters nucleosome structure and leaves DNA susceptible to MNase digestion (Chambers et al. 2012). However, biochemical studies undertaken so far from *H. sapiens* have only implicated the ANP32E histone chaperone in H2A.Z eviction (Mao et al., 2014; Obri et al., 2014), so the relationship between Ino80 and H2A.Z in mammals is yet to be thoroughly investigated.

Taken together, the influence of H2A.Z on the transcription of important oncogenes that lead to cancer, and the roles of H2A.Z in the regulation of chromosome segregation, provide two pathways by which H2A.Z may contribute to cancer. Making the mechanisms by which H2A.Z is regulated, for example, it's deposition and removal from chromatin, and post-translational modification, significantly important avenues for further investigation.

1.1.2.1.1 H2A.Z acetylation

Given the roles of H2A.Z in transcription, development, and chromosome segregation, the regulation mechanisms behind H2A.Z function are important to understand. Post-translational modification of histones by acetylation is widely associated with transcription, thus many studies have made correlations between H2A.Z acetylation and gene regulation.

In *S. cerevisiae*, H2A.Z is acetylated by the Esa1 catalytic subunit of the NuA4 histone acetyltrasferase (Keogh et al., 2006; Figure 2 A). This acetylation is used to regulate the incorporation of H2A.Z into chromatin by the SWR1 chromatin remodelling complex (Watanabe et al. 2013), with the Swc2 catalytic subunit binding to H2A.Z (Wu et al., 2005). Mass spectrometry has revealed acetylation occurs at four lysine residues (K3, K8, K10 and K14) in the N-terminus (Millar et al., 2006; Figure 1 B), with K14 being the most abundantly acetylated (Mehta et al., 2010). The acetylated N-terminal lysines are conserved in higher eukaryotes from *M. musculus* to *H. sapiens* (Pantazis & Bonner 1966; Boyne et al, 2006). The acetylation of H2A.Z in higher eukaryotes destabilises the nucleosome core (Ishibashi et al. 2009), making acetylated H2A.Z containing nucleosomes more susceptible to nuclease digestion.

In terms of transcription, genome-wide expression profiles in *S.* cerevisiae show that H2A.Z is hyperacetylated on K14 at promoters of active genes (Millar et al., 2006). Similar results have been observed at the promoters of active genes in higher eukaryotes (Bruce et al., 2005; Valdés-Mora et al., 2012). In addition, acetylated H2A.Z is present at highly active promoters in prostate cancer cell lines

(Valdés-Mora et al., 2012), where the acetylation of H2A.Z acts as a switch for transcription. Furthermore, H2A.Z is acetylated during early embryonic development in mice (Bošković et al., 2012) and for the maintenance of cell fates in *C. elegans* (Shibata et al. 2014), suggesting acetylation of H2A.Z may govern the transcription of genes early in mammalian development.

The functions of H2A.Z in chromosome segregation have been linked to H2A.Z acetylation, with rates of sister chromatid separation in *S. cerevisiae* occurring at the same frequency in *htz1* null cells as a *htz1(K-R)* acetylation mutant (where K3, K8, K10 and K14 have been mutated to arginine) (Sharma et al., 2013). Similarly in *S. pombe*, acetylated H2A.Z leads to chromosome segregation defects during anaphase (Kim et al., 2009). Therefore it is unsurprising that H2A.Z acetylation is being described as a key epigenetic modification in certain cancers.

1.2 Chromatin remodellers

Chromatin remodellers utilise ATP hydrolysis to rearrange or alter nucleosomes and histones, allowing for chromatin accessibility and repackaging. This can be achieved through nucleosome sliding, nucleosome eviction, or the complete exchange of histones. Their importance cannot be underestimated, as they catalyse the removal of chromatin barriers that would otherwise impede on vital cellular processes such as transcription and DNA replication. Remodellers share a key characteristic ATPase domain, which shares sequence homology with the SNF2 (super family 2) helicases, and hydrolyses ATP to catalyse the translocation of nucleosomes on DNA. The unique domains flanking the ATPase region govern remodeller function, and give rise to four families of chromatin remodellers: ISWI, CHD, SWI/SNF and INO80, each categorised by their specialised domains (for reviews, see van Vugt et al. 2007 and Clapier & Cairns 2009).

1.2.1 ISWI Remodellers

The ISWI family of chromatin remodellers typically contain remodellers composed of between 2-4 subunits (Hartlepp et al., 2005; Ito et al., 1999). Each contains C-terminal HAND-SANT-SLIDE domains in their catalytic ATPase subunit, which bind to linker DNA between nucleosomes (Yamada et al., 2011). The ISWI remodellers are thought to reposition nucleosomes in steps of 1 bp (Deindl et al., 2013), with additional roles in transcription, high-order chromatin structure assembly, and DNA replication (for review, see Corona & Tamkun 2004).

1.2.2 CHD Remodellers

Subunit number of remodellers within the CHD (Chromodomain-Helicase-DNA-binding) family varies hugely, with some, such as Chd1, existing only as monomers in eukaryotes (Woodage et al., 1997), and others with up to ten subunits, such as the NuRD complex in *H. sapiens* (Xue et al., 1998; Zhang et al., 1998, 1999). These remodellers are characterised by two N-terminal chromodomains (Delmas et al., 1993; Woodage et al., 1997), which, for CHD1 in *H. sapiens*, bind to methylated K4 on histone H3 (Flanagan et al., 2005; Sims et al., 2005). In *S. cerevisiae* the chromosodomains of Chd1 regulate ATPase contacts with DNA (Hauk et al., 2010). In addition, CHD family members have roles in chromatin assembly, transcription, development, and human disease (for review, see Marfella & Imbalzano 2007)

1.2.3 SWI/SNF Remodellers

The *SWI/SNF* (Switch/Sucrose Non-Fermenting) genes were first identified in two separate screens of genes in *S. cerevisiae* involved in class switching or sucrose fermentation (Haber and Garvik, 1977; Neigeborn and Carlson, 1984). Some of the *SWI* and *SNF* genes, identified during the screens, were later found to encode components of large chromatin remodelling complexes, now known as SWI/SNF (Smith et al. 2010), and the RSC complex (Cairns et al., 1996). Subsequently, homologous genes, and the complexes they encode, were found to be conserved in *D. malongaster* (Tamkun et al. 1992) and *H. sapiens* (Muchardt & Yaniv 1993;

Khavari et al. 1993; Chiba et al. 1994). In *H. sapiens*, the BAF (BRG1-associated factor) and PBAF (polybromo-BAF) complexes (homologous to *S. cerevisiae* SWI/SNF and RSC respectively) contain a single ATPase subunit, BRM or BRG1, and three core subunits: BAF155, BAF170, and BAF47, with BAF containing ARID1A/ARID1B, and PBAF containing BAF180 and BAF200, and up to 7-15 additional subunits. Remodellers of this family are characterised by the presence of bromodomains within their subunits. These domains are found in the C-terminus of BRM/BRG1, and six within BAF180. Bromodomains are characteristic of histone acetyltransferases (HATs) (Jeanmougin et al., 1997) and bind acetylated lysine residues (Dhalluin et al., 1999).

Studies in *S. cerevisiae* initially focused on SWI/SNF and RSC complexes in transcription (Biggar and Crabtree, 1999; Peterson and Herskowitz, 1992; Sudarsanam et al., 2000), then roles in DNA repair (Chai et al. 2005; Shim et al. 2005; Chambers et al. 2012), with focus on the influence of nucleosome remodelling by both complexes (Shim et al., 2007; Sinha et al., 2009). In addition, the RSC complex, promotes cohesion loading at DSB ends to enable repair by homologous recombination (Oum et al., 2011). Furthermore, advances in sequencing, have identified mutations in both BAF and PBAF complexes in multiple human cancers (for reviews, see Wilson & Roberts 2011; Masliah-Planchon et al. 2014). Given BAF and PBAFs functions, they could contribute to cancer progression from multiple pathways. Including repression of transcription at DSBs (Kakarougkas et al., 2013), in addition to the regulatory functions of PBAF subunits in cohesion loading, independent of transcription (Brownlee et al., 2014). These studies highlight the importance of chromatin remodelling complexes, and

how the loss of individual remodellers, and their specific remodelling activities, can have a significant detrimental impact on genome stability.

1.2.4 The INO80 family

Members of the INO80 (Inositol Requiring 80) family of chromatin remodellers contain multiple subunits that are often shared between complexes (Figure 3). These complexes are assembled around a catalytic core, which comprises of two ATPase domains, separated by an insert region, and an N-terminal helicase SANT-associated (HSA) domain. The family acquired its name after the *INO80* gene was identified in *S. cerevisiae* as regulating transcription in response to inositol depletion (Ebbert et al., 1999). Since, two complexes, SWR1 (Krogan et al., 2003) and INO80 (Shen et al., 2000), have been identified in *S. cerevisiae*, with homologous complexes in *H. sapiens*, SRCAP (Johnston et al., 1999) and INO80 (Jin et al., 2005), in addition to the TIP60 complex.

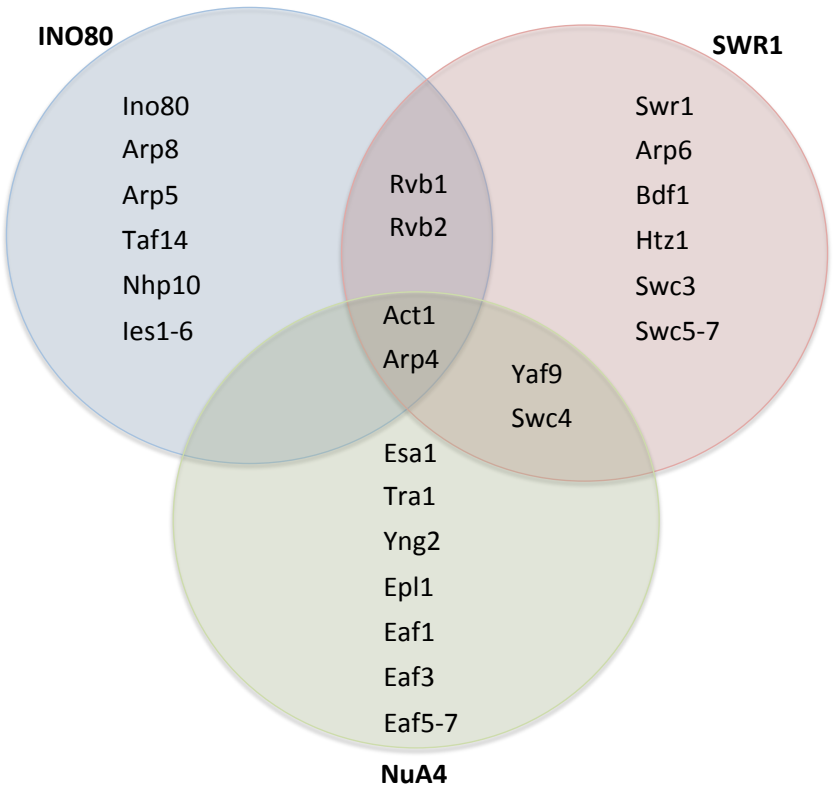

Figure 3: Subunits are shared between chromatin remodellers and chromatin modifying complexes in *S. cerevisiae.*

The INO80 and SWR1 chromatin remodellers share Rvb1 and Rvb2, the SWR1 complex and NuA4 share Yaf9 and Swc4, the Act1 and Arp4 subunits are found in INO80, SWR1, and NuA4. Adapted from: (Kapoor and Shen, 2014)

In *S. cerevisiae,* the SWR1 complex has 14 subunits, including the catalytic component, Swr1 (Krogan et al., 2003; Mizuguchi et al., 2004), and shares subunits, Arp4, Ruvb1 and Ruvb2, with INO80 (Shen et al. 2003; Figure 3), and subunits Arp4, Swc4 and Yaf9, with the yeast specific, histone acetyltrasferase (HAT) complex, NuA4 (Mizuguchi et al., 2004; Figure 3). The specific chromatin remodelling function of SWR1 is to displace the H2A-H2B conical histone dimer, and replace it with the H2A.Z-H2B variant dimer. This is achieved through binding of the Swr1 catalytic subunit N-terminus to H2A.Z dimers (Hong et al., 2014). The NuA4 HAT complex contributes to SWR1 incorporation of H2A.Z through its acetylation of H2A and H4 (Altaf et al., 2010). The catalytic component of NuA4, Esa1, is homologous to human Tip60 protein (Doyon et al., 2004), and, as previously mentioned, Esa1 acetylates H2A.Z on its N-terminal tail (Keogh et al., 2006; Figure 2 A). Additionally, in *H. sapiens* the TIP60 complex shares homologous subunits with the SRCAP complex, as NuA4 does with SWR1 in *S. cerevisiae*. However, unlike NuA4, the mammalian TIP60 complex contains an Swr1 orthologue, p400, and competes with SRCAP in the removal of H2A-H2B dimers (Choi et al., 2009). In *H. sapiens,* both the SRCAP and TIP60 complexes contain the mammalian specific subunit, YL1 (Cai et al., 2005), which is orthologous to Swc2, a H2A-binding protein in *S. cerevisiae* (Wu et al., 2005), and shares a C-terminal YL1_C domain with the INO80 subunit, Ies6.

As previously discussed, the incorporation of the H2A.Z variant in nucleosomes acts as a primer for transcription. However, mechanistic insights into the regulation of H2A.Z removal are largely unclear in *H. sapiens*, but evidence

from *S. cerevisiae* would implicate the SWR1 partner complex INO80 (Papamichos-Chronakis et al., 2011; Watanabe et al., 2015).

1.2.4.1 The INO80 complex

The INO80 chromatin-remodelling complex has 15 subunits in *S. cerevisiae* (Shen et al. 2003; Table 1) and 14 in mammals (Cai et al., 2007; Chen et al., 2011; Jin et al., 2005; Table 1). Both complexes share the catalytic ATPase core, Ino80, in addition to the highly conserved ATPases: Ruvb1 and Ruvb2, actin-related proteins: Arp5, Arp8, Act1 and Arp4, Actin and BAF53a in mammals respectively, and finally, two conserved Ino-eighty-subunits (IES), Ies2 and Ies6. In addition, the *S. cerevisiae* INO80 complex contains further IES subunits that are not found in mammals (Ies1, Ies3, Ies4 and Ies5) as well as yeast specific Nhp10 and Taf14 subunits (Figure 4 B). In turn, the INO80 complex in *H. sapiens* contains mammalian specific subunits: Amida, INO80E, NFRKB, MCRS1, INO80D, YY1 and UCH37.

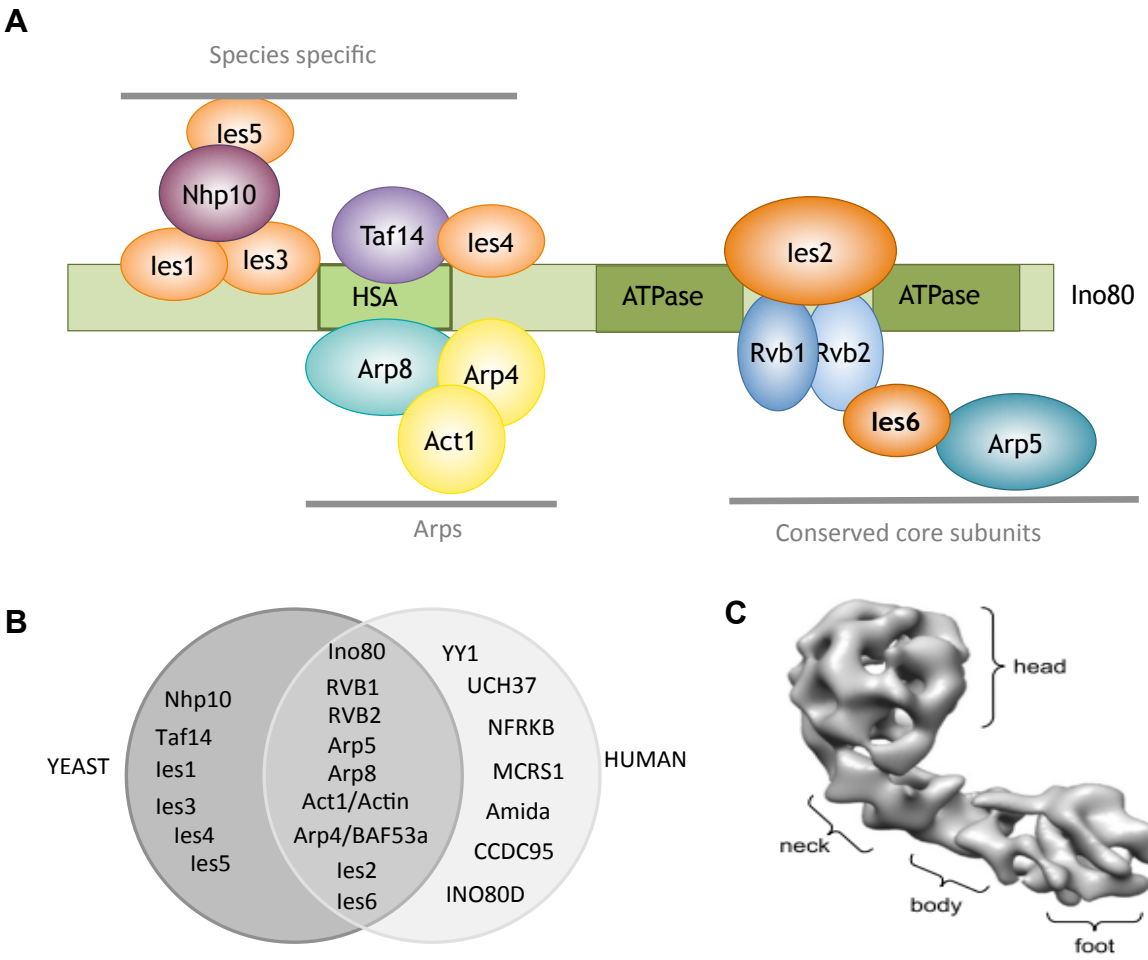

Figure 4: The INO80 complex is composed of multiple subunits, which are conserved in both *S. cerevisiae* and *H. sapiens*.

A. Schematic of the INO80 complex in *S. cerevisiae* showing. Subunit positioning depicts their interactions with the catalytic subunit, Ino80. Adapted from: (Watanabe and Peterson, 2010)

B. Schematic showing subunits of the INO80 complex conserved between *S. cerevisiae* and *H. sapiens.* Adapted from: (Jha and Dutta, 2009)

C. EM structure of the INO80 complex from *S. cerevisiae*. Adapted from: (Tosi et al., 2013)

All the subunits are known to assemble on the Ino80 catalytic core (Figure 4 A) either directly or indirectly through other subunit contacts. It is known that the actin-related proteins (Arps) bind HSA domains in other chromatin remodelling complexes in *S. cerevisiae* (Szerlong et al., 2010). Indeed, for Ino80, biochemical analysis has shown Act1, Arp4 and Arp8 assemble on the N-terminal HSA domain (Shen et al., 2003), in addition to yeast specific subunits Taf14 and Ies4 (Kapoor et al. 2013; Tosi et al. 2013). Act1, Arp4, Arp8 and Taf14 a bind to a specific 'TELY' motif within the HSA domain (Kapoor et al. 2013). Additional yeast specific subunits Ies5, Nhp10, Ies1 and Ies3 are known to bind to the very N-terminus of the protein before the HSA domain. The remaining core conserved subunits, Ies2, Ies6, Rvb1, Rvb2 and Arp5, are known to assemble on the 'insert' region between the two ATPase domains (Watanabe and Peterson, 2010; Figure 4 A).

Electron microscopy (EM) of the complex has revealed the shape and structure of the complex in *S. cerevisiae* (Tosi et al., 2013). This study revealed an 'embryo' shaped complex (Figure 4 C), with Rvb1/Rvb2 constituting the 'head' region, Ino80, Ies2, Arp5 and Ies6 within the 'neck', Nhp10, Ies1, Ies3 and Ies5 within the 'body' and Arp8, Arp4, Act1, Taf14 and Ies4 within the 'foot' region (Tosi et al., 2013).

Table 1: The subunits of the INO80 chromatin remodelling complex contain specialised domians.

Yeast	Humans	Domain Structure	Additionally part of…
Ino80	INO80	HSA, Snf2-like ATPase	-
Rvb1	RuvB1 (Tip49a, RUVBL1)	AAA^+ ATPase	SWR1
Rvb2	RuvB2 (Tip49b, RUVBL2)	AAA^+ ATPase	SWR1
Arp4	Baf53a (Arp4, ACTL6A)	Actin-fold	SWR1, NuA4
Arp5	Arp5 (ACTR5)	Actin-fold	-
Arp8	Arp8 (ACTR8)	Actin-fold	-
Act1	β-actin (ACTB)	DNAse I Nucleotide binding	SWR1, SWI/SNF, RSC
Ies1	-	-	-
Ies2	Ies2 (INO80B, PAPA-1)	Zinc-finger-HIT, PAP-1	-
Ies3	-	-	-
Ies4	-	-	-
Ies5	-	-	-
Ies6	Ies6 (INO80C, c18orf37)	YL1_C	-
Nhp10	-	HMG type-II	-
Taf14	-	YEATS	SWR1, RSC
-	YY1	Gli-Kruppel zinc finger	SRCAP, Tip60/p400
-	Uch37 (UCHL5)	UCH family	-
-	NFRKB (INO80G)	-	-
-	MCRS1 (MCRS2, MSP58, INO80Q)	FHA	-
-	Amida (TFTP1, INO80F)	-	-
-	INO80D (FL20309)	-	-
-	CCDC95 (FLJ90652, INO80E)	Coiled-coil	-

1.2.4.1.1 INO80 chromatin remodelling

In terms of the complexes ATPase function, *in vitro* incubation of purified INO80 complex from *S. cerevisiae* with nucleosomes or DNA, is sufficient to stimulate ATPase activity (Jin et al., 2005). In addition, it has been suggested that complex exhibits *in vitro* ATP-dependent DNA helicase activity (Shen et al., 2000), however, this is controversial, as a more recent study could find no evidence of DNA helicase activity (Watanabe et al., 2015). However, in *S. cerevisiae* ATP-dependent chromatin remodelling is clear, in the form of nucleosome sliding (Jónsson et al., 2004; Shen et al., 2003), nucleosome spacing (Udugama et al., 2011) leading to nucleosome eviction (Tsukuda et al., 2005), and H2A.Z dimer exchange (Watanabe et al., 2015).

The Rvb1 and Rvb2 proteins (Table 1) are essential ATPases in *S. cerevisiae* (Qiu et al., 1998), making them elusive subunits of the INO80 complex. They are closely related to the bacterial RuvB ATPase, a molecular motor which resolves Holliday junctions during homologous recombination in bacteria (West, 1996). EM has revealed they form double asymmetric rings *in vitro* (Torreira et al., 2008), which can be heterohexameric (Gribun et al., 2008; Puri et al., 2007) or homohexameric (Torreira et al., 2008). Both are found within the SWR1 chromatin remodelling complex (Mizuguchi et al., 2004; Figure 3), the NuA4 histone actyltansferase (Jha et al., 2008; Figure 3) and the R2TP (Ruvb1/2-Tah1-Pih1) complex (Zhao et al., 2005), which is important for the functions of the Hsp90 molecular chaperone (Zhao et al., 2005) (to be discussed in detail in Chapter 5).

In relation to INO80, Rvb1 and Rvb2 are required for stability of the complex, and for its chromatin remodelling activity (Jónsson et al., 2004). However, biochemistry has shown a dependency of the Arp5 subunit on Rvb1 and Rvb2 for efficient loading (Jónsson et al., 2004), so Arp5, or any additional accessory subunits that require Rvb1 or Rvb2 interaction for sufficient loading, may be effecting chromatin remodelling when lost. Indeed, more recent cross-linking studies have shown, Rvb1 and Rvb2 are associated with Ies2, Ies6, and Arp5 (Tosi et al., 2013). The link between Rvb2 and Ies6 could prove vital, as this study did not find any independent association between Ies6-Arp5 and the Ino80 catalytic core (Tosi et al., 2013). As Ies6 and Arp5 have been shown to depend on each other for stability of the Ies6-Arp5 module within the complex (Chen et al., 2013; Watanabe et al., 2015). Therefore, this cross-linking assay (Tosi et al., 2013) would suggest their only mechanism of association with the complex may be through contact with the Rvb2 subunit.

All the Arp family members contain an actin-fold domain (Table 1), which bares similarities to the actin nucleotide binding region (for review of Arps, see Boyer & Peterson 2000). Actin has two major domains, composed of four subdomains (S1, S2, S3 and S4), and a separate nucleotide-binding region. The subdomains are arranged on the outside of the protein with the nucleotide binding domain, known to bind ATP, in the centre between S2 and S3 (Kabsch et al., 1990). Of all the Arps within INO80, only Arp4 and Arp8 bind core histones (Harata et al., 1999; Shen et al., 2003) and only Arp4 binds ATP (Sunada et al., 2005). Furthermore, an actin mutant (*act1-2*), harbouring a point mutation in S2, shares phenotypes with a complete *ino80* deletion (Kapoor et al., 2013). In addition, intact INO80 complex, purified from *act1-2* expressing cells, has a reduced capacity to

slide nucleosomes (Kapoor et al., 2013). Suggesting Actin, and specifically S2, is vital for INO80 chromatin remodelling functions, regardless of the additional accessory subunits. However, this is not to say the remaining Arps do not contribute to chromatin remodelling, albeit indirectly, as nucleosome sliding is dependent on the presence of Arp5 (Shen et al., 2003; Watanabe et al., 2015) and, to a lesser extent, Arp8 (Shen et al., 2003; Watanabe et al., 2015), which other accessory subunits depend on for recruitment (Tosi et al., 2013).

Investigation of Ino80 regulation by various INO80 subunits within complexes purified from *H. sapiens* has revealed potential subunit dependencies for Ino80 ATPase function. Studies found that nucleosome sliding was abolished when contacts between Ino80 and Ies2 were removed, however, sliding was restored in the presence of increasing concentrations of independently purified Ies2 (Chen et al., 2013). Similarly for the Ies6-Arp5 module, nucleosome remodelling was partially restored in cells expressing an Ino80 mutant upon the addition of recombinant Ies6 or Arp5 protein, but was optimal when added together, however, this was still in the presence of Ies2, which had a greater influence on nucleosome sliding (Chen et al., 2013). Interestingly, they showed data to suggest that the Ies6-Arp5 complex has the capacity to bind nucleosomes in complexes that lack Ies2 (Chen et al., 2013), however, Ies6 has since been shown to not be required for nucleosome sliding in *S cerevisiae* (Watanabe et al., 2015). These studies highlight the interdependencies of subunits within the INO80 complex, making it critical to control for the loss of various subunits within each experiment.

In addition to chromatin remodelling, the INO80 complex is known to function in transcription (Shen et al., 2000), DNA repair (Van Attikum et al., 2004;

Downs et al., 2004; Morrison et al., 2004), replication (Falbo et al., 2009; Papamichos-Chronakis and Peterson, 2008; Shimada et al., 2008) and chromosome segregation, both in terms of cohesion (Ogiwara et al. 2007) and the maintenance of centromere structure (Chambers et al. 2012). Contribution to these biological processes is likely to arise from the complexes chromatin remodelling functions, including nucleosome sliding (Jónsson et al., 2004; Shen et al., 2003) and the exchange of H2A.Z/H2B dimers for free H2A/H2B dimers (Papamichos-Chronakis et al., 2011).

1.2.4.1.2 Transcription

INO80 is known to regulate around 20% of *S. cerevisiae* genes (Van Attikum et al., 2004; Jónsson et al., 2004), which is dependent on Rvb1 and Rvb2 (Jónsson et al., 2004). The deletion of either *arp5* or *arp*8 has also been shown to reduce the transcription of the *INO1* gene to levels comparable with deletion of the catalytic core, Ino80 (Van Attikum et al., 2004). Though, since these early transcriptional studies, DNA repair, replication and chromosome segregation have taken the primary focus of INO80 research.

1.2.4.1.3 DNA damage

DNA repair phenotypes first emerged after systematic deletion of specific INO80 subunits (Van Attikum et al., 2004). Deletions of *arp5* and *arp8* were shown to have Methyl methanesulfonate (MMS) sensitivity. MMS methylates DNA causing

bulky adducts that are thought to collide with replication machinery inhibit homologous recombination (HR) (Lundin et al., 2005). In addition to hydroxyurea (HU) sensitivity, an inhibitor of ribonucleotide reductase that blocks dNTP production (Koç et al., 2004). Both *arp5* and *arp8* had lowered transcription after MMS exposure of genes important for replication fork progression (*MRC1* and *TOF1*) (Van Attikum et al., 2004). In addition, both *arp*5 and *arp*8 are defective for growth in the presence of a HO endonuclease break that can only be repaired by the non-homologous end joining (NHEJ) pathway. In this strain, Ino80, Arp5 and Arp8 are all known to be recruited to the DSB site (Van Attikum et al., 2004; Morrison et al., 2004). However, the exact mechanism behind INO80 recruitment to DSBs remains controversial. Some studies suggest H2A phosphorylation at S129 in *S. cerevisiae*, a PTM regulated by Mec1 and Tel1 (ATM and ATR in *H. sapiens*) to mark the presence of a DSB (Downs et al., 2000), may serve to recruit Ino80 to sites of damage (Van Attikum et al., 2004; Kashiwaba et al., 2010; Morrison et al., 2004). However, other studies have found no link between H2A phosphorylation and chromatin remodeller recruitment (Bennett et al., 2013). Instead suggesting a model where remodellers are recruited by the early stages of the homologous recombination (HR) pathway or DNA repair.

Aside from the recruitment mechanisms of INO80, deletion of subunits *arp*8 or *nhp*10 impairs nucleosome eviction at DSB sites (Van Attikum et al., 2007; Tsukuda et al., 2005), a process that may provide access to DNA repair machinery. For instance, an *arp*8 deletion reduces Mre11 association with double strand breaks (Van Attikum et al., 2007), and causes a reduction in Rad51 recruitment to DSBs (Tsukuda et al., 2005), both indicating a role for the complex in promotion of HR. Furthermore, the deletion of either *arp*8 or *nhp*10, reduces Mre11

endonuclease resection (Van Attikum et al., 2007), a process that is critical for creating 3' ssDNA tracts to initiate repair by HR, and the DNA damage checkpoint, through the recruitment of Mec1.

The idea that INO80 subunits may be important for DNA checkpoints is supported by the fact that *arp*8 and *nhp*10 deletions show reduced levels of Mec1 at DSBs, and reduced Rad53 checkpoint kinase activation (Van Attikum et al., 2007), a process that occurs by Mec1 dependent phosphorylation. Furthermore, the INO80 subunit, Ies4 (Table 1), is phosphorylated by Mec1 and Tel1 in response to DNA damage, a process that activates downstream DNA damage checkpoint factors (Morrison et al., 2007).

Given the inconclusive data from *S. cerevisiae*, it cannot be concluded how Ino80 is recruited to DSBs, as the use of phosphorylated H2A remains controversial (Bennett et al., 2013; Kashiwaba et al., 2010; Van Attikum et al., 2004; Morrison et al., 2004). In addition, the complex promotes DNA checkpoint activation through Ies4 phosphorylation, and the Arp8 and Nhp10 subunits (Morrison et al., 2007). There are some contradictions within the data as to whether INO80 is involved in both NHEJ (Van Attikum et al., 2004; Morrison et al., 2004) and HR (Van Attikum et al., 2007; Tsukuda et al., 2005), however, multiple studies have suggested INO80 is present at DSBs and may be involved in promotion of the DNA damage checkpoint (Van Attikum et al., 2007; Tsukuda et al., 2005).

In *H. sapiens* the INO80 complex is recruited to site of laser (Kashiwaba et al., 2010) and ionising radiation (IR) (Gospodinov et al., 2011) induced damage, however, ɣ-H2A.X was not required for the recruitment or retention of Ino80 (Kashiwaba et al., 2010). When comparing Ino80 recruitment in YY1, Uch15,

Mcrs1, Arp4, Arp5, and Arp8 stable knockdowns, only the depletion of Arp8 prevented Ino80 recruitment to laser-induced damage sites (Kashiwaba et al., 2010). However, a separate study found cells depleted for Arp5 (knockdown efficiency of 20-30%) were sensitive to bleomycin, with reduced γ-H2A.X expression (Kitayama et al., 2009). However, it is important to remember Ies6 and Arp5 are dependent on each other for stability in the complex in *S. cerevisiae* (Chen et al., 2013; Watanabe et al., 2015), so this result should be considered as the loss of both subunits from the INO80 complex.

In contrast to the data from *S. cerevisiae*, there is some evidence to suggest Ino80 may be important for repair by HR in *H. sapiens*. Levels of DNA recombination at an I-SceI-induced break site have been observed as slightly reduced in Ino80 depleted cells (Gospodinov et al., 2011). Furthermore, this study showed Ino80 knockdown caused a reduction in ssDNA production at DSB ends (Gospodinov et al., 2011), a process that initiates HR, as well as the DNA damage checkpoint. This was shown to be dependent on Arp8, as depletion of Arp8 led to a reduction in RPA foci formation after IR induced DNA damage (Gospodinov et al., 2011). In addition, the INO80 mammalian specific subunit, Ying yang 1 (YY1), has been shown to function with RuvBL2 (homologue of *S. cerevisiae* Rvb2) to promote Rad51 focus formation after IR (López-Perrote et al., 2014), further suggesting that INO80 is important for HR in *H. sapiens*. Taken together with data from *S. cerevisiae*, it is clear that INO80 plays some role in DNA damage pathways, however, whether it contributes directly to NHEJ, HR, and checkpoints remains unclear.

1.2.4.1.4 Replication

Since sensitivity to both MMS and HU can highlight roles in replication, rather than DNA damage per se, many studies have found links between INO80 subunits and replication fork progression and stability using these sensitivity read outs. In *S. cerevisiae*, further analysis showed *ino80* null cells are sensitive to CPT, a compound that causes DSBs in S-phase, due to the replication fork colliding with topoisomerase I bound single strand breaks (SSB). However, this did not activate the Rad9 DNA damage checkpoint (Papamichos-Chronakis and Peterson, 2008), demonstrating *INO80* deletion caused reduced cell viability for reasons unrelated to the persistence of DSBs.

Further analysis of cell cycle progression in *ino80* null cells showed delayed entry into a prolonged S-phase, which, in the presence of HU causes replication fork stalling and collapse in both and *ino80* (Papamichos-Chronakis and Peterson, 2008; Shimada et al., 2008) or *arp*8 null strain (Shimada et al., 2008). Subsequently, Ino80 was shown to be recruited to the replication fork and required for fork progression under stress conditions (Papamichos-Chronakis and Peterson, 2008). In depth analysis of Ino80 recruitment at replication forks has brought up differences in the data, as it has been suggested to preferentially bind early firing origins (Shimada et al., 2006), and late origins (Vincent et al., 2008), as well as genome wide, at around 45% of the total autonomously replicating sequences (ARS) (Falbo et al., 2009). The data clearly demonstrates the presence of Ino80 at replication forks, however, the function of the complex is still unclear.

In contrast to previous analysis, where Rad53 kinase activation was said to be reduced in *arp8* or *nhp10* deletions (Van Attikum et al., 2007), studies on replication have not found results in agreement for the deletion of *INO80*. Using 2D gel analysis to examine replication fork progression, unlike a *rad53* deletion, *ino80* null cells were found to be proficient for replication fork maintenance and stabilisation at a single ARS (Falbo et al., 2009).

Multiple studies have suggested Ino80 might be involved in the DNA damage tolerance pathway (Falbo et al. 2009; Czaja et al. 2010; Niimi et al. 2012; Kato et al. 2012). This pathway, mediated by Rad18 and Rad6, is initiated during DNA replication when damage to the leading strand causes replication to stall and the introduction of a DSB upon replication fork collapse (Ulrich, 2007). Like *ino80*, mutants of this pathway are sensitive to MMS (Ulrich, 2007), and phosphorylated H2A was only found to accumulate in *ino80* null cells once they had progressed through S-phase.

Furthermore, the length of replicated DNA tracts in *arp8* mutants released from S-phase into MMS are significantly shorter than in wildtype (Falbo et al., 2009). In *S. cerevisiae*, the primary pathway to resolve MMS lesions during replication is through ubiquitination of proliferating cell nuclear antigen (PCNA), a sliding clamp protein complex that enables stalled replicative polymerase to be replaced with a translesion synthesis (TLS) polymerase (Lehmann et al., 2007). Cells lacking *ino80* or *arp8* have reduced levels of PCNA ubiqiutination in response to MMS (Falbo et al., 2009; Niimi et al., 2012), and INO80 promotion of PCNA ubiqiutination is dependent on Ino80 ATPase activity, as similar defects were observed in an ATPase mutant (Falbo et al., 2009). PCNA ubiqiutination is known

to be dependent on Rad18 (Hoege et al., 2002), and recruitment of Rad18 to ARSs is reduced in *ino80* null cells.

From the replication data, it is clear that Ino80 plays an important role in the maintenance of replication forks, especially when inhibited by replication stress induced DNA damaging agents. These findings could even account for some of DNA damage sensitivities previously observed in *S. cerevisiae*, as asynchronous *ino80* mutant cells have shown to be effective at repair of MMS, UV and IR induced regions (Czaja et al. 2010). Similarly, in *H. sapiens*, Ino80 is found to be important for the DNA damage tolerance pathway and PCNA ubiqiutination, with Ino80 also recruiting Rad18 to sites of DNA damage (Kato et al., 2012). Furthermore, Ino80 has been found to be phosphorlayted at its C-terminus, a feature of mammalian INO80 complex was proposed to be analogous to the phosphorylation of Ies4 by Mec1 and Tel1 (Morrison et al., 2007), which serves to regulate its functions in the DNA damage tolerance pathway, specifically PCNA ubiqiutination (Kato et al., 2012).

Additional data from *H. sapiens* supports the role of Ino80 at replication forks (Lee et al., 2014; Vassileva et al., 2014), in addition to suggesting the BRCA-1 associated protein (BAP1) as a mechanism of Ino80 recruitment and maintenance at replication forks (Lee et al., 2014). BAP1 is a de-ubiquitinating enzyme (Jensen et al., 1998) that is often mutated in certain cancers (Wood et al., 2007). This study demonstrated that BAP1 interacts with Ino80 through its HSA domain, an interaction that retains Ino80 at forks by de-ubiquitination, which prevents protein degradation by extending Ino80 protein half life (Lee et al., 2014). Subsequently, they observed Ino80 protein expression to be down regulated in BAP1-deficent cancer cell lines (Lee et al., 2014), proposing a mechanism by which

the INO80 chromatin remodeller may contribute to human cancers, similar to the BAF and PBAF complexes. Furthermore, this study highlighted the importance of Ino80 mediated replication in mouse development, a novel role for Ino80, which had previously been implicated only in the transcription of genes in the pluripotency network for blastocyst development (Wang et al., 2014).

1.2.4.1.5 Chromosome segregation

Additional pathways can contribute to human cancers, one avenue is through aneuploidy or polyploidy as a result of chromosome misegregation events (discussed later in more detail). Indeed, INO80 in *S. cerevisiae* has been linked to the maintenance of sister chromatid cohesion through its Arp8 subunit (Ogiwara et al., 2007). In this study, *arp8* null cells were shown to have separated sister chromatids, indicative of defects in sister chromatid cohesion. Subsequently, Ctf18, a protein that loads and unloads PCNA *in vitro*, was found to be decreased at replication forks in *arp8* null cells (Ogiwara et al., 2007). Both PCNA and Ctf18 are required for cohesion establishment at replication forks (Lengronne et al., 2006; Moldovan et al., 2006).

Further influences of INO80 on chromosome stability, which impact on the fidelity of chromosome segregation, have been highlighted by the role of Ino80 in the maintenance of centromere structure (Chambers et al. 2012). The discovery of this role resulted from the observation that either *ino80* or *ies6* null cells quickly become polyploid through a whole genome duplication event (Chambers et al. 2012). Further analysis revealed both *INO80* and *IES6* were important for the

maintenance of a centromeric plasmid (Chambers et al. 2012). In addition, their deletion caused irregular DAPI staining, indicative of errors in chromosome segregation, in addition to hypersensitivity to the microtubule destabilising drug benomyl (Chambers et al. 2012). Interestingly, both *ies6* and *ino80* null cells had increased levels of H2A.Z at the centromere, which made their DNA susceptible to MNase digestion (Chambers et al. 2012). This indicates that relaxed chromatin structure, as a result of H2A.Z misregulation in cells lacking Ino80 or Ies6, could be contributing to chromosome segregation problems.

In *H. sapiens*, INO80 has been linked to aneuploidy through the loss of the mammalian specific subunit YY1 (Wu et al., 2007; Table 1). On study demonstrated that YY1 knockdown results in a polyploid phenotype, in addition to structural chromosomal aberrations (Wu et al., 2007). Further studies have suggested Ino80 may interact with the microtubule and the E-hook domain of α-Tubulin (Park et al., 2011). Suggesting an interaction between Ino80 and spindle microtubules (Hur et al., 2010), and a requirement for Ino80 in microtubule assembly during mitosis, due to total loss of microtubule formation in metaphase Ino80 knockdown cells (Hur et al., 2010). However, these conclusions require further investigation due to the complexity of factors determining microtubule formation. Ino80 knockdown cells, exhibit problems with chromosome segregation. These included an inability to establish condensed chromosomes during prophase, in addition to segregation errors, resulting in the appearance of micronuclei and anaphase bridges (Hur et al., 2010).

Data from *S. cerevisiae* and *H. sapiens* demonstrates that the INO80 complex is important in conducting proper and controlled segregation of chromosomes, which, as previously discussed, is vital for maintaining genomic stability and for

the prevention of cancer. At least for chromosome segregation, it is clear that the Ies6 subunit of the INO80 complex completely mimics the functions of the catalytic component, Ino80.

1.2.4.1.6 Ies6

The Ies6 protein in *S. cerevisiae* and is highly conserved across multiple organisms (Figure 5 A), most notably at its C-terminus, which contains sequence homology to a domain defined as 'YL1_C' (Figure 5). The YL1_C domain was first identified from a study of the human protein YL-1 (Horikawa et al., 1995), where the N-terminal or central region was termed 'YL1 nuclear' and the C-terminal portion is defined as 'YL1_C' (Figure 5 C). Though the function of both these domains has not been rigorously determined, the data available suggests they have the capacity to bind DNA and are common to transcription factors (Horikawa et al., 1995). Indeed, previous work has shown Ies6 has the capacity to bind dsDNA and have preference for Y-fork structures (Fenwick, 2010). More recent work supports an Ies6 DNA binding function in a complex with Arp5 (Tosi et al., 2013), as well as nucleosome binding in complex with Arp5 (Chen et al., 2013). Previous work from Fenwick 2010 demonstrated that the presence of four mutataions within the YL1_C domain (Figure 5 B and C) were sufficient to disrupt DNA binding, which would indicate this domain is structurally significant to Ies6 function.

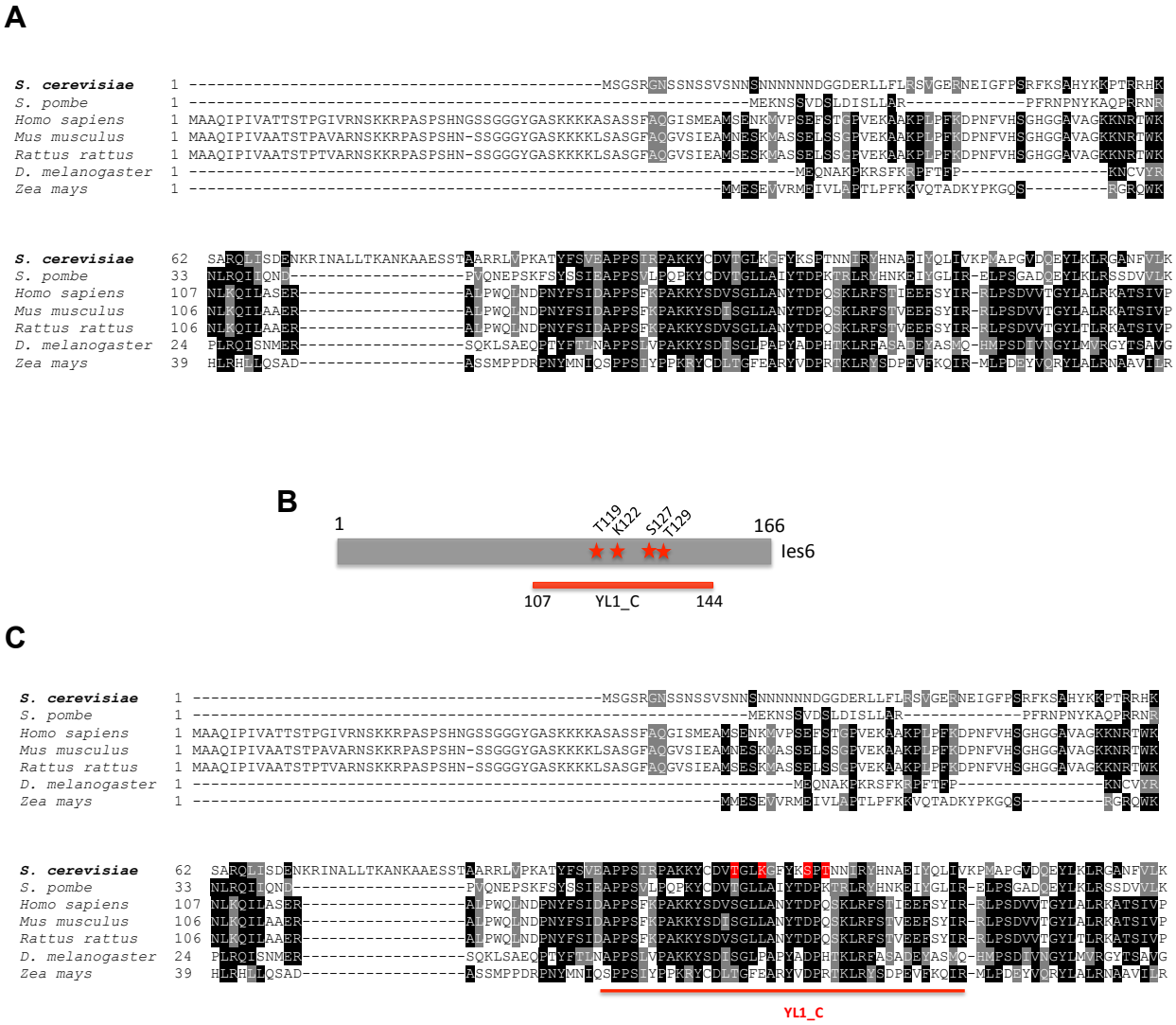

Figure 5: Ies6 is highly conserved across different organisms and contains a putitive DNA binding domain known as YL1_C

A. Multiple protein alignment of the Ies6 protein from different organisms. Produced using Clustal W and BoxShade. Consensus residues are highlighted in black and similar in grey.

B. Schematic depicting the mutagenesis of Ies6 residues previously conducted in Fenwick 2010.

C. Multiple protein alignment depicting the location of mutations created by Fenwick 2010

In addition YL1_C domain homology, providing a link to a DNA interaction interface, cross linking studies have shown interaction of Ies6 with Arp5 and Rvb2 (Tosi et al., 2013). From the method of cross linking used and the amino acid range, potential Arp5 and Rvb2 interaction 'domains' can be inferred. However, the lack of definitive structural information relating to Ies6 makes inferring the function of its putative subunit interacting 'domains' difficult.

Similarities between the phenotypes of *ies6* and *ino80* null cells in *S. cerevisiae* are striking; both are sensitive to HU, MMS and benomyl, with defects in growth, cell viability, ploidy maintenance, in addition to increased H2A.Z at centromeres, leading to altered centromere structure (Chambers et al. 2012). Furthermore, a recent study has implicated Ies6 as being critical to basic INO80 chromatin remodelling functions, such as nucleosome sliding and H2A.Z dimer exchange (Watanabe et al., 2015), however, in contrast to reports from *H. sapiens* (Chen et al., 2013) Ies6 was not important for nucleosome binding (Watanabe et al., 2015). However, still relatively little is known about Ies6 in relation to other functions of INO80, such as DNA repair, replication, or the mechanisms underlying the influence of Ies6 on H2A.Z incorporation at centromeres.

1.3 The process of faithful chromosome segregation

Chromosome segregation is a vital part of mitosis (M-phase of the cell cycle) which allows cells to generate daughter cells containing an equal number of chromosomes to the parent cell. The eukaryotic cell cycle consists of two main phases: interphase, and mitosis (M-phase). Interphase is composed of three stages: an initial growth phase (G1), which is interrupted by a period of DNA replication (S-phase), and followed by a final growth phase (G2) (Verdaasdonk and Bloom, 2011).

Mitosis is initiated following G2 and has a total of five steps: prophase, when the chromosomes are condensed, prometaphase, where microtubules search for chromosome kinetochores, metaphase, when chromosomes become bi-orientated, anaphase, when sisters separate to opposite poles, and telophase, where chromosomes decondense (Verdaasdonk and Bloom, 2011). Each step is critical for the production of viable daughter cells. However, metaphase and anaphase contain critical steps for achieving faithful chromosome segregation (Verdaasdonk and Bloom, 2011).

During metaphase, microtubules extend from the centrosomes at each pole of the cell. The microtubules attach to the kinetochores within the centromere of each sister chromatid and force exerted from the centrosomes pulls on the microtubules. This force causes the sister chromatids to line up along the metaphase plate. Once aligned, the microtubules pull the chromatids towards opposite poles of the cell. Here, cohesion proteins encase the sisters and create an opposing force. This tension signals that two identical copies of one chromosome

are to be separated at different poles. Upon the degradation of cohesin during anaphase, chromosomes are pulled towards the centrosomes by their centromeres. Once cohesion is removed and the replicated chromosomes are on opposite poles of the cell, the final stage, telophase, involves the formation of a nuclear membrane around each set of newly replicated chromosomes, followed by cytokinesis to produce two daughter cells (Verdaasdonk and Bloom, 2011)..

1.3.1 The structure and role of the centromere

The centromere is a complex chromatin structure, which contains characteristic PTMs, histone variants and associated chromatin proteins. Chromosome segregation is directed by the centromere, as it allows for the formation of the kinetochore to which the microtubules attach. Therefore, it is vital that chromosomes enter prophase with only a single centromere on each chromosome to prevent improper segregation.

The centromeric region of eukaryotic chromosomes is partly defined by specific DNA repeat sequences. In *S. cerevisiae* there are three conserved centromeric repeat sequences known as centromere DNA elements: CDEI, CDEII, and CDEIII. Their sequence lengths vary: CDEI is 8bp in length, CDEII is 26bp, and CDEIII can be between 78-86bp (Fitzgerald-Hayes et al., 1982) when combined, the sequence is sufficient to confer mitotic stability of plasmid DNA (Clarke and Carbon, 1980, 1983; Hieter et al., 1985).

In contrast, centromere sequences from higher eukaryotes, including *H. sapiens*, are governed in part by vast satellite repeats (Schueler et al., 2001).

Although, their DNA structure varies considerably, the proteins associated with all eukaryotic centromeric chromatin are highly conserved, and DNA sequences serve to recruit them. Namely, the histone H3 variant, CENPA (Cse4 in *S. cerevisiae*), which is unique to the centromere (Sullivan et al., 1994) and incorporated into the nucleosomes of centrometic chromatin (Stoler et al., 1995). The CENPA histone variant is essential for maintaining kinetochore structure (Van Hooser et al., 2001; Howman et al., 2000), making it vital for mitosis progression and proper chromosome segregation. In *S. cerevisiae,* CENPA is known to interact with suppressor of chromosome misegregation 3 (Smc3) via its centromere targeting domain (CATID), an interaction that enables Smc3 to act as a chaperone for CENPA (Zhou et al., 2011) by recruiting to its target nucleosomes.

It has been suggested that the H2A.Z histone variant regulates the formation of neocentromeres (NC), centromeres that occur ectopically and do not require DNA sequence elements, in *S. pombe* (Ogiyama et al., 2013). This study demonstrated that H2A.Z expression in ectopic neocentromeres served to inhibit Smc3 association, subsequently reducing CENPA nucleosome incorporation. Upon the removal of H2A.Z, Smc3 and CENPA association was restored, allowing for centromere stabilisation (Ogiyama et al., 2013).

Furthermore, H2A.Z has been found in the centric and pericentric chromatin of both *H. sapiens* and *Mus musculus* (Greaves et al., 2007). Within the centric chromatin, H2A.Z and dimethylated K4 H3 are arranged between subdomains on CENPA. This arrangement of H2A.Z is thought to organise the centromere structure (Greaves et al., 2007). In addition, H2A.Z loss in *S. pombe*, through the removal of Msc1 or Swr1 driven incorporation, leads to a loss of centromere silencing and chromosome segregation defects (Hou et al., 2010).

These findings suggest that H2A.Z may be important for determining chromatin architecture by CENPA exclusion resulting in defined and identifiable centromeric regions.

1.3.2 The importance of stable Kinetochore-Microtubule interactions

1.3.2.1 Kinetochore assembly

The kinetochore in *S. cerevisiae* is a multi-protein complex that assembles at the centromere to form a contact for microtubule attachment. The CBF3 complex (Ndc10, Ctf13, Cep3, Skp1) (Connelly and Hieter, 1996; Goh and Kilmartin, 1986; Lechner and Carbon, 1991), a centromere binding factor, interacts directly with centrometic DNA at the *CDEIII* element (Lechner and Carbon, 1991; Ng and Carbon, 1987). Three complexes, Ndc80 (Ndc80, Nuf2, Spc24, Spc25), COMA (Ctf19-Okp1-Mcm21-Ame1), and MIND (Mtw1p including Nnf1-Nsl1-Dsn1) bridge the gap between the CBF3 and the microtubule interacting complex DASH (De Wulf et al., 2003). The DASH complex, in conjunction with Dam1 and Ask1, then forms a ring around a single microtubule to establish the kinetochore-microtubule interaction (Miranda et al., 2005). Deletion of many of these proteins causes kinetochore mislocalisation or detachment from the microtubule. For example, *ndc80-1* mutants, where Ndc80 has been inactivated, show 'scattered' kinetochore foci, typical of microtubule detachment (De Wulf et al., 2003). Kinetochore detachments from the microtubule can induce, erroneous, merotelic kinetochore

attachments. This arises when microtubules from both poles are connected with the kinetochore of only one sister, which leads to chromosome segregation defects.

1.3.2.2 Erroneous kinetochore attachments

Attachments that achieve effective chromosome segregation are described as amphitelic, where the microtubules attach to opposite spindle poles during mitosis in a bi-polar arrangement (London and Biggins, 2014). However, there are various forms of erroneous attachment, including: monotelic, syntelic, and merotelic (London and Biggins, 2014). Merotelic attachments occur frequently during the early stages of mitosis and are a major driver of aneuploidy (Cimini et al., 2001, 2003).

Monotelic kineoteochore attachments, where the microtubules from a single pole attach to the kinetochore of only one sister, frequently occur during prometaphase due to the stochastic nature of the microtubule and spindle pole interaction (Alexander and Rieder, 1991). However, once the second sister kinetochore is located, bi-polar attachment is achieved, and chromosome segregation is unaffected. Syntelic attachments, where microtubules from a single spindle pole are attached to the kinetochores of both sisters (London and Biggins, 2014), and merotelic attachments, where the microtubules from both poles are connected with the kinetochore of one sister (London and Biggins, 2014) are the most detrimental to the dividing cell and are a leading cause of aneuploidy in *H. sapiens*. This leads to cancer predisposition and birth defects (Chi and Jeang, 2007; Cimini et al., 2001; Hassold and Hunt, 2001) (discussed later).

In order to prevent the misegregation of chromosomes, which can arise from undetected monotelic, syntelic, or merotelic kineotichore attachments, the cell has developed a network of proteins to monitor spindle pole tension, known as the spindle assembly checkpoint (SAC). This checkpoint detects erroneous microtubule attachments and halts the cell cycle until amphitelic attachments are achieved.

1.3.2.3 The spindle assembly checkpoint

Non-amphitelic kinetochore microtubule interactions are excluded from anaphase by the spindle assembly checkpoint (SAC), which signals a delay in anaphase onset (Chen et al., 1996; Gillett et al., 2004). The checkpoint in *S. cerevisiae* is composed of Mad1, Mad2, Mad3, Bub1, and Bub3, which are systematically recruited to the kinetochores (Hoyt et al., 1991; Li and Murray, 1991). In addition to Mps1, which phosphorylates Mad1 upon SAC activation (Hardwick et al., 1996), activated SAC proteins inhibit Cdc20 (Hwang et al., 1998), which activates the anaphase promoting complex (APC) (Visintin et al., 1997). Activation of the APC regulates the expression of the anaphase inhibitor Pds1 (Cohen-Fix et al., 1996), thus regulating the timing of anaphase entry.

SAC activation is induced upon the loss of tensional force between the sister chromatids (Stern and Murray, 2001) or in the presence of unattached kinetochores (Spencer and Hieter, 1992; Wells, 1996). This enables the cell to easily identify both monoteylic and syntelic kinetochore attachments, however, metrotelic attachments are significantly more difficult to detect, as neither

amphitelic or merotelic attachments signal to the cell that there is an unattached kineotochore and can produce tension across both sisters. The Ipl1 kinase (Aurora B in *H.* sapiens) is known to prevent kinetochores with merotelic attachments from entering anaphase. This is achieved by destabilising low tension attachments to generate un-attached kinetochores, thus initiating SAC activation (Pinsky et al., 2006; Tanaka et al., 2002).

Using these mechanisms the SAC can effectively monitor the potential risk of chromosomal misegregation through kinetochore defects. The creation of tensional force at the centromere, through kinetochore attachment, indicates chromosome polarity. However, additional mechanisms exist to create tensional force along the length of each sister chromatid to complement tension created at the centromere, and ensure sisters are segregated to opposite poles.

1.3.3 The SMC protein family increase chromosomal tension

Successful chromosome segregation during mitosis involves the disassembly of chromosomes in a controlled and concise manner. In part, this is achieved by structural maintenance of chromosomes (SMC) proteins. Proteins in the SMC family make up the core components of large protein complexes, namely condensin, cohesin and the SMC5/6 complex (Wood et al., 2010).

All SMC proteins are characterised by specific domains, which give them a distinctive triangular shape. This includes a pair of highly conserved Walker motifs, separated by two large coiled coils, with a central hinge domain. The domains are arranged so that the N-terminal Walker A, and C-terminal Walker B

motifs assemble side by side to form an ATP nucleotide binding domain (Löwe et al., 2001), a region known as the head domain. The coiled coils then run antiparallel, with the hinge domain at the proteins apex (Löwe et al., 2001). In both the condensin and cohesin complexes, two different SMC monomers are joined at their hinge domain to form a heterodimer. Additional non-SMC subunits within specific complexes assemble on the head domains. This arrangement of subunits gives complexes in the SMC family their distinct tripartite structure and a triangular shape.

1.3.3.1 The role of condensin

Condensin is a protein complex in the SMC family that is required for chromosome compaction throughout the cell cycle. In *H. sapiens* there are two distinct forms of condensin known as condensin I and condensin II. The two forms are defined by their non-SMC protein composition. Condensin II promotes compaction of chromosomes upon entry into mitosis, while condensin I assembles chromosomes in metaphase after the degradation of the nuclear envelope (Hirano, 2005). In all organisms, the condensin complex contains a heterodimer of SMC2 and SMC4, in addition to the non-SMC proteins, which are thought to regulate condensin (Kimura et al., 1998). In *S. cerevisiae*, where only condensin I exists, these proteins Ycs4, Ycg1, and Brn1 have direct homologues in *H. sapiens* (CAP-D2, CAP-G and CAP-H) (Hirano, 2002). Crystal structures obtained of vertebrate condensin demonstrate that CAP-H binds directly to the head domains of SMC2/SMC4, which recruits CAP-D2 and CAP-G through their HEAT domains (Onn et al., 2007). In *S.*

cerevisiae, all the non-SMC proteins of condensin are phosphorylated by the Cdc5 kinase during mitosis. This phosphorylation event is sufficient to activate the complexes DNA supercoiling function (St-Pierre et al., 2009).

In *S. cerevisiae*, mutation in either Smc2 or Smc4 causes pronounced chromosome condensation and segregation defects (Freeman et al., 2000; Strunnikov et al., 1995). The same defects are observed when mutating any of the non-SMC subunits, Ycs4, Ycg1, or Brn1 (Lavoie et al., 2004; Ouspenski et al., 2000; Poirier et al., 2002). This demonstrates the importance of maintaining an intact condensin complex to the cell during mitosis. However, additional data from *S. cerevisiae* has highlighted a requirement for condensin during interphase for the organisation of rDNA genes. Consequently, the mutation or deletion of any of the condensin subunits allows uncontrolled recombination of rDNA clusters, which become dispersed throughout the genome (Ambrosio et al., 2008). These results highlight the importance of chromosome condensation in preventing permissive recombination, in addition to promoting faithful chromosome segregation.

1.3.3.2 The role of cohesin

In addition to the importance of compaction, a second SMC complex, known as cohesin, is required to keep sister chromatids cohered during mitotic DNA replication. The mitotic cohesin complex in *S. cerevisiae* is composed of an Smc1 and Smc3 heterodimer, in addition to the non-SMC proteins, Scc3 and Scc1 (SA1/SA2 and RAD21 in *H. sapiens*) (Hirano, 2002). In meiosis, the Scc1 subunit is replaced by a meiosis specific kleisin, also known as Rec8 (Uhlmann et al., 1999).

Both mitotic and meiotic cohesin assemble into the triangular shape typical of SMC family members. The Scc3 subunit binds to Scc1, which bridges the head domains of Smc1 and Smc3, this makes contact with the Smc1 C-terminus and Smc3 N-terminus (Haering et al., 2002). Mutation in any of the cohesin subunits causes dramatic chromosome separation defects (Guacci et al., 1997; Michaelis et al., 1997).

Many different models exist to explain how cohesin may hold chromosomes together. Due to the ring structure of cohesin, the "embrace" model proposes that sister chromatids are topologically embraced by cohesin, which is assembled around the sisters through the cleavage of Scc1 by the protease Esp1 (separase) (Haering et al., 2002). Though, alternative models have since proposed that cohesin may oligomerise whilst bound to the DNA of each sister, thus holding them together. It has been proposed that cohesin complexes may join at the coiled coils in the "snap" model (Milutinovich and Koshland, 2003), or at the hinge domains in the "bracelet" model (Huang et al., 2005). Despite the mystery surrounding its mechanism of action, it is known that cohesin is bound to the sisters in prophase. This attachment provides suitable resistance during metaphase, when the chromatids are pulled towards the spindle poles by their kinetochores. The opposing force indicates the presence of a replicated chromosome pair that is to be divided between the resulting daughter cells. During the transition into anaphase, cohesin is cleaved by Esp1 to allow the sisters to be pulled to opposite poles (Ciosk et al., 1998). In the absence of precise, directed loading and release of mitotic cohesin, errors can arise during chromosome segregation that lead to genomic instability and disease.

1.3.4 The importance of efficient chromosome segregation

The roles of SMC protein complexes, condensin and cohesin, are critical to maintaining chromosomal stability. *In vivo*, mammalian cells lacking cohesin display chromosome misegregation errors, which include, lagging chromosomes, the failure to segregate their entire genome or cells containing multiple nuclei (Hauf et al., 2001). Defects in chromosome segregation that lead to chromosomal rearrangements and misegregation errors can cause or contribute to permanent states of chromosomal rearrangement. These include: changes in cellular ploidy, where whole chromosome number increases, or aneuploidy, when there is the gain or loss of one or more chromosomes. These alterations to chromosome number are common features of cancer genomes (Burrell et al., 2013). Ploidy and aneuploidy occur when subunits of the INO80 or pBAF chromatin remodelling complexes are removed (Chambers et al. 2012; Brownlee et al. 2014). This suggests the existence of wider influences on chromosome structure than condensin or cohesin presence alone, of which chromatin remodellers may play a significant role. However, segregation errors can occur through alternative mechanisms, including the misregulation of the centromere, kinetochores, microtubules or spindle poles. If these complexes are improperly assembled it can lead to erroneous kinetochore attachments.

1.3.4.1 Polyploidy

Alterations in ploidy cause reduced fitness and genome instability in cells due to the inefficiency of mitosis, for example, ploidy changes in *S. cerevisiae* cause a dependency for Bik1, a protein involved in kinetochore-microtubule attachment, which is nonessential in parental haploids (Lin et al., 2001). In the short term such changes in fitness are deleterious, however, they can influence an evolutionary advantage over their parental haploids when acquiring subsequent mutations. The period of instability following a genome duplication event is thought to increase the frequency of beneficial mutations, which overall can cause accelerated evolution in yeast (Selmecki et al., 2015).

In *H. sapiens*, whole genome duplication events, giving rise to polyploid or tetraploid cells, are characteristic of cancer (Carter et al., 2012; Zack et al., 2013). Increases in polidy influence cancer evolution, which leads to tumour heterogeneity (Burrell et al., 2013). Variations in gene expression within tumours, and between patients hinder the selection of targeted therapies.

1.3.4.2 Aneuploidy

Aneuploidy cells arise from misegregation events that cause the gain or loss of a chromosome. Similarly to irregularities in ploidy, the loss or gain of chromosomes is indicative of cancer in *H. sapiens* (Gordon et al., 2012). These specific alterations typically reoccur with high frequency across a single cancer type (Gordon et al., 2012). The specific effects of aneuploidy varies depending on the organism and the

chromosome affected, however, haploid *S. cerevisiae* strains containing an increase of one chromosome are slow to proliferate due to a delayed G1 phase (Torres et al., 2007). In developing mouse embryos, trisomy for chromosomes 1, 13 or 16 is lethal and causes developmental defects such a stunted growth (Williams et al., 2008). Similarly in *H. sapiens*, aneuploidy is a major cause of miscarriage, with trisomy of chromosome 16 occurring at a high frequency (Nagaoka et al., 2012). In addition, trisomy can give rise to birth defects, most notably Down syndrome, caused by trisomy of chromosome 21 (Patterson, 2009).

Given the importance of maintaining chromosome number during chromosome segregation a multitude of factors contribute to the successful division of chromosomes, including histone PTM, and chromatin remodellers.

1.4 Replication fidelity underpins basic cellular processes

Replication of DNA is a highly conserved cellular process, its basic function is replicate the parental chromosomes and pass on their genetic material to the daughter cells during mitosis or meiosis. In addition, replication machinery is called upon during multiple DNA repair pathways. It is highly orchestrated to ensure that replication origins are fired at the correct points during the cell cycle, and constantly monitored by both replication and S-phase checkpoints. The highly regulated nature of the replication process seeks to prevent, or at the very least minimise, errors in replication. Losing this tight regulation can contribute to cancer progression in *H. sapiens*.

1.4.1 Replicative barriers cause replication stress and genomic instability

Barriers that inhibit the progression of the replication fork can cause replication stress. If not removed, these barriers block replication fork progression and can induce replication fork collapse. This has a huge impact on the fidelity of DNA synthesis and can potentially induce errors that may lead to further genomic instability. Such barriers can occur completely naturally, for example, lesions may arise from DNA hydrolysis or metabolism (Lindahl, 1993), unusual DNA structures: such as triple H-DNA, left-handed Z-DNA, and slipped-strand S-DNA regions (Mirkin and Mirkin, 2007), collisions between replisomes and DNA bound

proteins or transcription machinery (Azvolinsky et al., 2009) can all contribute to replication stress.

The production of replication stress is a major cause of genomic instability (Aguilera and Gómez-González, 2008), and data would strongly suggest it influences cancer progression (Gaillard et al., 2015; Lecona and Fernández-Capetillo, 2014). For example, when replication stress is induced by aphidicolin, a compound that inhibits DNA polymerase function (Krokan et al., 1981), micro-deletion mutations occur, which highly resemble mutations consistently found in human tumours (Durkin et al., 2008). Furthermore, when mice are exposed to hydroxyurea (HU), mutated progenitor cells outcompete those that are healthy within the population, causing leukaemogeneis (Bilousova et al., 2005). Given the consequences of replication stress, eukaryotes have developed a surveillance system in the form of S-phase and replication checkpoints, which monitor replication fidelity and activate the DNA damage response pathway (DDR) when required.

1.4.2 Preventing replication stress

Mechanisms that oversee replication in eukaryotes are highly conserved pathways. In *S.* cerevisiae, the S-phase specific checkpoint is composed of the mediator of replication protein 1 (Mrc1), topoisomerase 1-associated factor 1 (Tof1) and chromosome segregation in meiosis protein 3 (Csm3) (Uzunova et al., 2014). Upon replication stress during S-phase, Mrc1 is phosphorylated by Mec1 (Alcasabas et al., 2001), and is also found in association with Tof1 and Csm3 at the replication

fork during unperturbed replication (Bando et al., 2009; Katou et al., 2003). The deletions of either *mrc1*, *tof1* or *csm3* are synthetically lethal with mutants that destabilise the Polα/primase (Nedelcheva et al., 2005), suggesting the S-phase checkpoint proteins function specifically to maintain replication fork progression. The activation of the S-phase checkpoint in *S. cerevisiae* is known to influence downstream factors that impact on replication. Including the timing of late origin firing (Santocanale and Diffley, 1998; Shirahige et al., 1998), which is also true in higher eukaryotes (Feijoo et al., 2001; Merrick et al., 2004), pausing normal replication progression.

Using both genetic and biochemical methods, the role of the Ies6 subunit of INO80 will be investigated. Considering currently published findings, the functionality of the Ies6 protein will be thoroughly examined to identify or confirm important domains. Subsequent mutation of these domains will allow insight into the potential roles of Ies6 within the INO80 complex. Key functions of Ies6 and Ino80 will be scrutinised, including DNA damage, the maintenance of ploidy and replication stress recovery.

This thesis aims to investigate the role of the Ies6 subunit of the INO80 complex in chromosome segregation, DNA replication and DNA repair. The Ies6 protein will be characterised for its DNA binding capacity and contribution of conserved residues to this function will be examined.

2 Materials and methods

2.1 Cloning and DNA manipulation

2.1.1 Polymerase chain reaction

Polymerase chain reactions were typically conducted using purified yeast genomic DNA (100-200 ng/reaction) or plasmid (10 ng/reaction) as a template. A typical reaction would contain 100 μM dNTPS (Fermentas), 1x Thermo Pol. Buffer (New England Biolabs), 500nM oligonucleotide primers (Sigma), 0.5 μl/50 μl of Pfu and 0.25 μl/50 μl of Taq polymerases (purified in house).

Table 2: Primers used in this study for cloning and mutagenesis.

Number	Name	Sequence (5'-3')	Application
1	F-ies6(K61A)	CAAGAAGACACGCATCAGCGAGGC	Primers to mutate residues of *IES6* in a pre-existing flag tagged pRS416 (flanked by NotI sites carried over from pGEM T-Easy).
2	R-ies6(K61A)	GCCTCGCTGATGCGTGTCTTCTTG	
3	F-ies6(R64A)	ACAAATCAGCGGCGCAGTTGATCT	
4	R-ies6(R64A)	AGATCAACTGCGCCGCTGATTTGT	
5	F-ies6(Q65A)	AATCAGCGAGGGCGTTGATCTCGG	
6	R-ies6(Q65A)	CCGAGATCAACGCCCTCGCTGATT	
7	F-ies6(R73A)	ACGAAAACAAGGCGATCAACGCCT	
8	R-ies6(R73A)	AGGCGTTGATCGCCTTGTTTTCGT	
9	F-ies6(S102A)	CGACGTACTTTGCCGTGGAAGCGC	
10	R-ies6(S102A)	GCGCTTCCACGGCAAAGTACGTCG	
11	F-ies6-S108A	GAAGCGCCACCGGCTATCAGGCCTG	
12	R-ies6-S108A	CAGGCCTGATAGCCGGTGGCGCTTC	
13	F-ies6(K113A)	TCAGGCCTGCCGCGAAGTACTGC	
14	R-ies6(K113A)	GCAGTACTTCGCGGCAGGCCTGA	

15	F-ies6(K114A)	GCCTGCCAAGGCGTACTGCGATG	
16	R-ies6(K114A)	CATCGCAGTACGCCTTGGCAGGC	
17	F-ies6-D117A	AGAAGTACTGCGCTGTTACTGGGTT	
18	R-ies6-D117A	AACCCAGTAACAGCGCAGTACTTCT	
19	F-ies6(Y115A)	TGCCAAGAAGGCCTGCGATGTT	
20	R-ies6(Y115A)	AACATCGCAGGCCTTCTTGGCA	
21	F-ies6-R133A	TACGAACAACATTGCGTATCACAAC GCA	
22	R-ies6-R133A	TGCGTTGTGATACGCAATGTTGTTC GTA	
23	F-ies6-E138A	ATCACAACGCAGCAATCTATCAGTT	
24	R-ies6-E138A	AACTGATAGATTGCTGCGTTGTGAT	
25	F-ies6(Y139A)	CAACATTCGGGCTCACAACGCA	
26	R-ies6(Y139A)	TGCGTTGTGAGCCCGAATGTTG	
27	F-ies6(Y145A)	CGCAGAAATCGCTCAGTTAATC	
28	R-ies6(Y145A)	GATTAACTGAGCGATTTCTGCG	
29	F-ies6-R159A	GTACTTAAAATTGGCAGGGGCCAAC TTC	
30	R-ies6-R159A	GAAGTTGGCCCCTGCCAATTTTAAG TAC	
31	SpeI-PIH1	ATGCTAGTATATATAGTGGCGT	Primers to amplify wildtype *PIH1* with SpeI and XbaI ends for integration into pRS415.
32	PIH1-XbaI	GAACAAATCTAGATTAACCG	
33	F-K58E	AAGATGAAGAAGTAGGGCGCTGAG	Primers to mutate conserved Lysines K58 and K106 within pRS416-*PIH1*.
34	R-K58E	GTCAGCGCCCTACTTCTTCATCTT	
35	F-K106E	CAGCAGGAGGACTAGTCCTCCTGC	
36	R-K106E	CGTATTCCGGCTAGTCCTCCTGCTG	
37	F-PIH1 STOP 167aa	AAGATGAAGAAGTAGGGCGCTGAG C	Primers to introduce a STOP condon at the 167th aa of *PIH1*.
38	R-PIH1 STOP 167aa	GCTCAGCGCCCTACTTCTTCATCTT	
39	F-RAD50check	TTTGAGTACTCGATAGAATTA	Primers to check *rad50* KO integration in the genome.
40	R-RAD50check	TCCACCGATACATCAATG	
41	F-CIN8delta	TATAAAAGCGCAAAAAATACAACAA GAAAGAATTTGTTTGcGGATCCCCG GGTTAATTAA	Primers to KO *cin8* using the Pringle method, and check for integration within the genome.
42	R-CIN8delta	CACTAGTTTGAATATATATTCGACTG AAAGGCAATATCAAgAATTCGAGCTC GTTTAAAC	
43	F-CIN8check	CATCTAAAGACTTCCTTTGTGACC	
44	R-CIN8check	TCTGTGAAAATTTGATTTAGGTTC	
45	F-SA3delta	TTCCTTCTTCATTAATTAGTCTCCGT ATAATTTGCAGATAcGGATCCCCGG GTTAATTAA	Primers to KO *sas3* using the

46	R-SAS3delta	TACATGTATATGCTTATATCCAATAT ATACCCATCGCCGCgAATTCGAGCT CGTTTAAAC	Pringle method, and check for integration within the genome.
47	F-SAS3check	GAAAATAGCACAGAAACAAAGCAT	
48	R-SAS3check	AAATTAATCGCACCCACAC	
49	Cy3-001	ACCCAGTTGACACCGTTTCTACAGG ATCGTTACATTAGCAGATACTGCAA	5' Cy-3 labelled oligonucleotide Complimentary sequence, annealed to create a dsDNA fragment.
50	gelshift-02	TGGGTCAACTGTGGCAAAGATGTCC TAGCAATGTAATCGTCTATGACGTT	

2.1.2 Site directed mutagenesis

Site directed mutagenesis was achieved by conducting two sequential PCR reactions from a wildtype template. Nested mutant primers, and primers flanking the gene ORF, were used in the first reaction to produce N-terminal and C-terminal gene fragments. These fragments were used as a template in the second reaction, where only the flanking primers were used. Resulting amplicons were full-length mutant alleles of the desired gene and used for cloning.

2.1.3 Restriction enzyme digestion

Vectors and amplified PCR products were cut the using the desired enzyme before being purified by agarose gel electrophoresis and ligated. Digestion reactions typically contained 1x NEB buffer, 1x BSA (as required), and 0.5 μl of enzyme per 10μl reaction volume. Reactions were mixed and digested at 37°C for between 1-2hrs.

2.1.4 Agarose gel electrophoresis

Gel electrophoresis was used to examine and purify DNA fragments after PCR reactions and before ligation. Gels contained 1-2% agarose (Melford), 1xTAE and 0.5 μg/ml of ethidum bromide (Sigma). DNA samples were loaded with 6x loading buffer (50 mM Tris, pH 8.0, 10 mM EDTA, pH 8.0, 50%, glycerol, 0.25% bromophenol blue, 0.25% xylene cyanol FF) and run in 1x TAE at 90-120 volts for 20 mins-1 hr, or until DNA had sufficiently migrated. DNA was imaged or extracted using a UV light source.

2.1.5 Ligation

Amplicons and vectors previously digested and purified were ligated using T4 DNA ligase. Typical reactions contained 1x Ligase buffer (New England Biolabs), 1 μl/10 μl reaction volume T4 DNA ligase (New England Biolabs) and the appropriate molar ratios of insert to vector. Ratios were calculated by dividing insert size by vector size, multiplied by the required molar ratio, multiplied by 100 ng vector, resulting number equals the nanogram amount of insert required in the reaction.

Table 3: Plasmids used or created during this study.

Plasmid	Host used	Source	Features
pRS416	*S. cerevisiae*	Stratagene	Centromeric yeast expression plasmid marked with URA3 and Ampicillin. T7 and T3 promoters flank the MCS.
pRS416-flag-*IES6*	*S. cerevisiae*	This study	Derivative of pRS416 with *IES6* cloned into MCS via NotI sites

pRS416-flag-*ies6(K61A)*	*S. cerevisiae*	This study	Derivative of pRS416 with *ies6(K61A)* cloned into MCS via NotI sites
pRS416-flag-*ies6(R64A)*	*S. cerevisiae*	This study	Derivative of pRS416 with *ies6(R64A)* cloned into MCS via NotI sites
pRS416-flag-*ies6(Q65A)*	*S. cerevisiae*	This study	Derivative of pRS416 with *ies6(Q65A)* cloned into MCS via NotI sites
pRS416-flag-*ies6(R73A)*	*S. cerevisiae*	This study	Derivative of pRS416 with *ies6(R73A)* cloned into MCS via NotI sites
pRS416-flag-*ies6(Y100A)*	*S. cerevisiae*	This study	Derivative of pRS416 with *ies6(Y100A)* cloned into MCS via NotI sites
pRS416-flag-*ies6(S102A)*	*S. cerevisiae*	This study	Derivative of pRS416 with *ies6(S102A)* cloned into MCS via NotI sites
pRS416-flag-*ies6(K113A)*	*S. cerevisiae*	This study	Derivative of pRS416 with *ies6(K113A)* cloned into MCS via NotI sites
pRS416-flag-*ies6(K114A)*	*S. cerevisiae*	This study	Derivative of pRS416 with *ies6(K114A)* cloned into MCS via NotI sites
pRS416-flag-*ies6(K114E)*	*S. cerevisiae*	This study	Derivative of pRS416 with *ies6(K114E)* cloned into MCS via NotI sites
pRS416-flag-*ies6(Y115A)*	*S. cerevisiae*	This study	Derivative of pRS416 with *ies6(Y115A)* cloned into MCS via NotI sites
pRS416-flag-*ies6(D117A)*	*S. cerevisiae*	This study	Derivative of pRS416 with *ies6(D117A)* cloned into MCS via NotI sites
pRS416-flag-*ies6(Y125A)*	*S. cerevisiae*	This study	Derivative of pRS416 with *ies6(Y125A)* cloned into MCS via NotI sites
pRS416-flag-*ies6(R133A)*	*S. cerevisiae*	This study	Derivative of pRS416 with *ies6(R133A)* cloned into MCS via NotI sites
pRS416-flag-*ies6(Y140A)*	*S. cerevisiae*	This study	Derivative of pRS416 with *ies6(Y140A)* cloned into MCS via NotI sites
pRS416-flag-*ies6(Y155A)*	*S. cerevisiae*	This study	Derivative of pRS416 with *ies6(Y155A)* cloned into MCS via NotI sites
pRS416-flag-*ies6(K114A,Y125A)*	*S. cerevisiae*	This study	Derivative of pRS416 with *ies6(K114A,Y125A)* cloned into MCS via NotI sites
pRS416-flag-*ies6(K114E,Y125A)*	*S. cerevisiae*	This study	Derivative of pRS416 with *ies6(K114E,Y125A)* cloned into MCS via NotI sites
pMAT10	Rosetta DE3	(Peränen et al., 1996) gift from Marko Hyvönen	Protein expression plasmid, which contains an N-terminal 6xHIS/MBP tag adjacent to the MCS, flanked by T7 and SP6 promoters. Carries an ampicillin resistance marker.
pMAT10-*IES6*	Rosetta DE3	This study	Derivative of pMAT10 with *IES6* cloned into the MCS via NcoI and XbaI sites.

pMAT10-*ies6(K114E,Y125A)*	Rosetta DE3	This study	Derivative of pMAT10 with *ies6(K114E,Y125A)* cloned into the MCS via NcoI and XbaI sites.
pRS426	*S. cerevisiae*	Stratagene	Yeast overexpression plasmid marked with URA3 and Ampicillin. T7 and T3 promoters flank the MCS.
pRS426-*HTZ1*	*S. cerevisiae*	Gift from Catherine Miller	Derivative of pRS426 with *HTZ1* cloned into MCS
pRS426-*htz1(K-Q)*	*S. cerevisiae*	Gift from Catherine Miller	Derivative of pRS426 with *htz1(K-Q)* cloned into MCS
pRS426-*htz1(K-R)*	*S. cerevisiae*	Gift from Catherine Miller	Derivative of pRS426 with *htz1(K-R)* cloned into MCS
pRS415	*S. cerevisiae*	Stratagene	Centromeric yeast expression plasmid marked with LEU and Ampicillin. T7 and T3 promoters flank the MCS.
pRS415-*PIH1*	*S. cerevisiae*	This study	Derivative of pRS415 with *PIH1* cloned into MCS via SpeI and XbaI
pRS415-*pih1(K58E)*	*S. cerevisiae*	This study	Derivative of pRS415 with *pih1(K58E)* cloned into MCS via SpeI and XbaI
pRS415-*pih1(K106E)*	*S. cerevisiae*	This study	Derivative of pRS415 with *pih1(K106E)* cloned into MCS via SpeI and XbaI
pRS415-*pih1*$^{(1\text{-}167aa)}$	*S. cerevisiae*	This study	Derivative of pRS415 with *pih1*$^{(1\text{-}167aa)}$ cloned into MCS via SpeI and XbaI
pRS415-*pih1(K58E)*$^{(1\text{-}167aa)}$	*S. cerevisiae*	This study	Derivative of pRS415 with *pih1(K58E)*$^{(1\text{-}167aa)}$ cloned into MCS via SpeI and XbaI
pRS415-*pih1(K58E)*$^{(1\text{-}167aa)}$	*S. cerevisiae*	This study	Derivative of pRS415 with *pih1(K106E)*$^{(1\text{-}167aa)}$ cloned into MCS via SpeI and XbaI

2.1.6 Bacterial media

All bacterial cultures were grown in Luria Bertani broth (LB) (10 g/L Bacto Tryptone, 5 g/L yeast extract, 10 g/L sodium chloride, pH 7.0), if plasmid selection was required; LB was supplemented with Ampicillin (100μg/ml). For growth on solid media, 5 g/L of agar was added.

2.1.7 Transformation

Competent cells were thawed on ice and mixed with 1 ng or less of plasmid DNA. Transformations were left on ice for 40 min, then heat shocked at 42°C for 90s. 500 μl of LB was added to the transformation, which was then incubated at 37°C for 30 min. Cells were pelleted by centrifugation and resuspended in 100 μl LB before plating onto drug containing medium.

2.1.8 Plasmid isolation from Bacteria

After transformation of XL1-Blue with the desired plasmid, were inoculated into 2 ml LB plus ampicillin, and grown at 37°C overnight. Cells were harvested by centrifugation at 7500 rpm in a microfuge and the DNA was isolated using either Miniprep (Qiagen) or Nucleospin plasmid (Machery-Nagel) kits as per the manufactures instructions.

Table 4: Bacterial strains used in this study.

Strain	Source	Genotype
XL1-Blue	Stratagene	endA1 gyrA96(nal^R) thi-1 recA1 relA1 lac glnV44 F'[::Tn10 proAB$^+$ lacI^q Δ(lacZ)M15] hsdR17(r_K^- m_K^+)
Rosetta DE3	Novagene	F$^-$ ompT hsdS$_B$(R_B^- m_B^-) gal dcm λ(DE3 [lacI lacUV5-T7 gene 1 ind1 sam7 nin5]) pLysSRARE (Cam^R)

2.2 Experiments in S. cerevisiae

Table 5: *S. cerevisiae* strains used or created during this study.

Strain Number	Description	Genotype	Source
JDY854	*ies6*	*MAT*a, *his3Δ1, leu2Δ0, met15Δ0, ura3Δ0*, *ies6Δ*::KanMx4	Euroscarf
JDY921	BY4741	*MATa, his3Δ1, leu2Δ0, met15Δ0, ura3Δ0*	Euroscarf
JDY922	BY4742	*MAT*α *his3Δ1, leu2Δ0, met15Δ0, ura3Δ0*	Euroscarf
JDY853	BY4743	*MAT*a/α, *his3Δ1/his3Δ1, leu2Δ0/leu2Δ0, LYS2/lys2Δ0, met15Δ0/MET15, ura3Δ0/ura3Δ0*	Euroscarf
JDY854	*ies6/IES6*	*MAT*a/α, *his3Δ1/his3Δ1, leu2Δ0/leu2Δ0, LYS2/lys2Δ0, met15Δ0/MET15, ura3Δ0/ura3Δ0, ies6Δ*::KanMx4*/IES6*	Chambers et al. 2012
JDY1021	*cin8/CIN8, ies6/IES6*	*MAT a/α, cin8Δ*::HIS3/*CIN8 ies6Δ*::KanX4/*IES6*	This study
JDY1022	*cin8*, *IES6*	*cin8Δ*::HIS3, *ies6*::KanX4 +pRS416-Flag-*IES6*	This study
JDY1023	*cin8*, *ies6 (K114E, Y125A)*	*cin8Δ*::HIS3, *ies6*::KanX4 +pRS416-Flag- *ies6 (K114E, Y125A)*	This study
JDY1015	*sas3/SAS3, ies6/IES6*	*MAT*a/α, *his3Δ1/his3Δ1, leu2Δ0/leu2Δ0, LYS2/lys2Δ0, met15Δ0/MET15, ura3Δ0/ura3Δ0, ies6Δ*::KanMx4*/IES6, sas3Δ*::HIS/*SAS3*	This study

JDY1016	*sas3*	*MATa, his3Δ1, leu2Δ0, met15Δ0, ura3Δ0, sas3Δ*::HIS3	This study
JDY1017	*sas3, ies6*	*MATa, his3Δ1, leu2Δ0, met15Δ0, ura3Δ0, ies6Δ*::KanMx4*, sas3Δ*::HIS	This study
JDY1018	*rad50/RAD50, ies6/IES6*	*MAT*a/α, *his3Δ1/his3Δ1, leu2Δ0/leu2Δ0, LYS2/lys2Δ0, met15Δ0/MET15, ura3Δ0/ura3Δ0, ies6Δ*::KanMx4*/IES6, rad50Δ*::HIS/*RAD50*	This study
JDY1019	*rad50*	*MATa, his3Δ1, leu2Δ0, met15Δ0, ura3Δ0, rad50Δ*::HIS3	This study
JDY1020	*rad50, ies6*	*his3Δ1, leu2Δ0, met15Δ0, ura3Δ0, ies6Δ*::KanMx4*, rad50Δ*::HIS	This study
JDY968	*ies6/IES6, htz1/HTZ1*	*MATa/α, his3Δ1/his3Δ1, leu2Δ0/leu2Δ0, LYS2/lys2Δ0, met15Δ0/MET15, ura3Δ0/ura3Δ0, ies6Δ::KanMx4/IES6, htz1Δ::HIS/HTZ1*	Chambers et al. 2012
JDY1029	*pih1*	*MAT*a, *his3Δ1, leu2Δ0, met15Δ0, ura3Δ0*, *pih1Δ*::KanMx4	Euroscarf

2.2.1 Media

Wildtype or strains containing endogenous deletions were grown on YPAD agarose plates (10% yeast extract (Melford), 20% peptone (Melford), 0.1%

adeinine (Sigma), 2% glucose and 3% agar (Melford)) or liquid YPAD medium, without agar. Strains expressing alleles were grown under selection using synthetic dropout media. Which was composed of: 1x YNB (6.7g per litre yeast nitrogen base w/o amino acids, Invitrogen), 1x Drop Out (40 μg/ml adenine, 20 μg/ml L-arginine, 100 μg/ml L-aspartic acid, 100 μg/ml L-glutamic acid, 20 μg/ml L-methionine, 50 μg/ml L-phenylalanine, 375 μg/ml L-serine, 200 μg/ml L-theronine, 30 μg/ml L-tyrosine, 150 μg/ml L-valine, 30 μg/ml Lysine, and 10ml 1M NaOH), 2% glucose and 0.5g agar/100 ml. Either 20 μg/ml uracil, 20 μg/ml histidine, 60 μg/ml leucine, or 40 μg/ml tryptophan were added, or omitted, depending on the selection marker required for each experiment. Sterile H_20 was then added to reach the final volume of media being prepared. Liquid drop out media was prepared by the same method, removing the agar and increasing the volume of sterile H_20.

2.2.2 Transformation

Overnight yeast cultures were sub-cultured to an optical density of 0.1 at 600 nm in 10 ml YPAD per transformation. Cultures were grown at 30°C with shaking until they reached an optical density of 0.5. Cells were then harvested at 2500 rpm for 5 min, washed in 1 ml sterile water and resuspended in 1 ml 1x TE/1x Lithum Acetate (10 mM Tris, pH 8.0, 1 mM EDTA, pH 8.0, 100 mM LiOAc) before pelleting and resuspuspention in 100μl 1x TE/1x Lithum Acetate/10 ml culture volume. In a separate tube 5 μg of salmon sperm single stranded DNA (Sigma) was added to ~0.2-1 μg of PCR product or plasmid DNA for integration or expression within the

host yeast cells. 50 μl of the cell suspension was added to DNA as required, followed by 300 μl fresh PEG4000 solution (40% PEG, 1x TE, 1x LiOAc) before being vortexed, pre-warmed at 30°C for 30 min and heat shocked at 42°C for 15 min. Cells transformed to express a plasmid, requiring selection on drop out media, were centrifuged, resuspended in 100 μl sterile water, and plated on the relevant drop out media. For the integration of DNA fragments into the genome, using a drug resistance gene, such as KanMX, cells were spun, resuspended in 500 μl of YPAD and incubated at 30°C with shaking for 1 hr. This allows for transcription of the gene marker before plating on the relevant drug containing media. All plates were incubated at 30°C for 3-4 days, or until colonies were large enough for re-streaking.

2.2.3 Sporulation and tetrad dissection

Heterozygous diploids were sporulated in synthetic complete, -ura or –his SPM (1% potassium acetate, 0.005% zinc acetate, 20 μg/ml uracil, 20 μg/ml histidine or 60 μg/ml leucine were added or omitted depending on selection required). Cells were incubated with shaking at 25°C for 5 days, then switched to 30°C for 3 days. Efficiency was checked under the microscope and 100 μl of cells were pelleted and resuspeneded in 200 μl 0.2 M sodium phosphate buffer. Zymoleyase 20T was added to 5 μM and tetrads were digested at 37°C for 15mins. The digested spores were plated on solid media and dissected using a tetrad-dissecting microscope. Plates containing the dissected spores were incubated 30°C until large enough for genotyping.

2.2.4 Genotyping

After transformation or tetrad dissection of a host strain expressing plasmids containing modified *ies6* or *pih1* alleles. Any clones or spores were verified by their growth on selection media at 30°C for 3 days, for *ies6, cin8, rad50, htz1* strains this was growth on -URA and for *pih1* strains this was growth on –HIS. Further verification was obtained by PCR where required.

2.2.5 Isolation of genomic DNA

Yeast cells were harvested from 10 ml of overnight culture by centrifugation at 2500 rpm. The pellet was washed in 1 ml of sterile water, spun at 13000 rpm, and resuspended in 200 μl phenol chlorform (Sigma), 200 μl acid-washed glass beads (Sigma) and 200 μl braking buffer (2% Triton-X-100, 1% SDS, 100 mM NaCl, 10 mM TrisCL pH 8.0, 1 mM EDTA). Cells were then mechanically lysed in a bead beater, and supernatant was transferred to a sterile eppendorf tube. 200 μl of 1xTE was added, this was mixed by inversion, and spun at 13,000 rpm for 3mins. The aqueous layer containing the DNA was then transferred to a sterile eppendorf and 1ml of 100% ethanol was added to precipitate it. The sample was spun at 13,000 rpm for 3mins, the supernatant was discarded, and the DNA pellet was resuspended in 400 μl 1xTE. To remove RNase contamination, the sample was incubated at 37°C for 15mins in the presence of 30 μg of RNaseA (Sigma). To finally precipitate the clean DNA, 5 μl of 7.5 M of ammonium acetate and 1 ml of

100% ethanol were added, mixed by inversion, and spun at 13,00 rpm for 5mins. The pellet was left to air dry before resuspention in 100μl 1x TE.

2.2.6 Growth curve analysis

Yeast cells were grown over night in appropriate medium, and inoculated at a low starting optical density (600 nm) in 10-15ml of pre-warmed media. Cells were incubated at 37°C for between 10-12hrs with shaking. Every hour, 1ml of culture was removed, and the number of cells was quantified by measuring the optical density at 600 nm. Optical density was plotted against time to monitor the growth rate over a give time period.

2.2.7 Chronic DNA damage exposure

Mid-log cultures, gown in either SC or YPAD were spotted onto YPAD or concentrations of HU, MMS or Benomyl from 5-fold serial dilutions, with a starting optical density at 600nm of 0.2. Plates were then incubated at 30°C (or 37°C when examining for temperature sensitivity) and imaged after 2-3 days.

2.2.8 Replication restart assay

Cells lacking endogenous *IES6* were transformed with either wildtype, *ies6(K114E/Y125A)* or a pRS416 empty vector. These cells were then grown in 2 ml

SC –ura overnight 30°C with shaking, cells were then arrested in 5 μg/ml alpha factor for 2 hours. Alpha factor was removed by washing in 3x 2 ml 4°C SC –ura. The culture was split at the final wash step into either SD –ura, or SD –ura, plus 0.2 M HU. The cells were then grown in the presence, or absence, of HU for 2, 4 and 6 hours. At each time point, the optical density (600 nm) was recorded and cells were diluted to obtain ~100 cells per 100 μl. Cells were plated on SD –ura without HU and grown at 30°C for 3-4 days before counting colonies.

2.2.9 Fluorescently activated cell sorting (FACS)

Cells, fixed in ice cold 70% ethanol, were pelleted, and resuspended in 0.5 ml 1 mg/ml RNaseA (Sigma), 100 mM Tris pH 7.5 before incubation at 37°C for 4 hours. Cells were then pelleted and resuspended in 0.5 ml 2 mg/ml proteinase K (Sigma), 50 mM Tris pH 7.5, before incubation at 50°C for 1hr. Finally, cells were spun and resuspended in 0.5ml of FACS buffer (200 mM TrisCl pH7.5, 200 mM NaCl, 78 mM MgCl2) to be stored at 4°C overnight.

The following day 25-50 μl of cells, suspended in FACS buffer, were added to 50 μg/ml propidum iodide, 50 mM Tris pH 7.5 in FACS tubes. Each sample was then sonicated at 25% amplitude for 8-10 seconds to create an even, single cell suspension. The samples were run on either a BD Calibur or BD Acuri FACS machine and the data was analysed in FlowJo (FlowJo LLC).

2.2.10 TCA precipitation

Cultures grown to mid-log were harvested by centrifugation and transferred to screw capped tubes. 5 pellet volumes of 20% TCA (trichloroacetic acid), and 1 pellet volume of acid-washed glass beads (Sigma) were added, and the cells were mechanically lysed in a bead beater. The resulting supernatant was transferred to a sterile eppendorf tube, and proteins were pelleted by centrifugation at 4°C for 15 min. The protein pellet was then repeatedly washed in 1ml 4°C acetone before being air-dried and resuspended in 1x SDS LB (NuPAGE LDS sample buffer, Invitrogen).

2.2.11 Chromatin fractionation

Mid-log cultures were arrested in G1 using 5 μg/ml alpha factor in YPAD and grown for 2 hours at 30°C with shaking. Cells were then washed three times in cold YPAD, and then resuspended in an equal volume of pre-warmed YPAD to starter culture. Both wildtype and *ies6* cells were grown at 30°C with shaking and 25 ml of cells were removed at timed intervals corresponding to their progression through the cell cycle. Sodium aside was added to 0.1% final and cells were kept on ice while later samples were collected. Once all samples were collected, cells were harvested at 3000 rpm and resuspended in 6.25 ml 10 mM DTT, 100 mM HePes pH 9.4 incubated at 30°C with shaking for 10 min. Cells were pelleted at 2500 rpm for 5 min at room temperature, and resuspended in 2.5 ml YPAD with 0.6 M sorbitol, plus 62.5 μl 1M Tris HCL pH 7.5 and 12.5 μl of 100 mg/ml zymolease 20-T. Cells

were then incubated 30°C with shaking for 45 min. This process was repeated, pelleting at 1800 rpm, room temperature for 3 mins resuspending in 2.5 ml YPAD with 0.7 M sorbitol plus 62.5 μl 1 M Tris HCL pH 7.5, and incubating at 30°C with shaking for 20 min. Finally, cells were harvested at 1500 rpm for 3 min at room temperature, gently washed three times in lysis buffer (0.4M sorbitol, 150 mM KOAc, 2 mM Mg acetate, 20 mM Hepes/KOH pH6.5). To lyse the cells, Triton X-100 was added to a final concentration of 1% and mixed by inversion. 90 μl was removed as whole cell extract (WCE), a further 100 μl was then removed (chromatin) and the remaining ~900 μl (concentrated chromatin) was centrifuged at 4°C, 1300 rpm for 30 min. The supernatant was then removed from both chromatin samples and precipitated using TCA (Supernatant). All samples from the fractionation were mixed with 4x SDS loading buffer before loading on a 12% polyacrylamide gel.

2.3 Biochemical protein analysis

2.3.1 SDS-PAGE

SDS-PAGE gels for the resolution of proteins were composed of resolving and stacking portions. The resolving component was typically 10-15% acrylamide (Severn Biotech, 30% acrylamide, 37.5:1 acrylamide: bisacrylamide), 0.38 M Tris Cl, pH 8.8, 0.1% SDS, and the stacking component was always 5% acrylamide (Severn Biotech, 30% acrylamide, 37.5:1 acrylamide: bisacrylamide), 25 mM Tris

Cl, pH 6.8, 0.2% SDS. Both phases of the gel were polymerized using 10 μl/ml of 10% APS (Sigma) and 1 μl/ml TEMED (Sigma). Gels were run at 100 volts until dye front had migrated through the stacking component, then 180 volts in 1x running buffer (25 mM Tris, 192 mM glycine, 0.5% SDS) until protein markers of the desired size had migrated sufficiently.

2.3.2 Western blotting

Proteins resolved using SDS-PAGE were transferred to a nitrocellulose membrane (Hybond ECL Nitrocellulose Membrane, GE Healthcare) in cooled transfer buffer (2x SDS running buffer, 20% methanol) for 1 hour under a 200mA current. Once complete the membrane was 'blocked' with excess proteins by incubation for 1 hour with 5% dried milk (Marvel) in TBST (20 mM Tris base, pH 7.6, 137 mM NaCl, 0.1% Tween 20). The membrane was then extracted from the milk and incubated with the primary antibody (see table bellow). Before incubation with the secondary antibody (see table bellow), the membrane was washed three times for 10 min in 1x TBST. Following secondary incubation, wash steps were repeated, and the membrane was visualized by enhanced chemiluminescence (ECL) using Western Lighting ECL (Perkin-Elmer). Finally, to visualize the resolved proteins,

Table 6: Antibodies used in this study.

Antibody	Optimal conditions	Source
α-flag	1:1000 dilution in TBST, 1hr at room temperature	Sigma
α-H2A	1:4000 dilution in TBST, 1hr at room temperature	In house
α-HIS	1:4000 dilution in TBST, 1hr at room temperature	Abcam
α-H2A.Z $K14^{Ac}$	1:3500 dilution in 5% milk, overnight at 4°C	Millapore
α-Mouse	1:4000 dilution in TBST, 45 min at room temperature	Sigma
α-Rabbit	1:10,000 dilution in TBST, 45 min at room temperature	Sigma

membranes were exposed to X-ray film (Konica Milota X-ray film AX, Data Services) and developed.

2.3.3 Protein staining by Coomassie

Proteins were resolved by SDS-PAGE (see above) and gels were stained in Coomassie (0.2% Coomassie Blue, 50% methanol, 10% glacial acetic acid) for 20 min. Coomassie was discarded and the gel was washed with de-stain (25% methanol, 10% glacial acetic acid) until protein bands became visible and background staining reduced.

2.3.4 Protein quantification by Bradford

Purified proteins were quantified using the Bradford method (Bradford, 1979) where Coomassie dye (Bio-Rad) was incubated with 1-2 μl of protein of unknown concentration for 5 min at room temperature. The absorbance at 595 nm was recorded, and the concentration was determined by plotting a standard curve of the 595 nm absorbance vs. the absorbance of known concentrations of BSA (NEB).

2.3.5 Ies6 protein expression and purification

Rosetta DE3 competent cells (Table 2.3) were transformed (see above) with the protein expression plasmids of interest. Cells were then grown at 37°C overnight

in 100 ml LB with ampicillin. The following day, cells were sub-cultured into 1 litre of LB with ampicillin at an optical density of 0.05 at 600nm. Cultures were grown at 37°C for 2-3 hours until they reached an optical density of 0.5 at 600 nm, then allowed to cool before adding 1mM IPTG (isopropylbeta-D-thiogalactopyranoside) (Sigma). Proteins were then expressed overnight at 18°C with shaking.

The following day, cells were harvested by centrifugation at 5,000 rpm for 10 min, at 4°C, pellets and kept on ice, then resuspended in 15 ml lysis buffer (50 mM Na phosphate buffer pH8, 500 mM NaCl, 10% glycerol, 1 M urea, 10 mM imidazole pH 7.5, 10 mM beta-mercaptoethanol, 1 µg/ml pepstatin A, 0.5 µg/ml aprotinin, 1 µM leupeptin, 100µg/ml ABSF). The suspension was sonicated on ice in 10-second bursts, for 4 min total, at 35% amplitude. Soluble proteins from the resulting lysates were separated by centrifugation at 4°C, 15000 rpm for 20 min. Supernatant, containing soluble proteins, was removed and run over talon resin (HIS-select; Sigma) in a protein purification column (Bio-Rad). The resin was washed with lysis buffer and final eluted with 6x 0.5ml of elusion buffer (lysis buffer, plus 250mM imidazole pH7.5.) The majority of the protein was eluted in fraction 2, which was subsequently carried over for dialysis.

2.3.6 Dialysis of recombinant Ies6 and mutants

Eluted protein from the ies6 purifications were injected into Slide-A-Lyser cassettes (G2, 10K MWCO; Fisher Scientific), which were pre-soaked in 4°C dialysis buffer (25 mM Tris pH8, 200 mM KCl, 10% glycerol, 1 mM $MgCl_2$, 1 mM DTT). The cassettes were then floated, and left stirring at 4°C for 2 hours. After the initial 2

hour period the dialysis buffer was changed and the samples were left stirring at 4°C overnight.

2.3.7 Preparation of fluorescent oligonucleotides

Oligonucleotides were annealed in 100 nM stocks by combining 1 μM of Cy3-labbeled oligonucleotide with an excess (2 μM) of unlabelled oligonucleotide in annealing buffer (50 mM Na phosphate buffer pH8, 60 mM NaCl). The oligonucleotides were boiled in a hot block for 10 minuets and then allowed to gradually cool in the block overnight.

2.3.8 EMSA

Varying concentrations of recombinant MBP, Ies6, and any mutant forms (from 0.5μM to 3μM) were incubated with 100nM of fluorescently labelled oligonucleotides in EMSA buffer (20mM Tris HCL, 16 mM KCL, 8% glycerol, 0.8 mM DTT, 3.84 mM $MgCl_2$, 0.2 mg/ml BSA). Proteins were added in 0.5-3 μM amounts to create a concentration gradient. Samples were mixed gently by pipetting, pulse spun and incubated at 4°C for 1 hour.

DNA binding reactions were loaded onto a pre-equilibrated 1x TAE, 5% acrylamide gel (30% acrylamide, 29:1 acrylamide: bisacrylamide), run at 4°C, 120 volts for 2-3 hours in 1x TAE. Loading dye containing 1x orange G was used in a

free lane to track migration. Complexes were sufficiently migrated when the dye reached roughly 1 inch from the gel bottom. All gels were imaged using a Fugi FLA-5100 phospho-imager (Cy-3, 600V).

3 Results

3.1 Genetic and biochemical analysis of Ies6

The INO80 complex is a multi-protein complex with established roles during transcription (Shen et al., 2000), DNA repair (Van Attikum et al., 2004; Downs et al., 2004; Morrison et al., 2004), replication (Falbo et al., 2009; Papamichos-Chronakis and Peterson, 2008; Shimada et al., 2008), the displacement of H2A.Z (Van Attikum et al., 2007; Papamichos-Chronakis et al., 2011) and chromosome segregation (Ogiwara et al. 2007; Chambers et al. 2012). Given the board functionality of such chromatin remodelling complexes, they call upon their large numbers of auxiliary subunits to make significant contributions towards these biological processes. For example, within the SWR1 chromatin remodelling complex, the Swc2 subunit enables the exchange of the core histone H2A for the variant histone H2A.Z through its interaction with H2A.Z (Wu et al. 2005, Hong et al. 2014). However, many of the subunits within the INO80 complex have not been explicitly linked to particular functions of the complex.

Within the INO80 complex it is known that deletion of the catalytic component, Ino80, inhibits growth (Shen et al. 2000; Chambers et al. 2012) and causes sensitivity to DNA damaging agents, including: UV, IR, MMS, HU, and benomyl (Shen et al. 2000; Attikum et al. 2004; Papamichos-Chronakis & Peterson 2008; Chambers et al. 2012). Interestingly, of its 15 auxiliary subunits, only the deletion of *IES6* phenocopies the deletion of *INO80* for growth and DNA damage sensitivity (Chambers et al. 2012). In addition to a shared abbarant morphology

and irreguar DAPI staining, typical of strains with chromosome segregation problems (Chambers et al. 2012). These shared phenotypes of *ies6* and *ino80* null mutants indicate a strong requirement for Ies6 within the INO80 complex. Critically, this study was the first to link Ies6 to the role of Ino80 in maintaining ploidy. It was revealed that Ies6 and Ino80 are both required for the regulation of H2A.Z at the centromere (Chambers et al. 2012), which prevented improper chromosome segregation by maintaining centromere structure. This was demonstrated by mapping nucleosome positions after MNase digestion, revealing a more accessible chromatin structure, as well as increased H2A.Z at the centromere when assessed using chromatin imunopercipitation (ChIP) in the *ies6* and *ino80* deletion strains.

Though Ies6 has been implicated in the prevention of polyploidy through the maintenance of H2A.Z at the centromere (Chambers et al. 2012), information relating to the structure of the Ies6 protein is scarce. Only one study has made significant genetic and biochemical inferences about the structure and function of Ies6 (Fenwick, 2010). In this study, Ies6 was demonstrated to bind double stranded DNA, with a preference for Y-fork structures (Fenwick, 2010). Furthermore, DNA binding was abolished with the incorporation of four alanine substations at T119, K122, S127 and T129 (Fenwick, 2010). Sequence alignments demonstrate these mutations reside within the YL1_C domain (Fenwick, 2010; Figure 6 A and B), which is common to DNA binding proteins and transcription factors (Horikawa et al., 1995). Subsequently, this is considered the putative DNA binding domain of Ies6 (Fenwick, 2010).

Additional regions of the Ies6 protein have been highlighted as potential regions for interaction with other auxiliary subunits of the INO80 complex (Tosi et

al., 2013). This study used EM to reveal the overall shape of the INO80 complex and the assembly positions of all the subunits (Tosi et al., 2013). Using disuccinimidyl suberate (DSS) they were able to cross-link lysine residues within a distance of approximately 30 angstroms (Å) (Leitner et al., 2013). This method revealed close structural interactions between the subunits of the INO80 complex and enabled the topology of the complex to be mapped for the first time (Tosi et al., 2013). Using Ies6 peptide sequences retrieved in this study, the Arp5 and Rvb2 interacting regions were defined (Figure 6 B and C). However, given the potentially vast distance of up to 30Å between each cross-linked lysine residue, any residues that establish the interactions *in vivo* may be far from the lysines that cross-linked in the study (Tosi et al., 2013).

The application of these potential interacting domains to the protein alignment revealed that previous mutations are within both the YL1_C domain and the Rvb2 interacting peptide region (Figure 6 C and D). However, plenty of unscreened residues, with better conservation in higher eukaryotes, are yet to be examined.

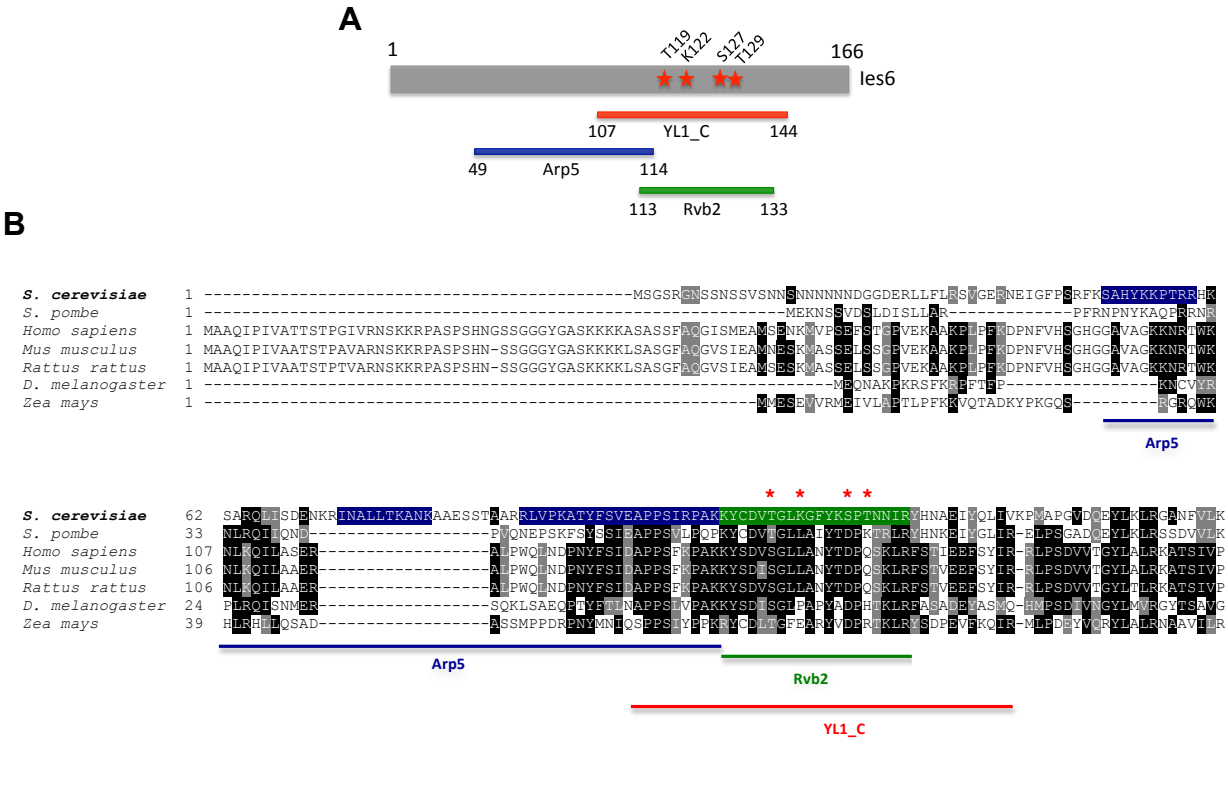

ies6 Mutation (Fenwick, 2010)	Located in which Ies6 domain?		
	Arp5	Rvb2	YL1_C
T119		✓	✓
K122		✓	✓
S127		✓	✓
T129		✓	✓

Figure 6: Ies6 from *Saccharomyces cerevisiae* contains two potential protein interaction domains in addition to a putative DNA binding region.

A. Schematic highlighting the position of previously mutated residues (Fenwick, 2010) within the Ies6 protein.

B. Alignment of Ies6 from higher eukaryotes showing the protein conservation and location of Arp5 (blue) and Rvb2 (green) interacting regions and the YL1_C domain (red). Red asterisk mark mutations from Fenwick, 2010.

C. Peptide sequences and interacting lysine residues (bold and underlined) involved in the Ies6-Arp5 (blue) and Ies6-Rvb2 (green) cross-links (Tosi et al., 2013), and the amino acid sequence of the YL1_C domain (red).

D. Table summary of previously mutated residues (Fenwick, 2010) and their location within the Ies6 protein regions.

3.1.1 Dissection of the Ies6 protein

To investigate the possible function of conserved residues within the YL1_C domain and the potential Arp5 and Rvb2 interacting regions, a total of 13 residues were selected for mutagenesis. These residues were selected based on their location within each interacting region or domain (Figure 7 B) and their conservation in higher eukaryotes (Figure 7 A). Due to the unconserved nature of the Ies6 N-terminus, some residues within the potential Arp5 interacting region were selected from an alignment of conservation within *Saccharomyces* (SGD protein blast – alignment not shown).

The residues selected for mutagenesis can be divided into three overlapping categories depending on their position within the two interacting regions and the YL1_C domain. These are, the Arp5 interacting region (K61, R64, Q65, R73, Y100 and S102) and the YL1_C domain (Y140) and Rvb2 interacting region (K113, K114, Y115, D117, Y125, R133). The position of the Rvb2 interacting region within the YL1_C domain resulted in the majority of mutations overlapping (Figure 7 C).

A

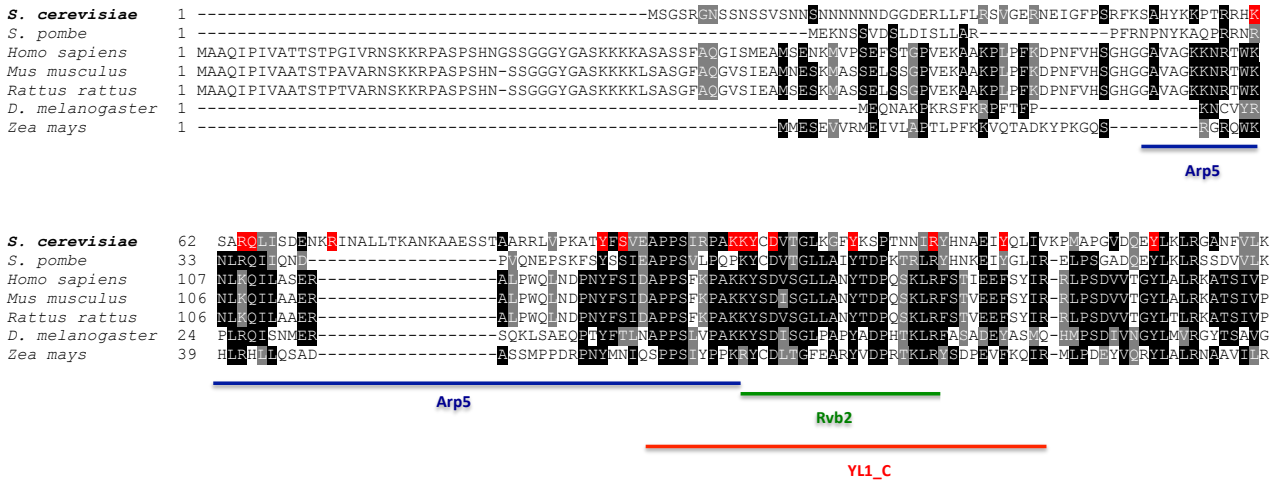

B

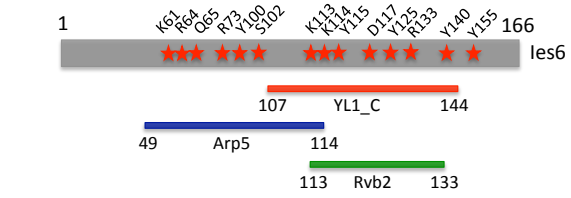

C

ies6 Mutation (This study)	Located in which Ies6 domain?		
	Arp5	Rvb2	YL1_C
K61	✓		
R64	✓		
Q65	✓		
R73	✓		
Y100	✓		
S102	✓		
K113		✓	✓
K114		✓	✓
Y115		✓	✓
D117		✓	✓
Y125		✓	✓
R133		✓	✓
Y140			✓
Y155			

Figure 7: Residues selected for mutagenesis were highly conserved and within Arp5 and Rvb2 interacting regions or the YL1_C domain.

A. Alignment of Ies6 from higher eukaryotes showing conservation and location of residues selected for mutagenesis (highlighted red). The Arp5 (blue line) and Rvb2 (green line) interacting regions and the YL1_C domain (red line) are marked.

B. Schematic representation of the mutagenized residues and their location within the Ies6 protein.

C. Table to summarise the location for the mutagenized residues within the Ies6 protein regions.

3.1.2 Point mutations tested within the potential Arp5 interacting region did not cause drug sensitivity.

Cellular response to DNA damage is frequently used as a preliminary screen of genetically modified alleles to compare their phonotype to wildtype and knockouts for a gene of interest. These assays provide an insight into gene function within specific cellular pathways through exposure to chronic levels of specific drugs and monitoring their fitness over time. For example, the three drugs that will be used to screen mutants within this study are MMS, HU and benomyl. These all probe for functionality within the pathways of DNA repair, replication and chromosome segregation. MMS methylates causes bulky adducts in the DNA which are thought to collide with replication machinery inhibit homologous recombination (HR) (Lundin et al., 2005), HU is and inhibitor of ribonucleotide reductase which blocks dNTP production (Koç et al., 2004) and Benomyl inhibits microtubules through competitive binding to tubulin (Quinlan et al., 1980).

As previously discussed, *ino80* mutants are sensitive multiple DNA damaging agents (UV, IR, MMS, HU and benomyl (Shen et al. 2000; Attikum et al. 2004; Papamichos-Chronakis & Peterson 2008; Chambers et al. 2012)), with the *ies6* null strain phoncopying the *ino80* null for HU and benomyl sensitivity (Chambers et al. 2012). Therefore, all the single residue substitutions of *ies6* were tested on HU, MMS and benomyl. The mutants were produced by PCR and verified by sequencing the whole open reading frame (ORF) to ensure there were no secondary mutations. The *ies6* alleles containing mutations within the potential

Arp5 interacting region (K61, R64, Q65, R73, Y100 and S102) (Figure 8 A) had no phenotype when screened for HU, MMS or benomyl sensitivity (Figure 8 B).

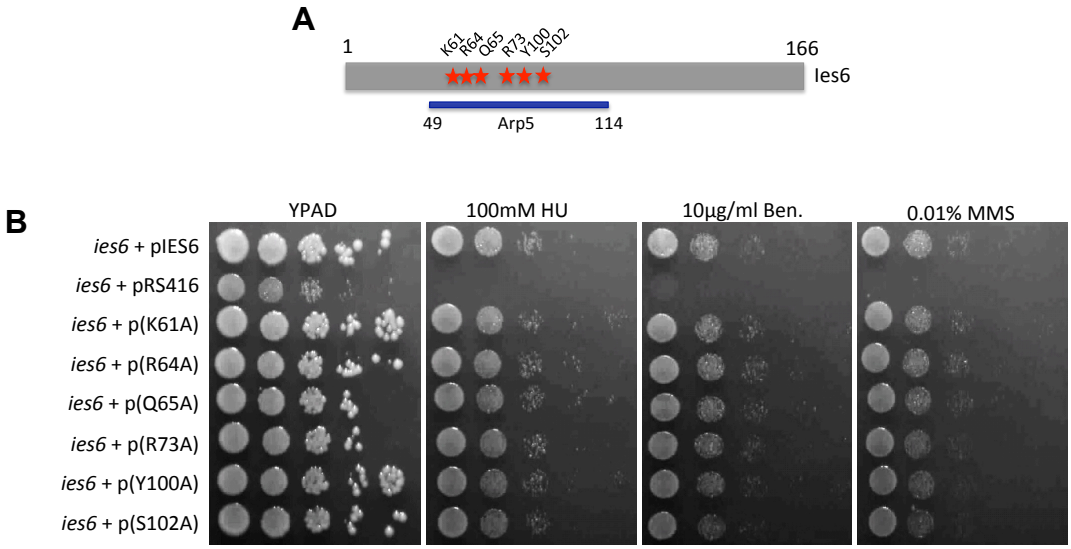

Figure 8: Sensitivity of mutations within the potential Arp5 interacting region to HU, Benomyl and MMS.

A. Schematic of the Ies6 protein showing position of each residue mutated and the location of the Arp5 interacting region (blue).

B. The *ies6* null strain (JDY854) was transformed with plasmids carrying mutated alleles of *ies6*, the resulting transformants, were plated on YPAD and drug containing media from 10x serial dilutions and grown at 30 °C for 72 hours. All the mutations tested from the Arp5 interacting region had no influence on sensitivity to HU, Benomyl or MMS.

3.1.3 Point mutations tested within the potential Rvb2 interacting region or the YL_C domain did not cause drug sensitivity.

Given the lack of phenotypes upon screening conserved residues within the Arp6 interacting region, mutations in conserved residues within the potential Ruvb2 interacting region, or the YL1_C domain (Figure 9 A) were screened using HU, MMS and benomyl. All mutations within these regions were produced by PCR and verified by sequencing across the whole open reading frame (ORF) to ensure there were no secondary mutations.

Surprisingly, the mutation of the selected conserved residues within the Rvb2 binding region (K113, K114, Y115, D117, Y125, R133) or the YL1_C domain (Y140) produced no phenotype when exposed to concentrations of HU, benomyl or MMS (Figure 9 B).

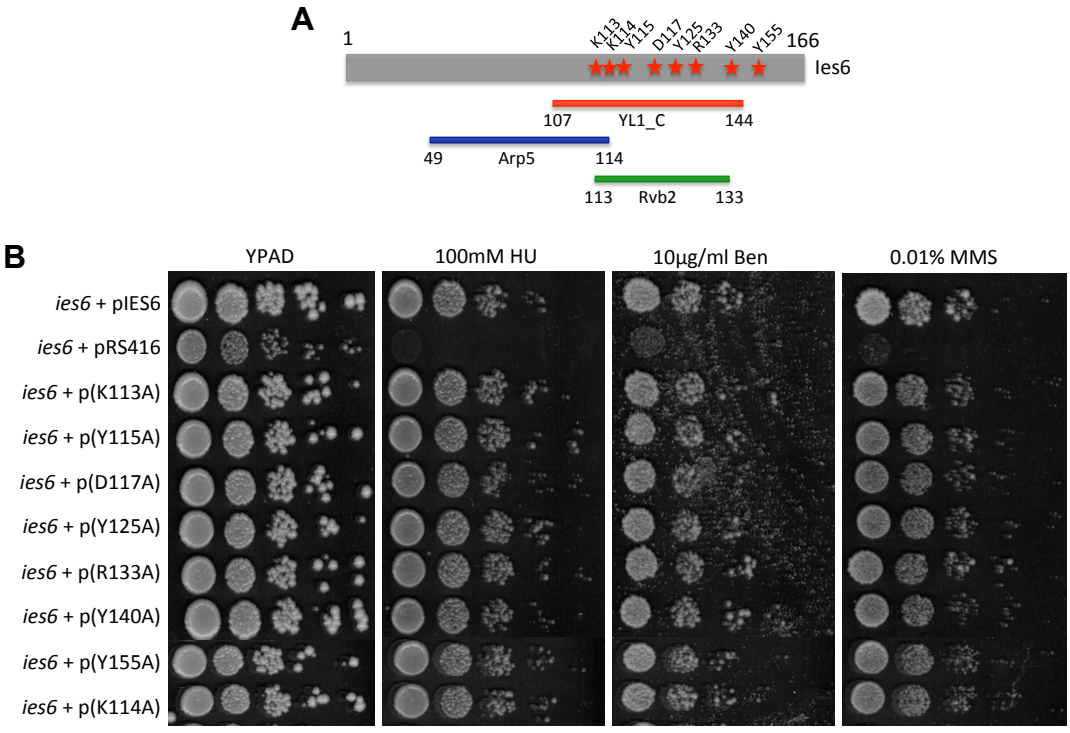

Figure 9: Sensitivity of mutations within the potential Rvb2 binding region and YL1_C putative DNA binding domain to HU, Benomyl and MMS.

A. Schematic of the Ies6 protein showing position of each residue mutated and the location of the Arp5 interacting region (green) and the YL1_C domain (red).

B. The *ies6* null strain (JDY854) was transformed with plasmids carrying mutated alleles of *ies6*, the resulting transformants, were plated on YPAD and drug containing media from 10x serial dilutions and grown at 30 °C for 72 hours. All the mutations tested from the Rvb2 interacting region and YL1_C domain had no influence on sensitivity to HU, Benomyl or MMS.

3.1.4 Single residue substitutions within Ies6 are stably expressed *in vivo*.

Given the lack of sensitivity of mutated residues to HU, MMS or benomyl, cells expressing a selection of *ies6* alleles within the highly conserved C-terminal region of the protein were screened by western blot using an N-terminal FLAG-tag. This is was important to measure possible degradation of the mutated form of the protein by proteolysis. Destabilisation of the protein structure as a result of mutagenesis can lead to lower expression levels in the cell.

Western blot analysis revealed mutations within the Rvb2 interacting region and YL1_C domain were expressed to the same level as the wildtype protein. Therefore, these mutations are unlikely to be improperly folded or subject to proteolysis (Figure 10 B).

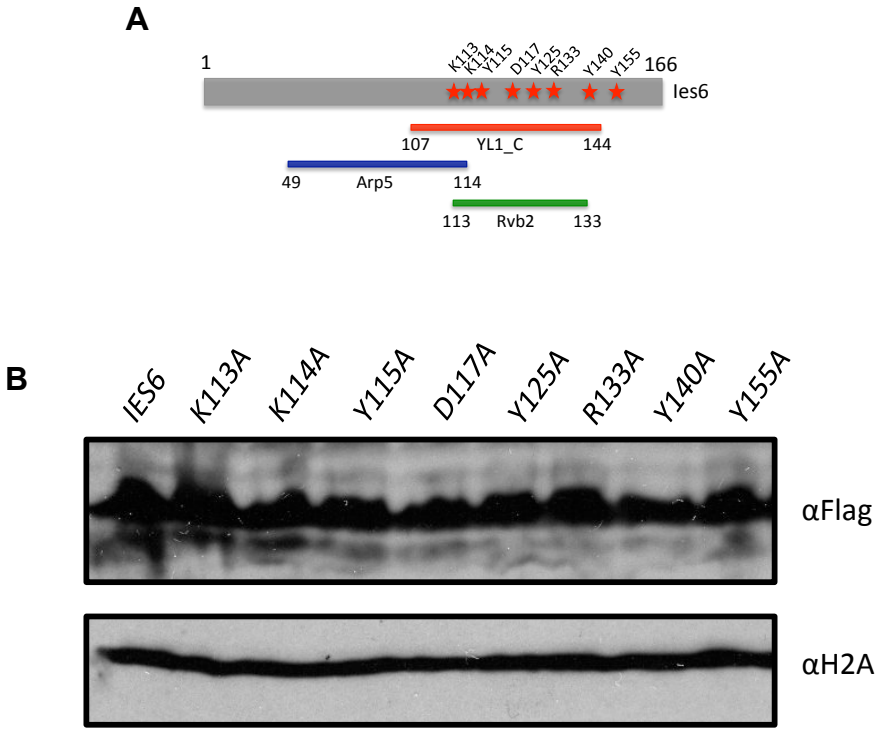

Figure 10: Single point mutants of *ies6* within the Rvb2 interacting regions and YL1_C domain are expressed to wildtype levels *in vivo.*

A. Schematic of the Ies6 protein showing the amino acid positions of the two interacting regions and the YL1_C domain.

B. Cells expressing flag tagged *ies6* alleles (the *ies6* null strain (JDY854) transformed with expression plasmids) were grown to mid-log phase, proteins were extracted and the lysates analysed by western blotting. Blots were probed for flag (top panel) and H2A as a loading control (bottom panel).

3.1.5 *ies6 (K114E, Y125A)* is defective for growth.

During the production of single point mutants, a double mutant containing glutamine substitution at K114 and an alanine substitution at Y125 was obtained. It was verified by sequencing the ORF of *IES6* to ensure it contained no other secondary mutations. Both residues are conserved and are located within the Rvb2 interacting region and YL1_C domain (Figure 11 A).

The double mutant was routinely tested along side all other single point mutants on HU, MMS and benomyl. During culturing, it was apparent that cells expressing the *ies6 (K114E, Y125A)* mutant allele had a slower growth rate than the wildtype, however, faster than the *ies6* null. Given the initial observation of growth, the growth rate of wildtype, *ies6* and *ies6 (K114E, Y125A)* strains was quantified by measuring their optical density (600 nm) over a 10-hour period.

As previously discussed, *ies6* null cells have an aberrant cellular morphology related to their chromosome segregation defects (Chambers et al., 2012). As optical density measurements are dependent on the light refraction at 600 nm wavelength, which is influenced by cell size, curves were produced from three independent isolates to reduce the effect of this variable.

The resulting curve confirmed that the *ies6 (K114E, Y125A)* expressing strain had a growth defect intermediate to the wildtype and *ies6* null (Figure 11 B). The intermediate growth phonotype indicates that, while Ies6 functions are not completely compromised, some have been altered sufficiently in the *ies6 (K114E, Y125A)* mutant to slow progression through the cell cycle.

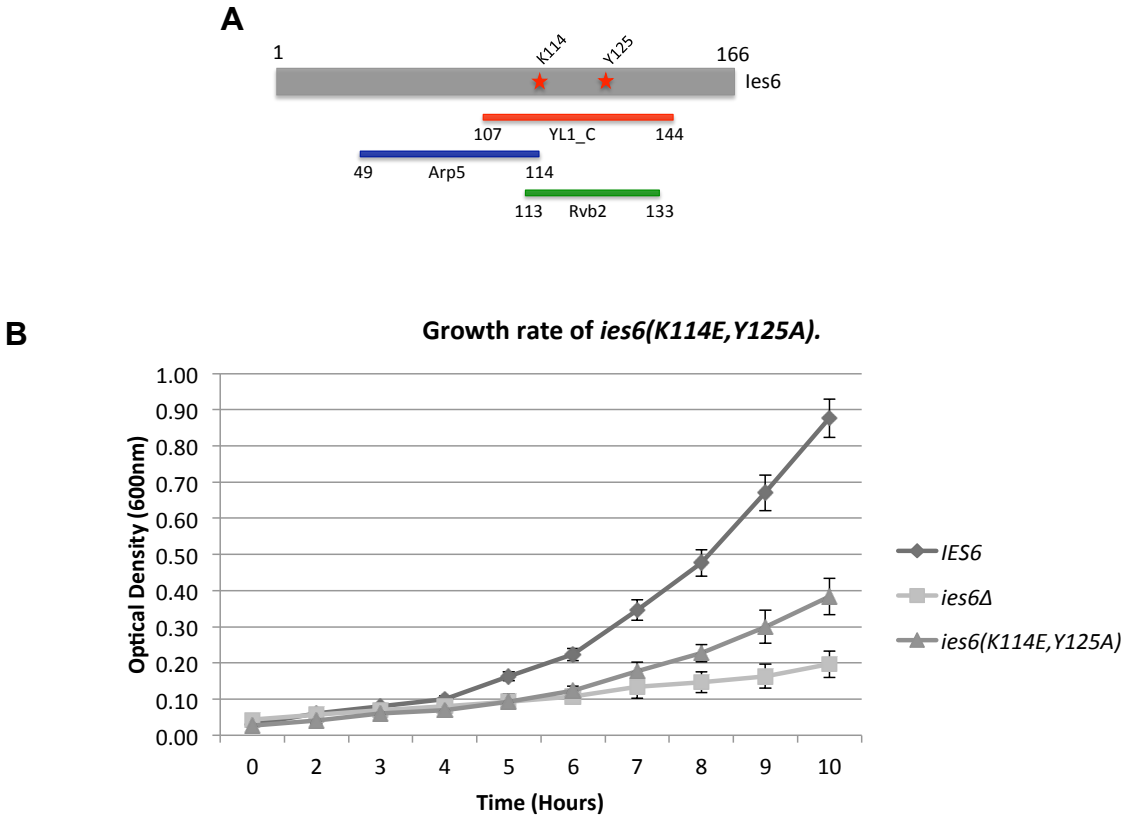

Figure 11: *ies6 (K114E, Y125A)* cells have a growth defect that is intermediate of wildtype and the *ies6* null.

A. Schematic of the Ies6 protein showing the location of the K114 and Y125 residues (red stars) in relation to the Arp5 (blue line) and Rvb2 (green line) interacting regions and the YL1_C domain (red line).

B. Optical density of cells endogenously deficient for *ies6* were grown for 10 hours at 30°C while expressing either an empty vector, *IES6* or *ies6(K114E,Y125A)* complementation plasmid. Error bars represent standard deviation.

3.1.6 The *ies6 (K114E, Y125A)* allele is sensitive to HU but not benomyl

To examine the cause of slow growth in cells expressing the *ies6 (K114E, Y125A)* mutant, these cells were subjected to screening with MMS, HU and benomyl. They were compared to wildtype and *ies6*, in addition to the corresponding single point mutants: *ies6 (K114E)* and *ies6 (Y125A)*, and the same mutant with and alanine substitution at K114, *ies6 (K114A, Y125A)*, and the corresponding single *ies6 (K114A)*. The results demonstrated that *ies6 (K114E, Y125A)* had a clear sensitivity to 100 mM HU, well above the 20 mM that is lethal to the *ies6* null strain (Figure 12 B). This intermediate sensitivity was later quantified by assessing colony forming ability on increasing concentration of HU (Figure 13 C).

Critically, this sensitivity was only observed in *ies6 (K114E, Y125A)* mutant and not in the *ies6 (K114A, Y125A)* mutant, or the *ies6(K114E), ies6(K114A),* or *ies6(Y125A)* single mutants (Figure 12 B). This observation indicates the substitution to glutamine at K114, in combination with an alanine substitution at Y125, inhibits the survival of *ies6 (K114E, Y125A)* to HU, whether the dose is chronic (Figure 12 B) or acute (Figure 13 C). Furthermore, the *ies6 (K114E, Y125A)* mutant was seen to be insensitive to benomyl (Figure 12 B). This was confirmed through quantification of colony forming ability on increasing benomyl concentrations (Figure 13 B).

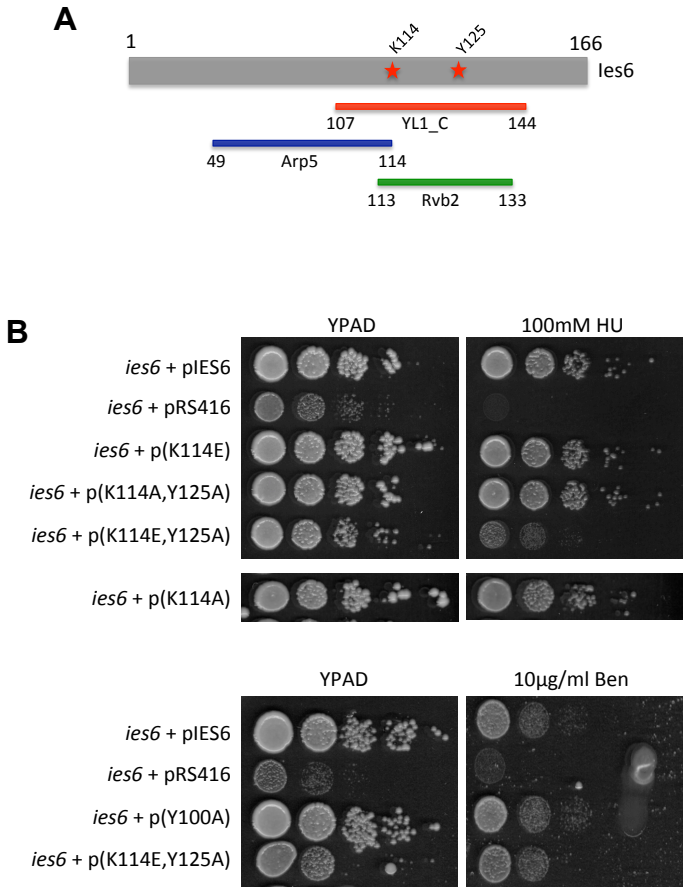

Figure 12: Cells containing the *ies6* allele K114E, but not K114A, in combination with Y125A, are sensitive to HU.

A. Schematic of the Ies6 protein showing the amino acid positions of the two interacting regions (Arp5 – blue bar, Rvb2 – green bar), the YL1_C domain (red bar) and the locations of the two point mutations (stars).

B. The *ies6* null strain (JDY854) was transformed with plasmids carrying mutated alleles of *ies6*, the resulting transformants, were plated on YPAD and drug containing media from 10x serial dilutions and grown at 30 °C for 72 hours.

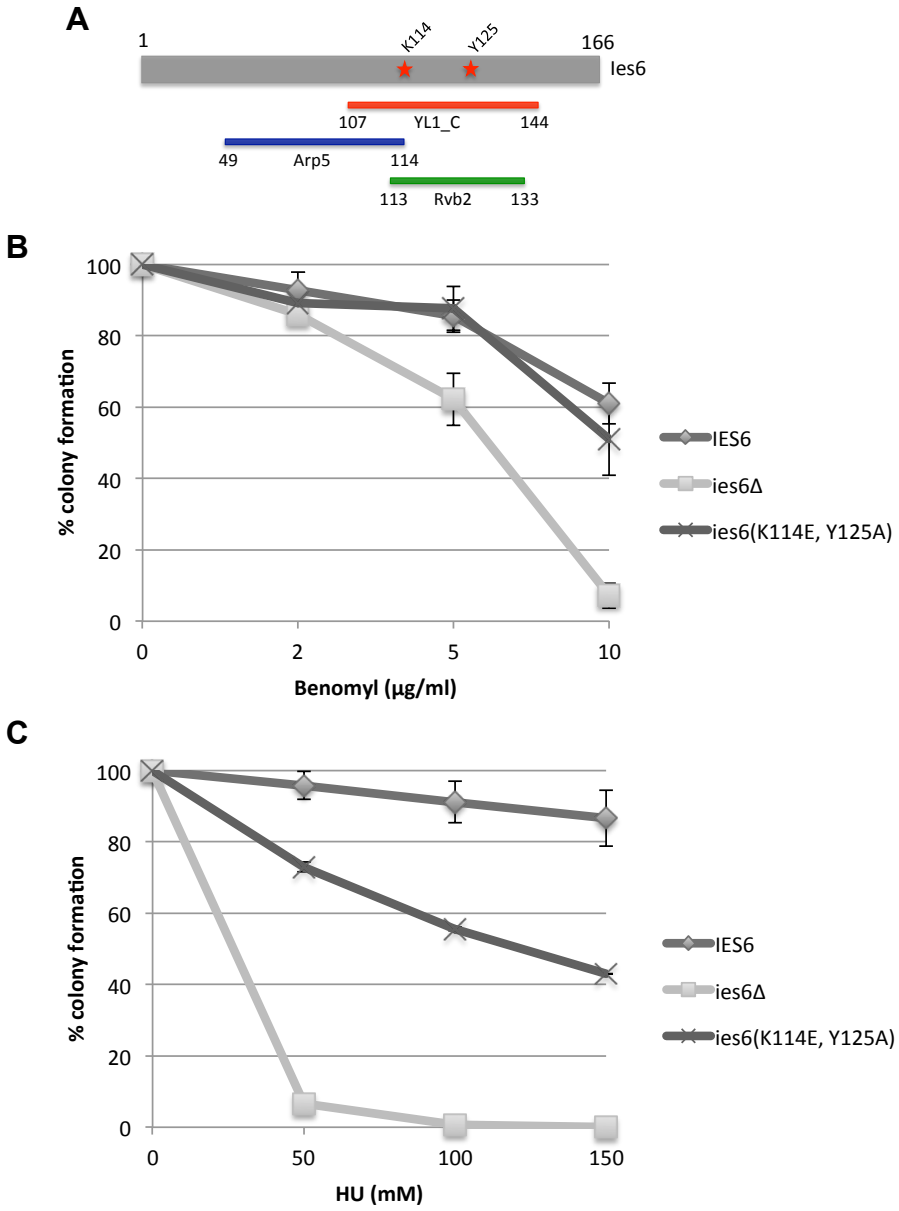

Figure 13: Quantification of *ies6(K114E,Y125A)* sensitivity to benomyl and HU.

A. Schematic of the Ies6 protein showing the amino acid positions of the two interacting regions (Arp5 – blue bar, Rvb2 – green bar), the YL1_C domain (red bar) and the locations of the two point mutations (stars).

B. *ies6* null cells (JDY854) transformed with either an empty vector, *IES6* or *ies6(K114E,Y125A)* expression plasmid were exposed to mid-log. ~100 cells were plated onto rich media or media containing benomyl.

C. *ies6* null cells (JDY854) transformed with either an empty vector, *IES6* or *ies6(K114E,Y125A)* expression plasmid were exposed were grown to mid-log. ~100 cells were plated onto rich media or media containing HU. Graphs shows the number of colonies formed on the drug containing media vs. untreated. Error bars are plotted using the standard deviation.

(Data provided by Melinda Ductor Peters)

3.1.7 The *ies6 (K114E, Y125A)* allele is stably expressed *in vivo*

As the *ies6 (K114E, Y125A)* mutant exhibited HU sensitivity it was vital to check its expression compared to wildtype due to potential destabilisation of the protein structure. Such destabilisation could make the mutated form of the protein a target for degradation by proteolysis. Cell lysates from wildtype, *ies6* null*, ies6 (Y125A)*, *ies6 (K114E), îes6 (K114E, Y125A)*, *ies6 (K114A)* and *ies6 (K114A, Y125A)* were analysed by western blot and probed using anti-flag antibody (Figure 14 B).

Interpretation of the blot was difficult due to the low level of Ies6 observed when probed with anti-flag, despite equal loading on the H2A control blot. However, *ies6 (K114E, Y125A)* appeared to be underexpressed compared to either the *ies6 (Y125A)* or *ies6 (K114E)* mutants, but was more comparible to the *ies6 (K114A)* and the *ies6 (K114A, Y125A)* mutant. Quantification confirmed these observations (Figure 14 C), however, they could not be attributed to loading, given that the H2A control was consistent throughout and requires repeating to obtain a suffcient comparison to wildtype. However, the previuous result, demonstring the ability of *ies6 (K114E, Y125E)* recover from benomyl induced DNA damage (Figure 13 C), confirms that the Ies6 (K144E, Y125A) protein is suffciently folded to conduct at least some of it's functions.

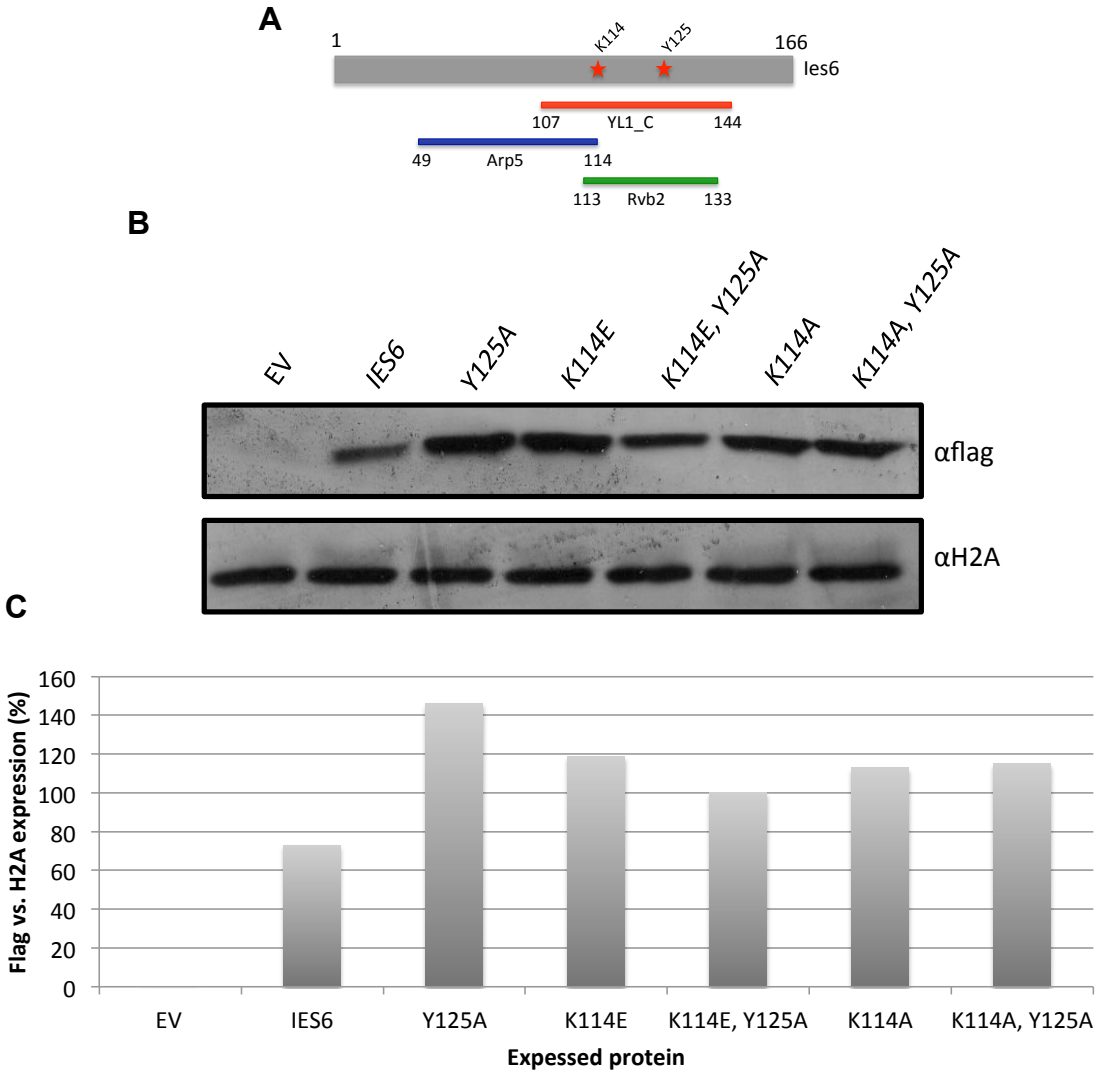

Figure 14: Double mutants of *ies6* within the Ruvb2 binding domain are expressed to wildtype levels *in vivo.*

A. Schematic of the Ies6 protein showing the amino acid positions of the two interacting regions (Arp5 – blue bar, Rvb2 – green bar), the YL1_C domain (red bar) and the locations of the two point mutations (stars).

B. *ies6* null cells (JDY854) transformed with either an empty vector, *IES6* or *ies6(K114E,Y125A)* expression plasmid were grown to mid-log phase, proteins were extracted and lysates were analysed by western blotting. Blots were probed for flag (top panel) and H2A as a loading control (bottom panel).

C. Quantification of the total expression of flag tagged Ies6, Ies6 (Y125A), Ies6 (K114E), Ies6 (K114E, Y125A), Ies6 (K114A) and Ies6 (K114A, Y125A) compared to equivalent H2A loading control. The difference between flag and H2A expression is displayed normalised to Ies6 (K114E, Y125A).

3.1.8 Expression of the ies6 (K114E, Y125A) mutant does not cause an increase in cellular ploidy.

Previous studies have demonstrated *ies6* null cells duplicate their genome after approximately 30 generations (3-4 days incubation at 30˚C) causing an increase in ploidy (Chambers et al. 2012). Ploidy maintenance defects in *ies6* null cells are attributed to problems with H2A.Z removal due to increased H2A.Z incorporation at the centromeres (Chambers et al. 2012). Inability to remove H2A.Z from the centromere is thought to cause a relaxation of the chromatin structure, leaving the chromatin vulnerable to digestion with micrococcal nuclease (MNase), which is supported by sensitivity to benomyl (Chambers et al. 2012).

Given the observation that the *ies6 (K114E, Y125A)* mutant was not sensitive to benomyl it was deemed unlikely that the growth defect observed (Figure 11 B) would be due to an issue with chromosome segregation. However, to confirm ploidy status of the *ies6 (K114E, Y125A)* mutant, the DNA content of newly sporulated *ies6* null haploids expressing the *ies6 (K114E, Y125A)* allele (generated from an *IES6/ies6* heterozygous diploid) was recorded over a 10-day period.

As previously observed (Chambers et al. 2012), the *ies6* cells quickly duplicated their genome after approximately 30 generations (3-4 days growth). However, the *ies6 (K114E, Y125A)* expressing cells did not duplicate their genome and maintained a haploid DNA content comparable to the wildtype control (Figure 15 B).

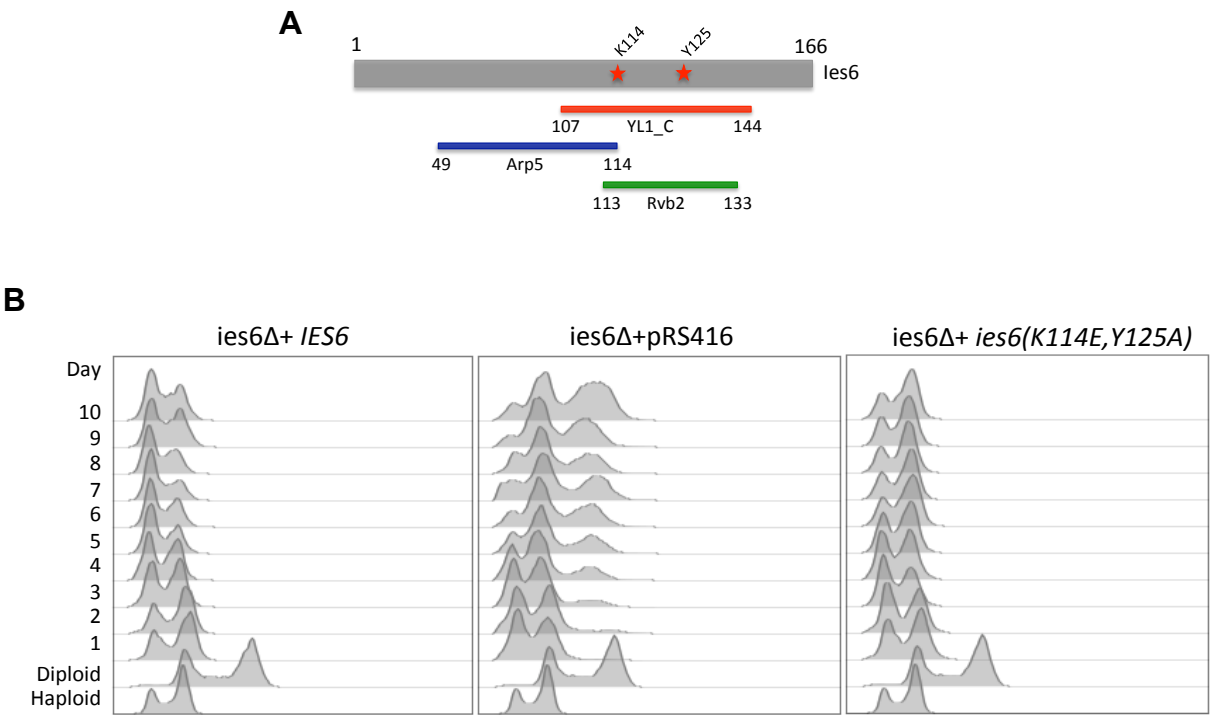

Figure 15: The increase in ploidy seen in an *ies6* null is not observed in an *ies6 (K114E, Y125A)* mutant.

A. Schematic of the Ies6 protein showing the amino acid positions of the two interacting regions (Arp5 – blue bar, Rvb2 – green bar), the YL1_C domain (red bar) and the locations of the two point mutations (stars).

B. FACS analysis was conducted on mid-log cultures, which were sampled for 10 days from newly derived *ies6* haploids expressing an empty vector, *IES6* or *ies6 (K114E, Y125A).* The *ies6* null strain expressing the empty vector became polyploid after 3days (equal to 30 generations; middle panel) as previously observed (Chambers et al., 2012).

3.1.9 *ies6 (K114E, Y125A)* inhibits replication progression after exposure to HU.

The sensitivity of *ino80* null strains to HU has been widely characterised due to its role in the relief of replication stress (Falbo et al., 2009; Papamichos-Chronakis and Peterson, 2008; Shimada et al., 2008). The deletion of *ies6* is known to phenocopy the deletion of *ino80* for sensitivity to HU (Chambers et al. 2012). Given the similarity between these two phonotypes, it is not unreasonable to assume that Ies6 is in some way contributing to the function of Ino80 in the relief of replication stress. As the *ies6 (K114E, Y125A)* mutant was only sensitive to HU, it was likely that replication fork recovery after HU stalling would be inhibited in the *ies6 (K114E, Y125A)* mutant.

Using an assay to measure recovery from replication stress (Shimada et al., 2008), the ability of the *ies6 (K114E, Y125A)* mutant to recover from HU meditated inhibition of replication was measured by comparing colony formation on rich media after exposure to HU in liquid media. The number of colonies formed provided a measurement of the number of cells that successfully overcame the inhibition of ribonucleotide reductase.

Compared with wildtype, *ies6* nulls cells were increasingly sensitive to fork stalling and could not recover to produce viable colonies (Figure 16 B and C). However, the *ies6 (K114E, Y125A)* mutant was able to produce more colonies than the *ies6* null, but still fewer than observed for wildtype under the same conditions (Figure 16 B and C).

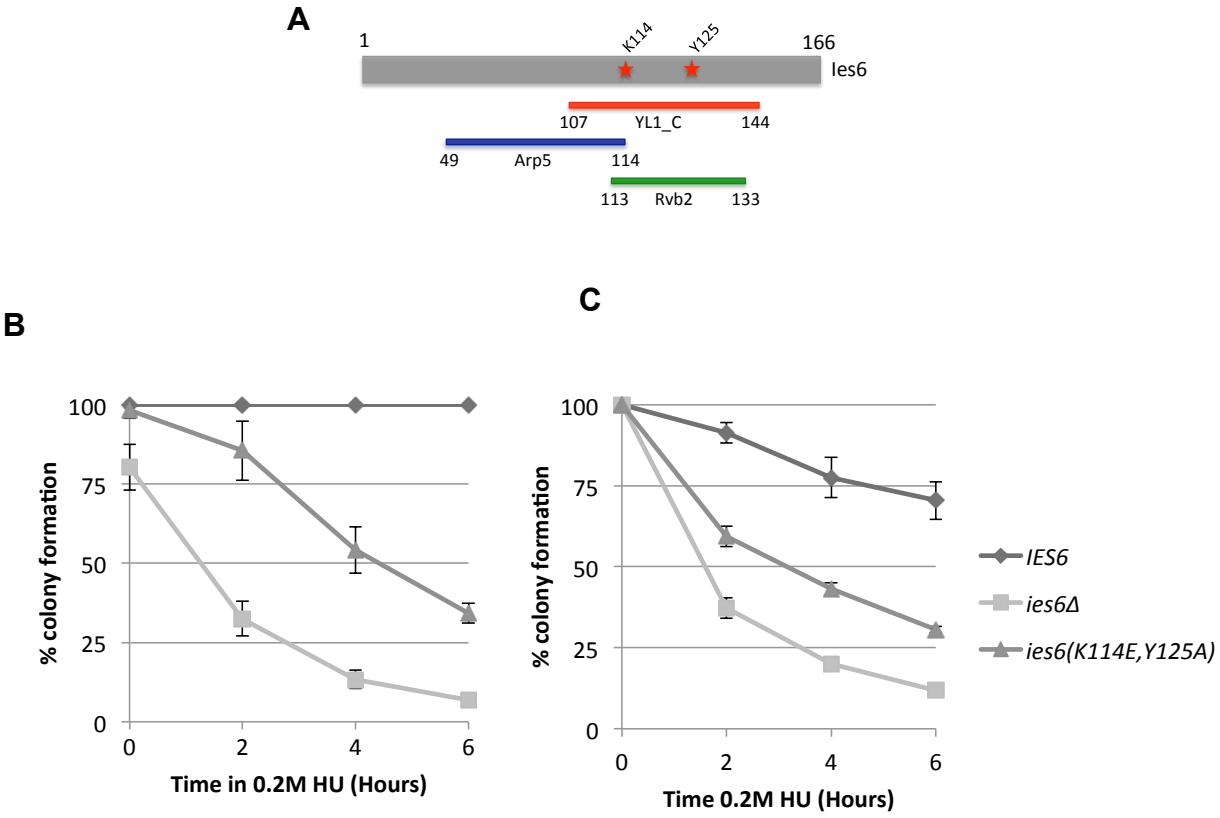

Figure 16: *ies6(K114E, Y125A)* is susceptible to replication fork collapse.

A. Schematic of the Ies6 protein showing the amino acid positions of the two interacting regions (Arp5 – blue bar, Rvb2 – green bar), the YL1_C domain (red bar) and the locations of the two point mutations (stars).

B. *ies6* null cells (JDY854) transformed with either an empty vector, *IES6* or *ies6(K114E,Y125A)* expression plasmid were exposed to 0.2 M HU for 2, 4 and 6 hours before plating onto drug free media and grown for 3 days at 30°C. Percentage colony formation of each mutant, on HU, vs. wildtype percentage formation on HU. Error bars represent the standard deviation of triplicates.

C. Percentage colony formation of strains on HU vs. untreated plates. Error bars represent the standard deviation of triplicates.

3.1.10 *ies6 (K114E, Y125A)* does not inhibit DNA binding.

Recombinant Ies6 protein has been shown to independently bind DNA *in vitro* (Fenwick, 2010), or as part of a complex with Arp5 (Tosi et al., 2013). Given that mutations within *ies6 (K114E, Y125A)* form part of the YL1_C domain, which is the putative DNA binding domain, it was reasonable to assume that both residues might contribute to Ies6 DNA binding. Furthermore, the HU sensitivity and impaired recovery of stalled replication forks in this mutant indicate a significant change in the functionality of the mutant protein.

In order to examine this hypothesis, wildtype and Ies6 (K114E, Y125A) MBP-tagged proteins were purified from *E. coli* at concentrations sufficient for DNA biding reactions (Figure 17 B). The proteins were purified under denaturing conditions and returned to their native fold using dialysis. During purification, a small proportion of the protein within each sample was degraded, giving rise to high molecular weight bands in both purifications (Figure 17 B). Given that degradation is a consequence of the purification protocol and appears consistently in all purifications, it was not considered to be a significant variable when proceeding with the DNA binding assay.

Despite K114 and Y125 being within the YL1_C domain of Ies6, the Ies6 (K114E, Y125A) mutant retained its ability to bind dsDNA to wildtype levels (Figure 17 C), this has been clarified through quantification of the levels of free probe within Ies6 and Ies6 (K114E, Y125A) lanes compared to the no protein control (Figure 18 B).

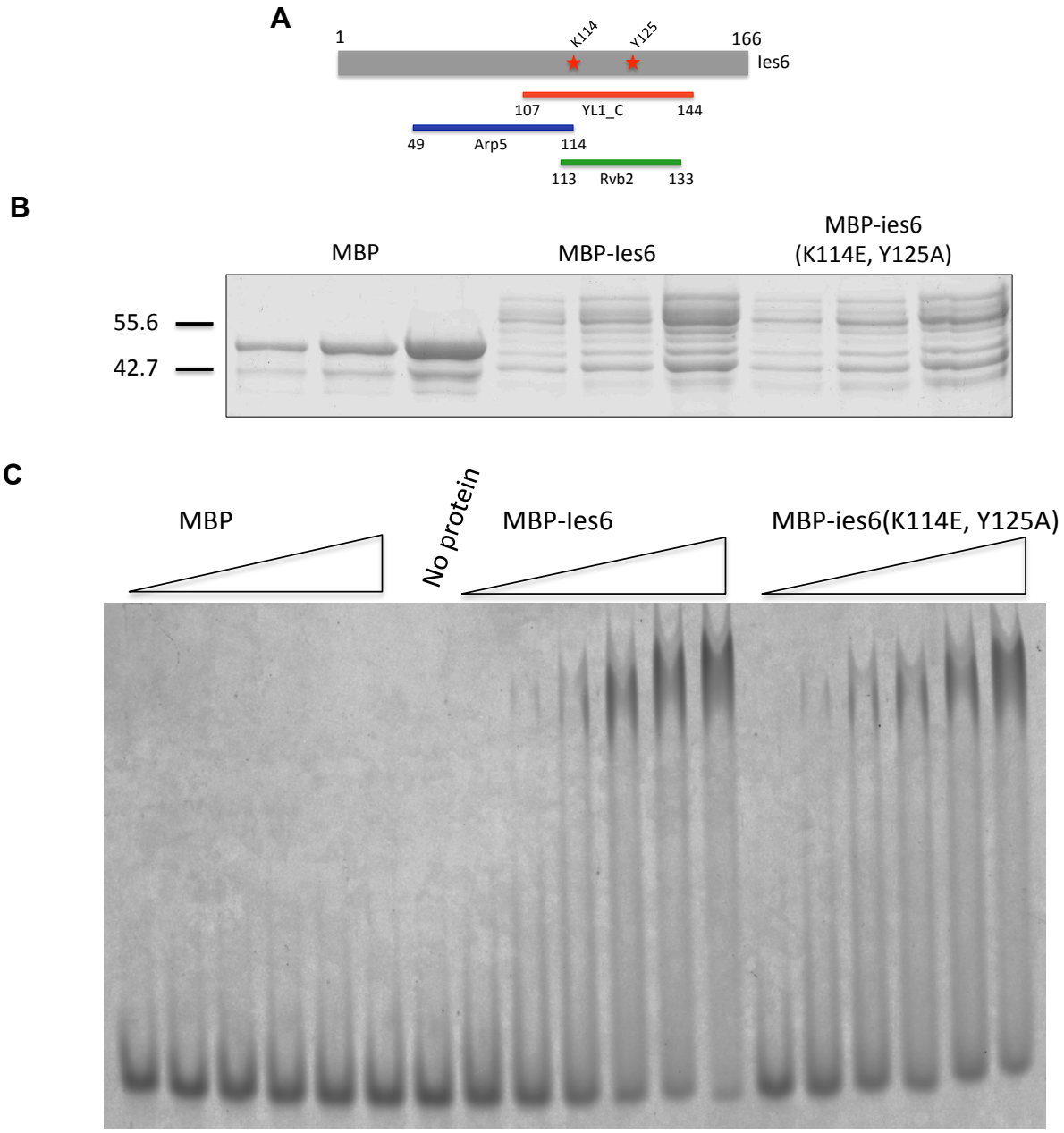

Figure 17: Recombinant ies6(K114E,Y125A) binds dsDNA

A. Schematic of the Ies6 protein showing the amino acid positions of the two interacting regions and the YL1_C domain.

B. Concentrations of eluted proteins from *E. coli* expressing MBP, MBP-Ies6 or MBP-ies6(KII4E,Y125A) were determined by Bradford assay. These were then run on an SDS page gel at 1, 2 and 5µM concentrations and stained with Coomassie.

C. Fluorescently labelled dsDNA was incubated with either MBP, MBP-Ies6 or MBP-ies6(K114E,Y125A) recombinant protein (at 0.5µM, 1.5µM, 2 µM, 2.5 µM and 3µM concentrations) purified from *E.coli.* Bound complexes were then analysed by SDS page and scanned using Fugi FLA-5100 phospho-imager.

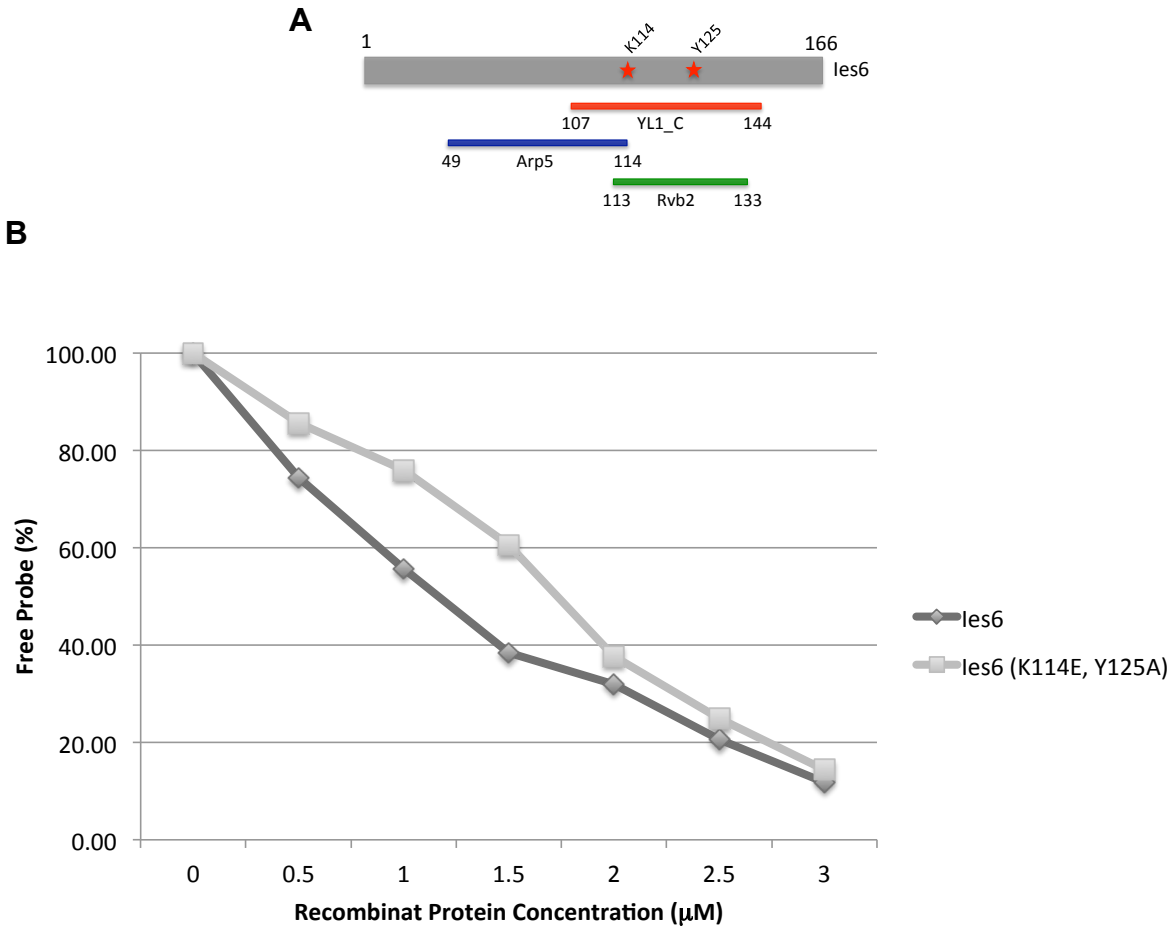

Figure 18: Quantification of the remaining free probe confirms the DNA binding capacity of Ies6 (K114E, Y125A)

A. Schematic of the Ies6 protein showing the amino acid positions of the two interacting regions and the YL1_C domain.

B. Quantification of free probe density using ImageJ. Intensities of free probe for Ies6 and Ies6 (K114E, Y125A) at each concentration (0.5-3µM) was normalised to the density of the no protein (0µM) control. The amount of free probe in react reaction is expressed as a percentage of the total observed in the no protein control

3.1.11 Truncation of ies6 at the C-terminus is sufficient to abolish DNA binding.

To investigate the presence of a DNA binding region with the C-terminus, and with the observation that Ies6 (K114E, Y125A) was still able to bind DNA, truncations were produced (Alžběta Kalendová) that retained only the N-terminus (Ies6 (1-76 aa)) or C-terminus (Ies6 (77-134 aa)) of Ies6. The truncation expressing the C-terminal portion of the protein contained the entire YL1_C domain (Figure 16 A), thus was hypothesised to retain its DNA binding capacity.

Recombinant truncated proteins were purified from *E. coli* (Figure 19 B), as observed with previous purifications of the wildtype and Ies6 (K114E, Y125A) (Figure 17 B), a small proportion of the protein in each was degraded (Figure 19 B). This degradation is a consequence of the purification protocol, thus it appears equally in all the samples tested and does not affect binding of the wildtype recombinant protein, or the comparability of the wildtype and mutant binding within each assay.

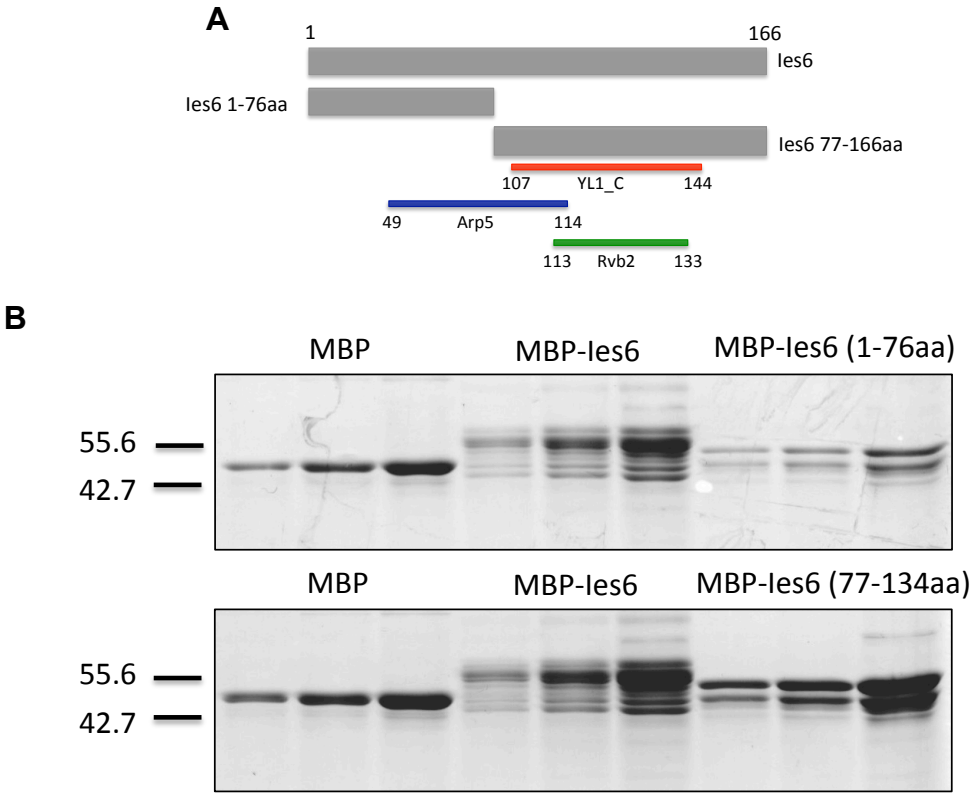

Figure 19: Coomassie stained gels of truncated proteins purified from *E.coli*

A. Schematic of the Ies6 protein showing the amino acid positions of the two interacting regions and the YL1_C domain.

B. Proteins eluted from cells expressing MBP, MBP-Ies6 and MBP-Ies6 77-166 aa were quantified by Bradford assay. These were run on an SDS page gel at 1, 2 and 5μM concentrations and stained with Coomassie. MBP-Ies6 1-76 aa was quantified by Bradford but a loading error means it appears less concentrated. All proteins were added to the same concentration in all subsequent DNA binding reactions.

The purified proteins: Ies6, Ies6 (1-76 aa) and Ies6 (77-134 aa) were assayed for DNA binding capacity. As predicted, the N-terminal portion of Ies6, Ies6 (1-76 aa), had no affinity for dsDNA, while the C-terminal portion containing the YL1_C domain, Ies6 (77-134 aa), retained a DNA binding that appeared to be slightly reduced compared to wildtype (Figure 20 B). Quantification of the levels of free probe within the Ies6 and Ies6 (77-134 aa) reactions demonstrates DNA binding of Ies6 (77-134 aa) at lower concentrations (1-2 μM protein) was reduced compared to wildtype. However, the level of binding was equal in both the wildtype and Ies6 (11-134 aa) at the higher protein concentrations (2.5 and 3 μM) (Figure 21 B).

This observation conclusively demonstrates that the DNA binding component of Ies6 is within the C-terminal, YL1_C domain, portion of the protein. Though, precise mutation of single amino acids failed to determine which residues were important for YL1_C function, abrogated binding upon the loss of the Ies6 YL1_C domain, demonstrates that it is required for Ies6 DNA binding.

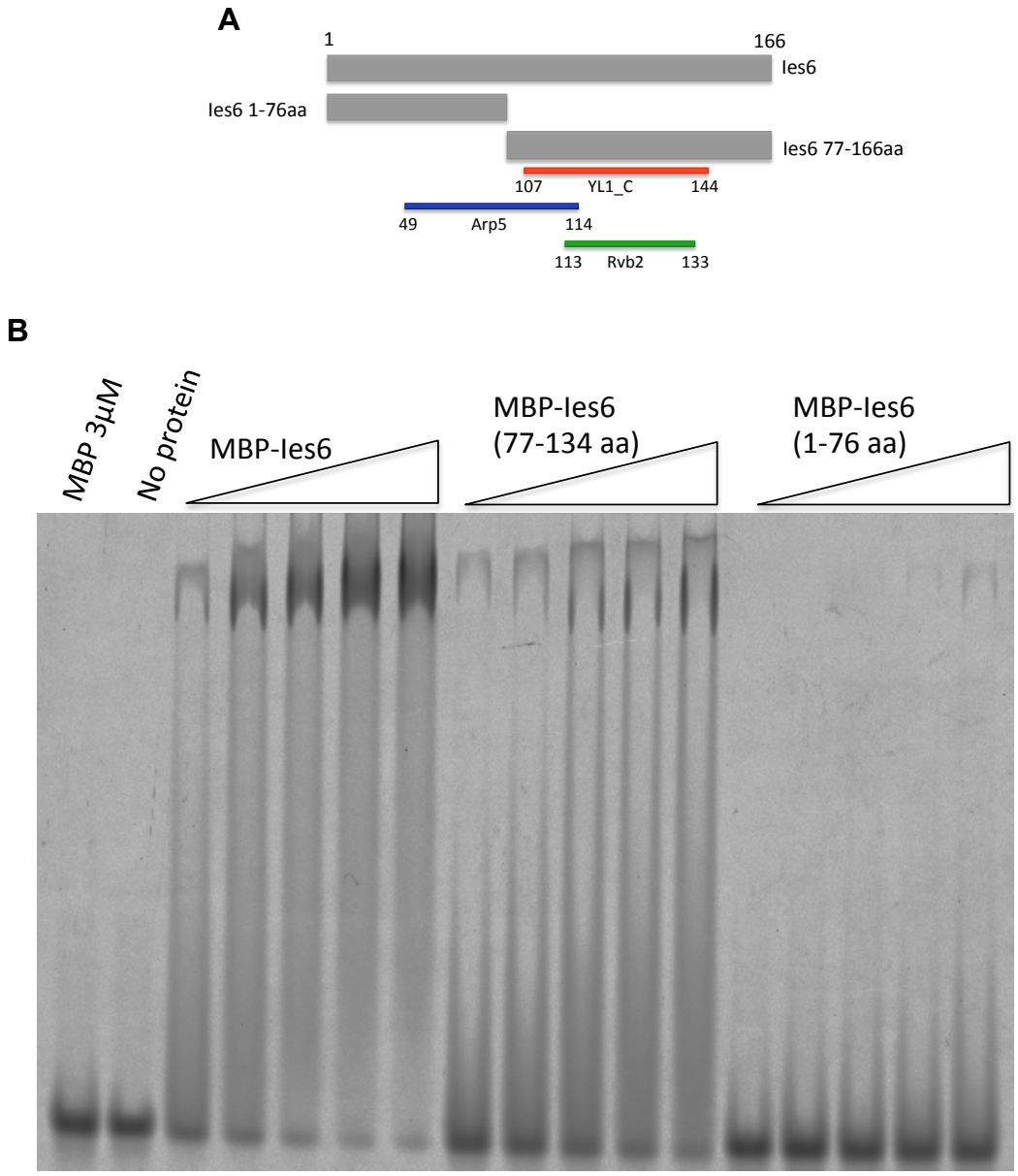

Figure 20: The C-terminus of Ies6 can bind DNA but the N-terminus cannot.

A. Schematic of the Ies6 protein showing the amino acid positions of the two interacting regions and the YL1_C domain with the truncated versions of the Ies6 protein.

B. Fluorescently labelled dsDNA was incubated with recombinant MBP, MBP-Ies6, MBP-Ies6 (77-134 aa) and MBP-Ies6 (1-76 aa) (at 1μM, 1.5μM, 2 μM, 2.5 μM and 3μM concentrations) purified from *E.coli.* Bound complexes were then analysed by SDS page and scanned using Fugi FLA-5100 phospho-imager.

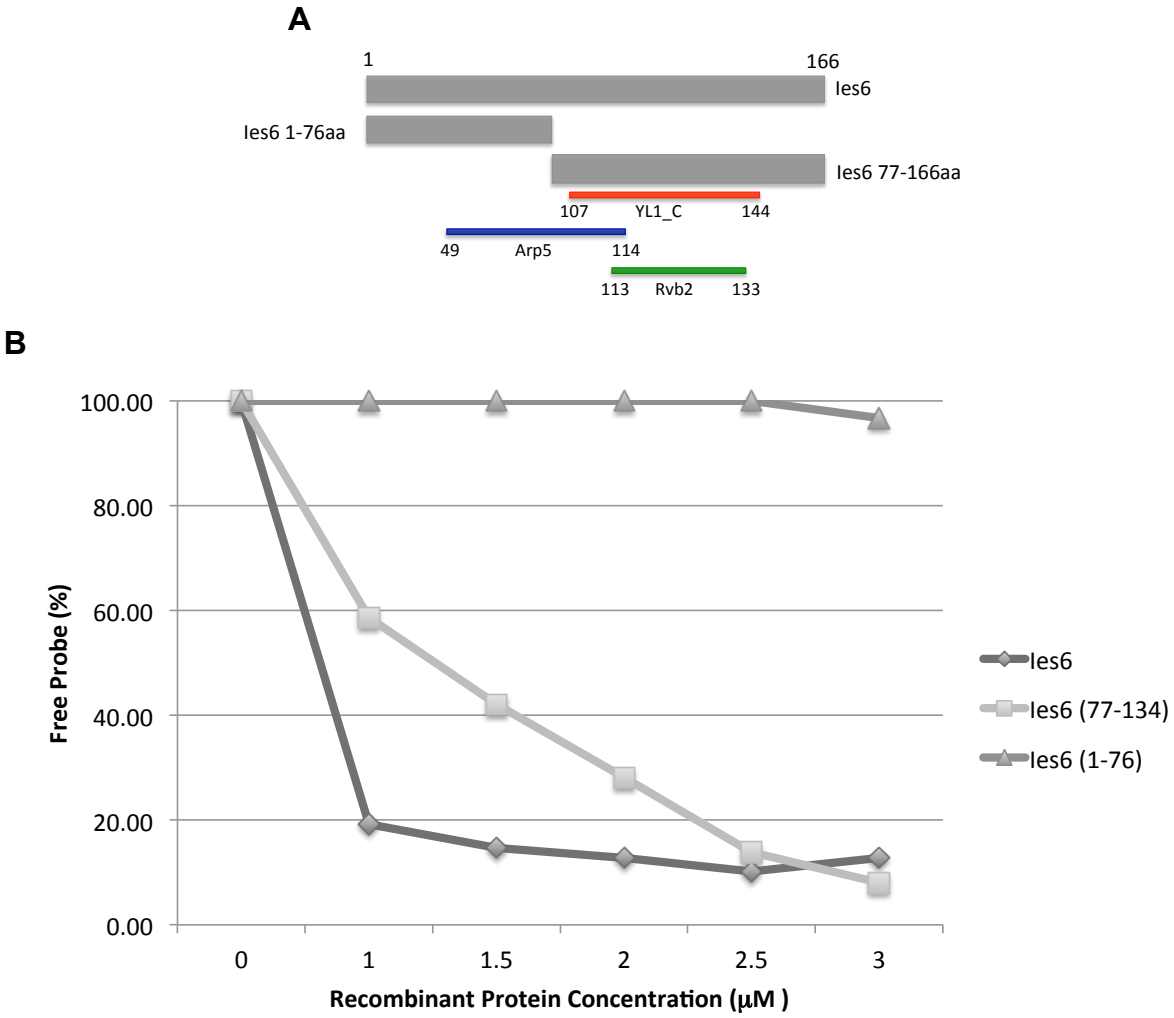

Figure 21: Quantification of the remaining free probe confirms Ies6 (1-76) does not bind to DNA, and DNA binding reduced at lower concentrations Ies6 (77-134).

A. Schematic of the Ies6 protein showing the amino acid positions of the two interacting regions and the YL1_C domain with the truncated versions of the Ies6 protein.

B. Quantification of free probe density using ImageJ. Intensities of free probe for Ies6, Ies6 1-76 aa and Ies6 77-134 aa at each concentration (1-3µM) was normalised to the density of the no protein (0µM) control. The amount of free probe in react reaction is expressed as a percentage of the total observed in the no protein control.

3.2 *IES6* genetically interacts with DNA damage and Chromosome segregation pathways.

The INO80 complex is known to be involved in DNA repair (Van Attikum et al., 2004; Downs et al., 2004; Morrison et al., 2004), chromosome segregation (Ogiwara et al. 2007, Chambers et al. 2012) and H2A.Z removal (Van Attikum et al., 2007; Papamichos-Chronakis et al., 2011). As previously discussed, phenotypic screens on DNA damaging agents can provide preliminary insight into gene function. In addition, these assays can be used to infer genetic relationships between genes within pathways that perform necessary cellular functions. Specific subunits of the INO80 complex are known to genetically interact with genes in the *RAD52* DNA damage response pathway (*RAD52, RAD55* and *RAD9*) through the *ARP8* and *NHP10* genes that encode the Arp8 and Nhp10 subunits of the INO80 complex (Morrison et al., 2004). Specifically, spores that are *arp8Δ* and *rad52Δ* defective exhibit a synthetic growth phenotype (Morrison et al., 2004). Furthermore, the deletion of *arp8* or *nhp10* in conjunction with *rad59* causes increased HU sensitivity at 50mM (Morrison et al., 2004).

RAD52 forms part of the highly conserved Rad52 epistasis group, composed of: *RAD50, RAD51, RAD52, RAD54, RAD55, RAD57, RAD59, RDH54* (*TID1*)*, MRE11* (*RAD58*) and *XRS2*, all of which cause recombination defects when mutated (Symington, 2002). Due to the importance of the Rad52 epistasis group, it was deemed sufficient to only select one gene (*RAD50*) for genetic comparison with *IES6.*

In addition to *RAD50,* other candidate genes were chosen using information submitted to the *Saccharomyces* genome database (SGD). These were: *CIN8* due to its role in chromosome segregation, and its synthetic sickness with *ies6* (Pan et al., 2004), and *SAS3*, as the catalytic core of the NuA4 histone chaperone and its synthetic sickness with *ies6* (Lin et al., 2008).

These previously characterised genetic interactions between IES6 and genes involved in DNA repair and chromosome segregation were utilised to further characterise the *ies6 (K114E, Y125A)* mutation. Ultimately, expression of the *ies6 (K114E, Y125A)* mutant in conjunction with the deletion of genes required for DNA repair or chromosome segregation will demonstrate whether the *ies6(K114E, Y125A)* mutant is defective for multiple Ies6 functions, or, whether it is only defective in one and proficient for all others, known as a separation of function. As the *ies6 (K114E, Y125A)* mutant displayed HU sensitivity it is likely to be important for pathways relating to DNA repair and not those influencing chromatin dynamics or chromosome segregation.

3.2.1 Double knockouts of *ies6*, *cin8* are synthetic lethal.

The gene *CIN8*, which is important for mitotic spindle assembly and chromosome segregation (Hoyt et al., 1992; Roof et al., 1992), was selected to combine with the *ies6 (K114E, Y125A)* allele. A previous study observed that *ies6* null was synthetic sick when combined with a *cin8* deletion strain (Pan et al., 2004). In order to express the *ies6 (K114E, Y125A)* allele within a *cin8* background, a *cin8, ies6* double knockout was obtained by crossing.

In contrast to the previous study, when the progeny of an *IES6/ies6*, *CIN8/cin8* heterozygous diploid were genotyped, only *CIN8/IES6* spores were obtained (Figure 22 A). This indicated a synthetic lethal interaction between *cin8/ies6* rather than a synthetic sickness, as previously stated. Both genes were segregating in a manner that produced only *CIN8/IES6* or *cin8/ies6* genotypes due to the close proximity of the *IES6* and *CIN8* genes, which were only 33kb apart on chromosome V. When constructing the heterozygous diploid, the *cin8* knockout construct was integrated on the same chromosome as the *ies6* knockout cassette, causing them to co-segregate during mitosis (Figure 22 B).

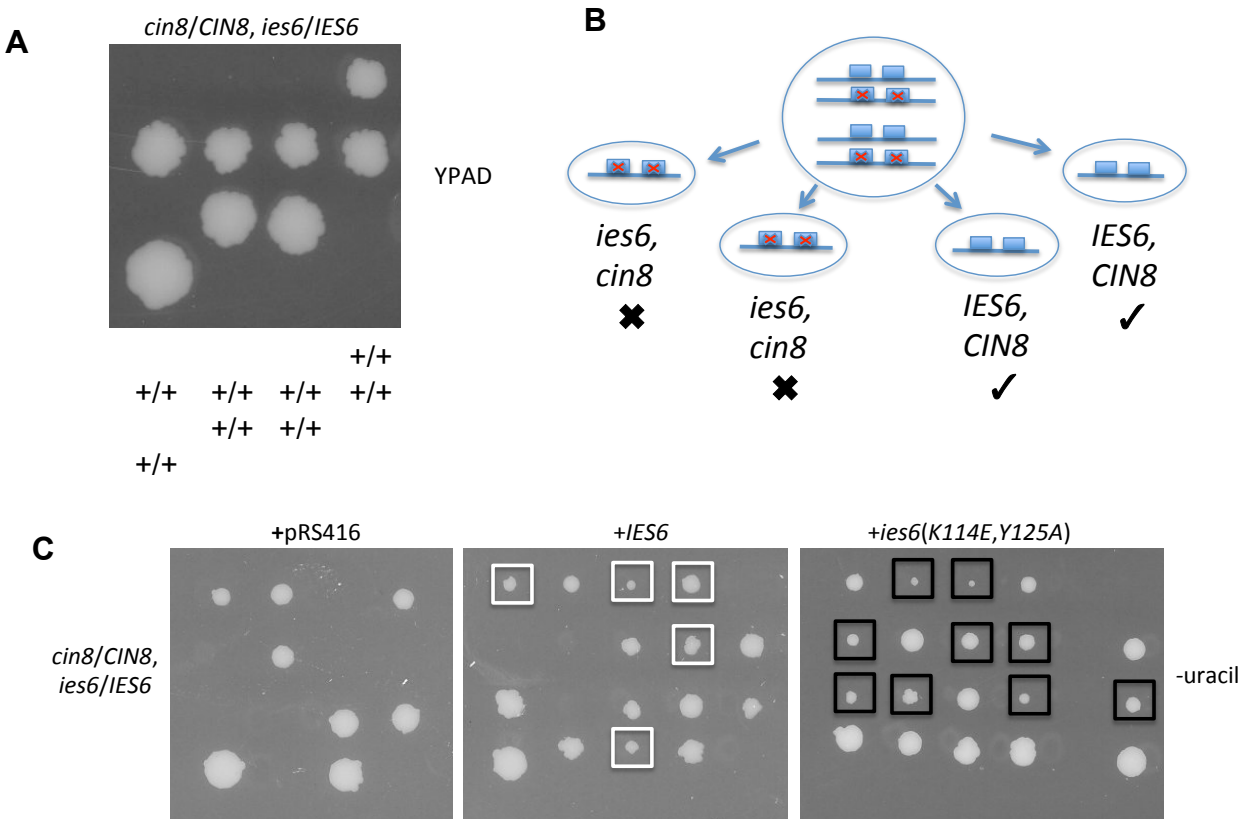

Figure 22: *cin8/ies6* double knockouts cause synthetic lethality, which can be rescued through ectopic expression of *IES6* or *ies6 (K114E,Y125A).*

A. Heterozygous diploids containing *IES6/ies6* and *CIN8/cin8* were dissected onto rich media and grown at 30°C for 3-5 days.

B. Diagrammatic representation of co-segregation occurring during meiosis in the *cin8/ies6* cells that are synthetic lethal.

C. Heterozygous diploids of *cin8/CIN8, ies6/IES6* (JDY1021) expressing either an empty vector, *IES6* or *ies6(K114E,Y125A)* complementation plasmids were dissected onto selective media. White boxes indicate a *cin8, ies6 +IES6* spore and black boxes indicate a *cin8, ies6 +ies6(K114E,Y125A)* spore. Genotypes were verified by re-growth on selection media followed by PCR.

3.2.2 Expression of wildtype *IES6* or *ies6 (K114E, Y125A)* rescues *cin8, ies6* synthetic lethality

The observation that *cin8, ies6* cells caused a synthetic lethality was confirmed by the ability of *IES6* or *ies6 K114E, Y125A)* to rescue the phenotype. Genotyping of the progeny from crosses of *CIN8/cin8*, *IES6/ies6* heterozygous diploids, expressing an *IES6* plasmid, confirmed that expression of the *IES6* gene was sufficient to restore Ies6 functions and rescue the synthetic lethality of the *cin8, ies6* double knockouts (Figure 22 C).

Given the synthetic lethality of *cin8, ies6* cells the only method of obtaining a *cin8, ies6 (K114E, Y125A)* mutant was to express it within the *CIN8/cin8*, *IES6/ies6* heterozygous diploid and analyse the progeny. Providing that expression of the *ies6 (K114E, Y125A)* allele was sufficient to rescue the functions of Ies6 required during meiosis. Indeed, the expression of the *ies6 (K114E, Y125A)* allele was sufficient to rescue the synthetic lethality observed in the *cin8, ies6* knockout (Figure 22 C).

3.2.3 *cin8, ies6 (K114E, Y125A)* mutants are partially growth defective.

Colonies derived from *cin8, ies6 (K114E, Y125A)* spores varied in size comparatively to those derived from *cin8* mutants expressing the *IES6* plasmid, or the *CIN8, IES6* wildtype (Figure 22 C). Quantification of their growth rate revealed only a mild growth defect, however, this was equal to the *ies6 (K114E, Y125A)* allele alone (Figure 23). This observation suggests that *cin8* and *ies6 (K114E, Y125A)* do not genetically interact within pathways critical for cell growth.

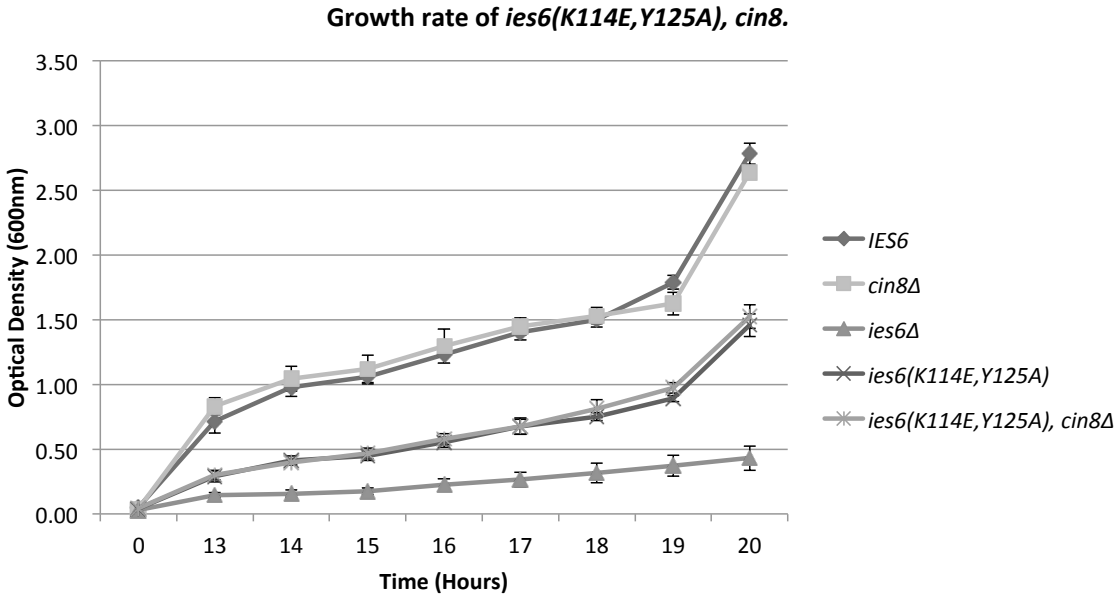

Figure 23: Growth defects observed in the *ies6(K114E,Y125A), cin8* mutant is comparable to an *ies6(K114E, Y125A)* single mutant.

Genotyped spores produced from the sporulation of heterozygous diploid of *cin8*/*CIN8*, *ies6*/*IES6* (JDY1021) containing *IES6* or *ies6 (K114E, Y125A)* expression plasmids were used to analyse the growth defects resulting from various *ies6* and *cin8* genotypes.

These genotypes were: *IES6* (wildtype), *ies6*, *cin8* (*ies6*, *cin8* +pRS416- Flag-*IES6*, JDY1021), *ies6* (*ies6* +pRS416- Flag-*IES6*), *ies6 (K114E, Y125A)* (*ies6* +pRS416- Flag-*ies6 (K114E, Y125A)*) and *ies6 (K114E, Y125A), cin8* (*ies6*, *cin8* +pRS416- Flag-*ies6 (K114E, Y125A)*). Each spore was grown for 20 hours at 30°C. Error bars represent standard deviation of triplicates.

3.2.4 *cin8, ies6 (K114E,Y125A)* mutants are sensitive to HU, but not MMS or benomyl

Further screening of the *cin8*, *ies6 (K114E, Y125A)* cells with DNA damaging agents known to inhibit Ies6 functions (HU, MMS and benomyl) were conducted for further characterisation of the *cin8, ies6 (K114E, Y125A)* mutant.

Comparisons to the HU, MMS and benomyl plates revealed that *cin8*/*ies6 (K114E, Y125A)* cells have a slight sensitivity to HU at 20mM, however, not significantly greater than the *ies6 (K114E, Y125A)* single allele (Figure 24). Sensitivity of the *cin8*/*ies6 (K114E, Y125A)* cells to MMS at 0.01% and benomyl at 10 μg/ml were identical to the *ies6 (K114E, Y125A)* allele alone, therefore cannot be attributed to a relationship between *cin8* and *ies6 (K114E, Y125A)*.

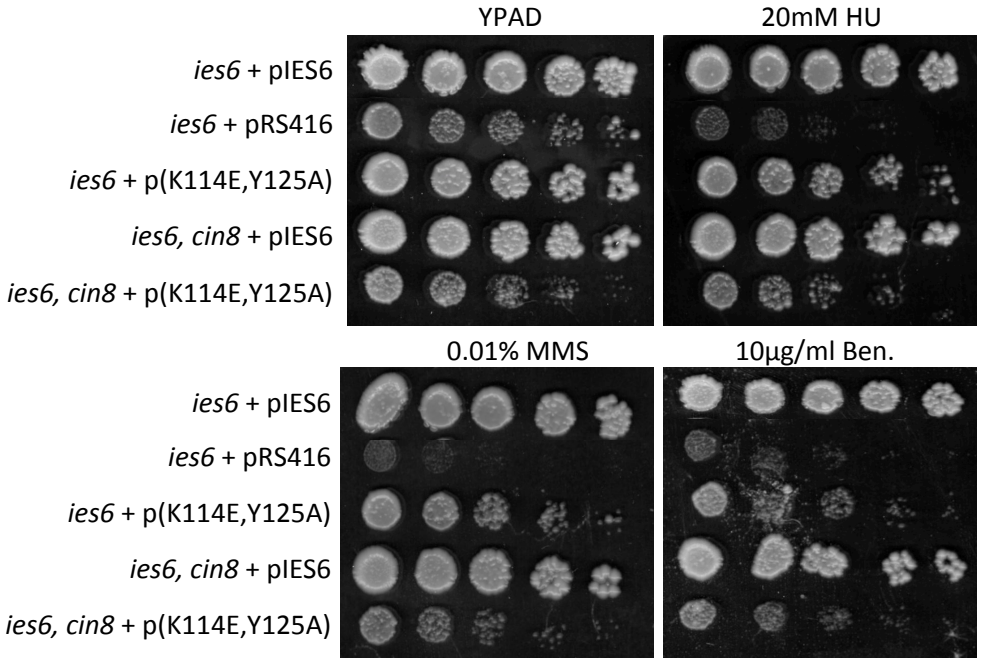

Figure 24: Sensitivity of *cin8, ies6(K114E,Y125A)* cells to benomyl and HU.

Genotyped spores produced from the sporulation of heterozygous diploid of *cin8*/*CIN8*, *ies6*/*IES6* (JDY1021) containing *IES6* or *ies6 (K114E, Y125A)* expression plasmids were used to analyse the drug sensitivity of the various *ies6* and *cin8* genotypes. These genotypes were: *IES6* (wildtype), *ies6, cin8* (*ies6, cin8* +pRS416-Flag-*IES6*, JDY1021), *ies6* (*ies6* +pRS416- Flag-*IES6*), *ies6 (K114E, Y125A)* (*ies6* +pRS416- Flag-*ies6 (K114E, Y125A)*) and *ies6 (K114E, Y125A), cin8* (*ies6, cin8* +pRS416- Flag-*ies6 (K114E, Y125A)*). Plates were incubated at 30°C for 3 days. There was a slight sensitivity to HU when *ies6, cin8* cells were expressing the *ies6 (K114E, Y125A)* plasmid.

3.2.5 Double knockouts of *sas3*, *ies6* are synthetic sick.

The second gene, *SAS3*, was utilised due to it's published interaction with *IES6* (Lin et al., 2008). Double knockouts for analysis with *ies6 (K114E, Y125A)* were obtained from the progeny of an *IES6/ies6*, *SAS3/sas3* heterozygous diploid. Consistent with previous reports, the *ies6/sas3* double knockouts were synthetically sick when compared to the corresponding wildtype and each single mutant (Figure 25 A).

The reduced growth of the *ies6, sas3* double knockouts compared to either single, indicates that there is an additive genetic effect on fitness when both genes have been removed. This suggests that the *SAS3* and *IES6* genes may be contributing to different pathways for functions influencing cell growth. Quantification of their growth rate demonstrated that *ies6, sas3* cells were significantly impaired, and achieving only a single doubling of optical density after 20 hours of incubation (Figure 25 C). However, cells were not quantified using a haemocytometer, which would eliminate any discrepancies in optical density resulting from cell size.

Considering their significant delay in progression through the cell cycle, it is reasonable to assume that a compensatory pathway, usually active in the absence of *IES6*, has now been removed through the deletion of *sas3*, causing an additive effect on growth impairment. To investigate this hypothesis, DNA damaging agents, which test known pathways of Ies6 function (HU, MMS and benomyl), were used to screen the *ies6, sas3* double knockouts.

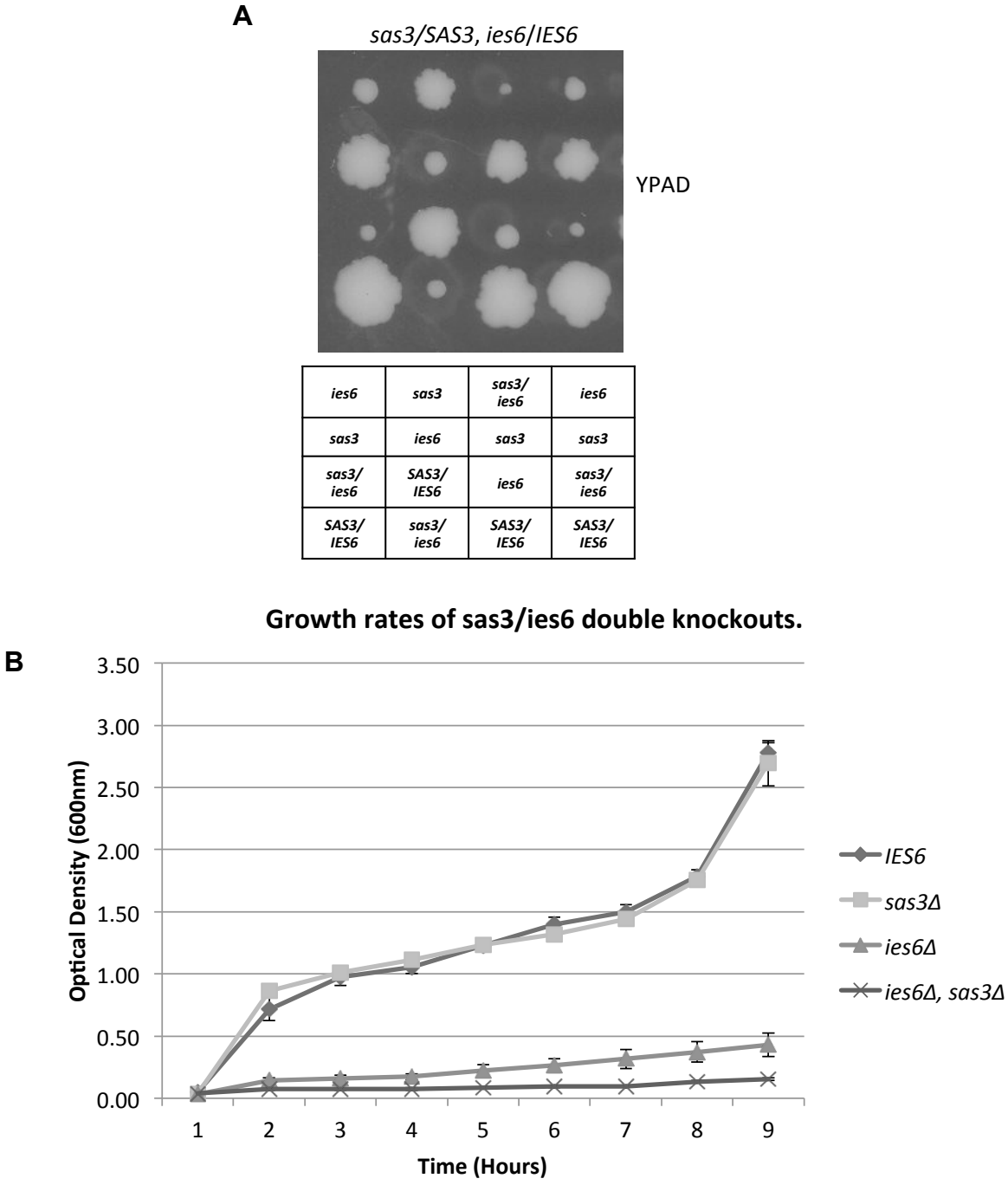

Figure 25: *ies6/sas3* are synthetic sick in BY4741.

A. Heterozygous diploids carrying both the wildtype and a deletion of *IES6* and *SAS3* (*ies6*/*IES6*, *sas3*/*SAS3*, JDY1015) were sporulated and dissected onto rich media and grown at 30°C for 3-5 days.

B. The resulting spores containing *sas3* and *ies6* deletions were growth defective. The optical density (260 nM) of wildtype, *ies6, sas3* (JDY1016), or *sas3, ies6* (JDY1017) spores was measured periodically during 20 hours of growth at 30°C. Error bars represent standard deviation.

3.2.6 *sas3, ies6* knockouts are sensitive to HU

The genotyped spores from a single tetrad, the progeny of an *IES6/ies6*, *SAS3/sas3* heterozygous diploid, were grown to mid-log and plated on varying concentrations of HU, MMS and benomyl within ranges where sensitivity had previously been observed for the *ies6* null. These concentrations were far too high and completely lethal to the *ies6/sas3* double knockout (data not shown). After testing a range of doses for each damaging agent, optimal concentrations for observation of comparative sensitivities were obtained. Within these ranges it was evident that *ies6, sas3* double knockouts were more sensitive to 10 mM HU compared to *ies6* (Figure 26). However, benomyl and MMS sensitivity was similar to that observed for the *ies6* null (Figure 26).

Due to the additive effect on HU sensitivity when combining the *ies6* and *sas3* deletion mutants, it is possible that these two genes are acting in separate pathways, which may contribute to replication. Insensitivity to MMS and benomyl suggests that any relationship between *IES6* and *SAS3* is not required for MMS or benomyl exposure.

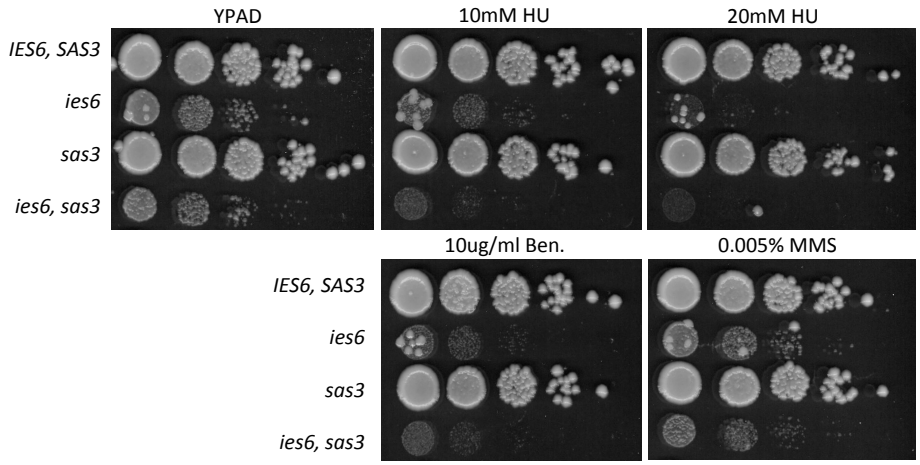

Figure 26: Sensitivity of *sas3*, *ies6* to HU, benomyl and MMS.

Spores from the previous growth curve analysis (wildtype, *ies6, sas3* (JDY1016) and *ies6, sas3* (JDY1017)) that were generated from the sporulation of the heterozygous diploid *ies6/IES6, sas3/SAS3* (JDY1015), were grown to mid-log and plated from serial dilutions and incubated at 30°C for 3 days. The *sas3, ies6* cells were more sensitive to 10mM HU than *ies6*, but insensitive to benomyl or MMS.

3.2.7 *sas3, ies6 (K114E,Y125A)* cells are partially growth defective and insensitive to DNA damaging agents.

Analysis of the *ies6 (K114E, Y125A)* mutant had indicated a sensitivity to 100 mM HU. Subsequent characterisation demonstrated this HU sensitivity was a result of an inability to recover from replication fork stalling, causing cell lethality. Characterisation of the *ies6, sas3* double knockout demonstrated a sensitivity to extremely low doses of HU (10 nM). Given this increased sensitivity, it was logical to test whether the expression of the *ies6(K114E, Y125A)* was able to rescue the increased sensitivity of *sas3, ies6* double knockouts, or if the additive effect of the *sas3, ies6* knockout was due to the influence of residues mutated within the *ies6 (K114E, Y125A)* allele.

Quantification demonstrated the *ies6 (K114E, Y125A), sas3* strain had a growth rate that was similar to the *ies6 (K114E, Y125A)* allele alone (Figure 27 A), indicating that the mutation of K114 to glutamine and Y125 to alanine within Ies6 had no adverse effect on the function of the Sas3 protein. Furthermore, the *ies6 (K114E, Y125A), sas3* strain was insensitive to high doses of HU, MMS and benomyl (Figure 27 B).

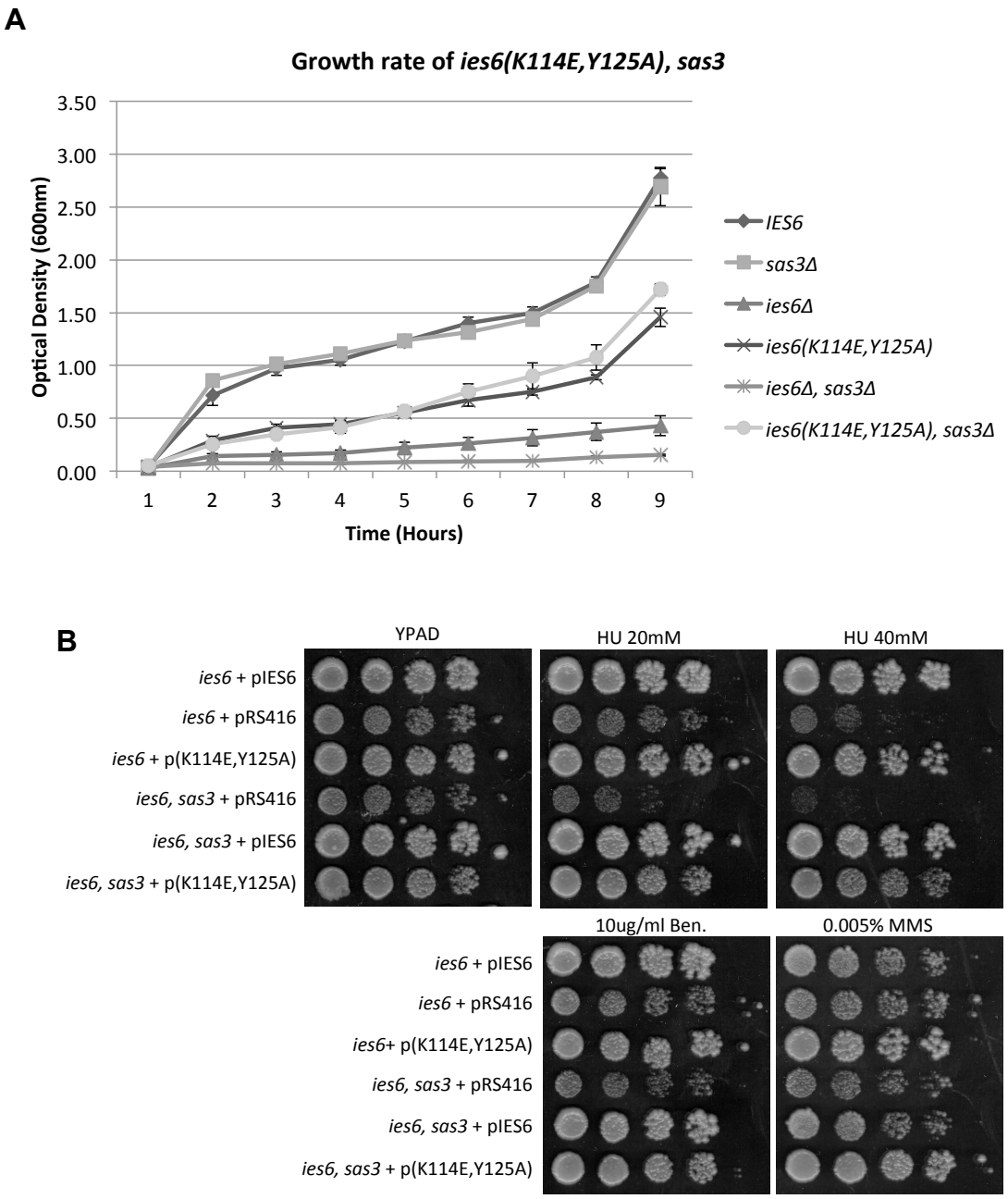

Figure 27: *ies6 (K114E,Y125A)*, *sas3* cells have an intermediate growth defect, but are insensitive to DNA damaging agents.

A. Cells endogenously deficient for *ies6* (JDY854), *sas3* (JDY1016) or *sas3, ies6* (JDY1017) were transformed with either an empty vector, *IES6* or *ies6 (K114E, Y125A)* expression plasmid. These cells were then grown for 20 hours at 30°C to measure growth rate by optical density at 260 nM. Error bars represent standard deviation of triplicates.

B. Transformed cells used to assay growth, *ies6* (JDY854), *sas3* (JDY1016) or *sas3, ies6* (JDY1017) containing either an empty vector, *IES6* or *ies6 (K114E, Y125A)* expression plasmid, were grown to mid-log and plated from serial dilutions. Plates were incubated at 30°C for 3 days.

3.2.8 Double knockouts of *rad50*, *ies6* are synthetic sick.

To examine the synthetic sickness of the final gene, *RAD50*, selected due to its interaction with *ARP8* and *NHP10* (Morrison et al., 2004), progeny from *IES6/ies6, RAD50/rad50* heterozygous diploids were obtained and genotyped (Figure 25 B). Similarly to *sas3, ies6* cells (Figure 25 A), spores genotyped as *rad50, ies6* double knockouts formed smaller colonies than either single mutant or wildtype (Figure 25 B).

Quantifying of growth rate revealed *rad50, ies6* cells showed a significant defect, as observed with the *sas3, ies6* cells, and only completed a single doubling during the 20 hour incubation period (Figure 28 B). Such a significant delay is consistent with *RAD50* and *IES6* acting within two separate pathways that promote cell cycle progression, as the loss of either gene alone did not have a significant effect on the cell cycle. To further the understanding of the pathways relating to Ies6 function critical to the reduced fitness of the *rad50, ies6* mutant, they were assayed for sensitivity to HU, MMS and benomyl.

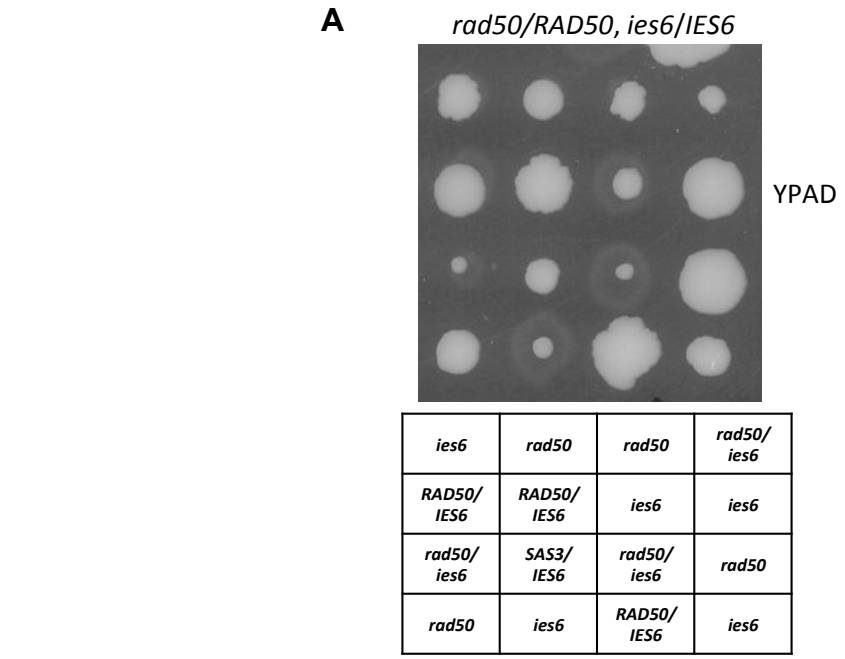

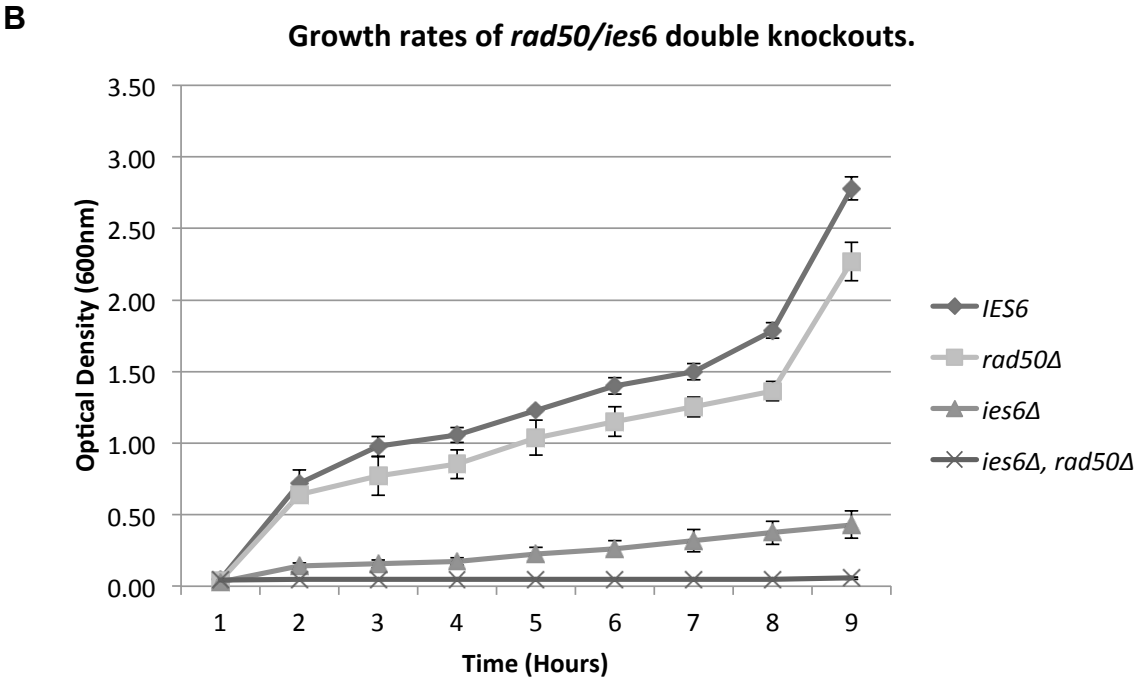

Figure 28: *ies6/rad50* are synthetic sick in BY4741.

A. Heterozygous diploids carrying both the wildtype and a deletion of *IES6* and *RAD50* (*ies6*/*IES6*, *rad50*/*RAD50*, JDY1018) were sporulated and were dissected onto rich media and grown at 30°C for 3-5 days.

B. The optical density (260 nM) of wildtype, *ies6, rad50* (JDY1019), or *rad50, ies6* (JDY1020) spores was measured periodically during 20 hours of growth at 30°C. The resulting spores containing *rad50* and *ies6* deletions were growth defective. Error bars represent the standard deviation of triplicates.

3.2.9 *rad50, ies6* knockouts are sensitive to HU and MMS.

Similarly to the *ies6, sas3* knockouts, the *ies6, rad50* double knockouts were screened for their sensitivity to HU, benomyl and MMS. In contrast to the *sas3, ies6* double knockouts, *rad50, ies6* cells required much lower doses of HU, benomyl and MMS were to visualise the sensitivity ranges, as the dose ranges applicable to *ies6* null cells were lethal (data not shown).

Consistent with the function of *RAD50* in the DNA damage response, *rad50* null cells were sensitive to 0.00125% MMS (Figure 24), far lower than the 0.01% range where *ies6* null cells become sensitised. Subsequently, the deletion of both *rad50* and *ies6* in the *rad50, ies6* knockout resulted in and additive sensitivity at 0.00125% MMS, and lethality at 0.025% (Figure 29). This additive effect on MMS sensitivity suggests that the *RAD50* and *IES6* genes could be acting in separate pathways for DNA damage or replication, as MMS sensitivity can be measure of stalled replication due to forks colliding with bulky methyl groups.

Furthermore, the *rad50* null was also sensitive to 10 mM HU comparatively to the *ies6* null, where sensitivity is observed at 80 mM HU. In contrast, sensitivity was observed at 5mM HU for the *rad50, ies6* double knockout. The additive effect on HU would suggest that *RAD50* and *IES6* may be contributing to separate pathways for replication stress recovery.

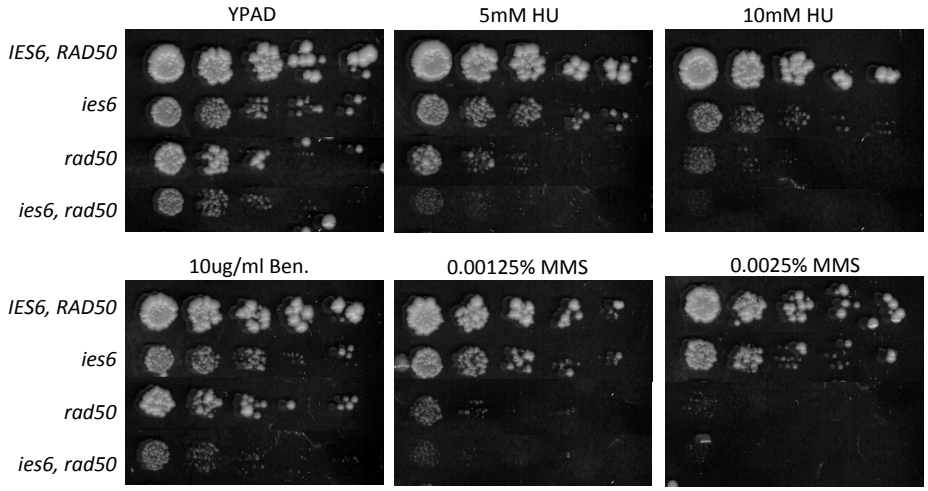

Figure 29: Sensitivity of *rad50*, *ies6* cells to HU, benomyl and MMS.

Spores from the previous growth curve analysis (wildtype, *ies6, rad50* (JDY1019) and *ies6, rad50* (JDY1020)) that were generated from the sporulation of the heterozygous diploid *ies6/IES6*, *rad50/RAD50* (JDY1018), were grown to mid-log and plated from serial dilutions and incubated at 30°C for 3 days. The *rad50*, *ies6* cells were sensitive to HU and MMS, but not benomyl.

3.2.10 *rad50, ies6 (K114E, Y125A)* mutants have no additional growth defects, but are sensitive to HU and MMS.

Following the observation that the *ies6, rad50* double knockout is increasingly sensitive to both HU and MMS, the functionality of the *ies6 (K114E, Y125A)* allele within this interaction was tested.

Analysis of the *rad50*, *ies6 (K114E, Y125A)* growth rate demonstrated a growth defect that was intermediate of the wildtype and the *ies6, rad50* double knockout, however, no greater than the single *ies6 (K114E, Y125A)* allele (Figure 30 A). This similarity to the *ies6 (K114E, Y125A)* allele would suggest that the K114 and Y125 residues of Ies6 have no effect on the *RAD50, IES6* genetic pathway. However, to further ascertain the effect of the *ies6 (K114E, Y125A)* allele on *IES6* function with *RAD50*, the *rad50, ies6 (K114E, Y125A)* mutant was screened for its sensitivity to HU, benomyl and MMS.

Subsequently, the *rad50, ies6 (K114E, Y125A)* strain was screened for sensitivity to HU, MMS and benomyl to examine their genetic interactions for and possible contributions towards the pathways of replication, DNA damage and chromosome segregation. Given that the *ies6 (K114E, Y125A)* allele is HU sensitive, it was likely that its expression in the *ies6/rad50* double knockout may increase sensitivity above either the *ies6 (K114E, Y125A)* allele or *rad50* null. Consistent with the results previously observed for the *ies6, rad50* double knockout, sensitivity was observed at 10 mM HU and 0.00125% MMS (Figure 30 B).

Surprisingly, addition of the *ies6 (K114E, Y125A)* allele to this strain rescued the sensitivity to HU, MMS and benomyl (Figure 30 B). The mechanism behind the rescue of *rad50* sensitivity is unclear, however, the levels of growth on each drug

were comparable to other strains. Growth on HU was comparable to the *ies6* null, where as growth on MMS was significantly reduced compared to *ies6,* but significantly better than *rad50*, and growth on benomyl was comparable to the *ies6 (K114E, Y125A)* allele. With no discernable pattern emerging further analysis is required to quantify the level of recue observed. Overall these observations suggest that the K114 and Y125 residues of Ies6 may be important for replication, but is potentially in a separate pathway to *rad50*.

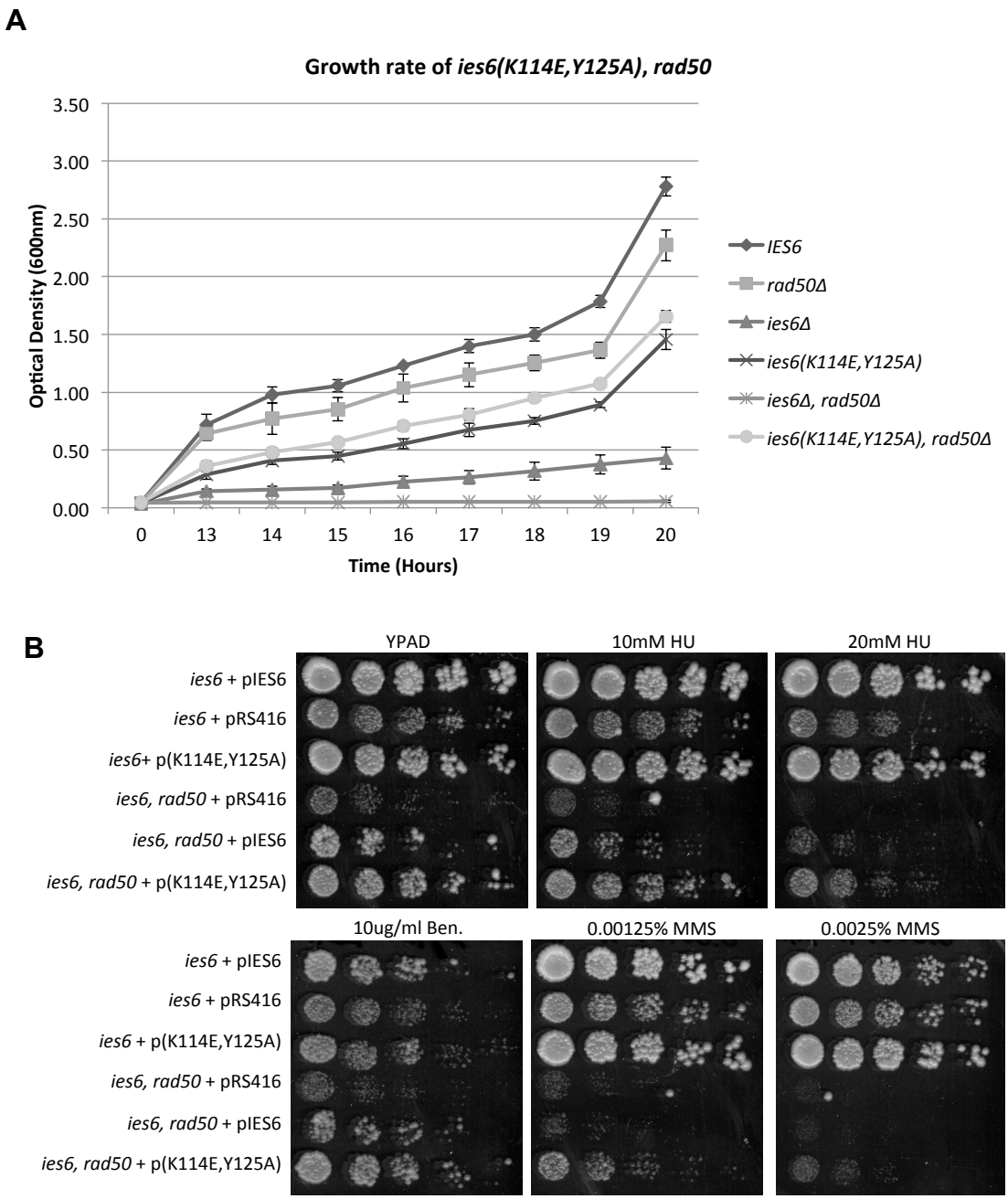

Figure 30: *ies6(K114E,Y125A)*, *rad50* cells have a partial growth defect and are sensitive to MMS and HU, but not benomyl.

A. Cells endogenously deficient for *ies6* (JDY854), *rad50* (JDY1019) or *rad50*, *ies6* (JDY1020) were transformed with either an empty vector, *IES6* or *ies6 (K114E, Y125A)* expression plasmid. These cells were then grown for 20 hours at 30°C to measure growth rate by optical density at 260 nM. Error bars represent standard deviation.

B. Transformed cells used to assay growth, *ies6* (JDY854 *rad50* (JDY1019) or *rad50, ies6* (JDY1020) containing either an empty vector, *IES6* or *ies6 (K114E, Y125A)* expression plasmid, were grown to mid-log and plated from serial dilutions. Plates were incubated at 30°C for 3 days.

Table 7: Comparison of the *rad50/sas3/cin8* combinations with *ies6 (K114E, Y125A)* demonstrate there is a separation of function. Only when *ies6 (K114E, Y125A)* combined with *rad50* deletion, is their an increase in sensitivity to HU and MMS.

Testing…	Mutant	Growth	MMS (0.005-0.01%)	HU (10-20mM)	Benomyl (10µg/ml)
-	WT	++++	++++	++++	++++
-	*ies6*	+	++	++	+
-	*ies6(K114E, Y125A)*	++	++++	++++	++++
DNA repair	*rad50*	++++	-	+	++++
	ies6/rad50	+	-	-	+
	ies6(K114E, Y125A)/rad50	++	+	+	++++
Chromosome Segregation	*cin8*	++++	++++	++++	++++
	ies6/cin8	-	-	-	-
	ies6(K114E, Y125A)/cin8	++	++++	+++	++++
Histone mobility	*sas3*	++++	++++	++++	++++
	ies6/sas3	+	++	+	+
	ies6(K114E, Y125A)/sas3	++	++++	++++	++++

Insensitive (++++)
Slight sensitivity (+++)
Intermediate sensitivity (++)
Highly sensitive (+)
Lethal (-)

3.3 The contribution of H2A.Z acetylation to wildtype cellular ploidy in *ies6* null cells

Cells deficient for *ino80* or *ies6* spontaneously undergo a genome duplication event, with associated phenotypes of a slow cell cycle progression, HU sensitivity and benomyl sensitivity (Chambers et al. 2012). This genome duplication event is coupled with an increase of H2A.Z at centromeres, which is detrimental to centromere structure and function (Chambers et al. 2012). Defects in the centromere structure are thought to cause chromosome instability and segregation errors in the *ino80* and *ies6* null cells, leading to the observed genome duplication (Chambers et al. 2012). Additionally, *ies6* null cells demonstrated decreased levels of K14 acetylation by western blot and H2A.Z overexpression exacerbates the rate at which *ies6* null cells undergo a whole genome duplication event (Chambers et al. 2012).

The INO80 complex in *S. cerevisiae* is known to be involved in H2A.Z removal (Van Attikum et al., 2007; Papamichos-Chronakis et al., 2011). In *S. cerevisiae*, the SWR1 complex incorporates H2A.Z through an interaction with the YL1 histone-binding domain of the Swc2 catalytic subunit (Wu et al., 2005). This incorporation additionally requires Esa1-dependent acetylation of the H2A.Z histone's N-terminal tail (Keogh et al., 2006). However, such a requirement for acetylation upon H2A.Z removal by the INO80 complex has not yet been identified.

Cells deficeint for both *ino80* and H2A.Z acetylation, carrying the *htz1 (K-R)* set of point mutations (disrupting the acetylated lysines in the N-terminal tail) miss-incorporate H2A.Z across the genome and are HU sensitive (Papamichos-

Chronakis et al., 2011). However, the *htz1 (K-R)* allele alone was not observed to have HU sensitivity (Papamichos-Chronakis et al., 2011). Furthermore, the *htz1 (K-R)* has been linked to a lack of sister chromatid cohesion, which results in increased chromosome separation (Sharma et al., 2013).

Considering the data that suggests the INO80 complex, namely Ino80 and Ies6, play important roles in the removal to H2A.Z (van Attikum et al. 2007; Papamichos-Chronakis et al. 2011; Chambers et al. 2012) it was logical to examine the relationship between H2A.Z acetylation and Ies6 more closely, specially how the presence of H2A.Z acetylation influences the genome duplication event.

3.3.1 Cells expressing a H2A.Z acetylation mimic do not increase cellular ploidy regardless of *ies6*.

Deletion of either *ies6* or *ino80* causes a rapid increase in ploidy after approximately 30 generations, equal to 3-4 days (Chambers et al. 2012). Furthermore, this study demonstrated H2A.Z overexpression exacerbates the *ies6* polyploid phenotype (Chambers et al. 2012). To better understand the possible relationship between the INO80 complex and H2A.Z acetylation, newly generated *ies6* and *htz1* null haploids, expressing the *htz1 (K-Q)* mutant were produced. The *htz1 (K-Q)* mutant contains glutamine substitutions at K3, 8,10 and 14 (Yu et al., 2013). Substitution of lysine with glutamine mimics acetylation due its similar structure and charge, which can replace acetylation in vivo (Li et al., 2002). Cells deficient for both *ies6* and *htz1*, but expressing the *htz1 (K-Q)* plasmid were

monitored by FACS over a 10 day period, enough to grow beyond 30 generations, which is the approximate time at which *ies6* cells become polyploid.

As expected, *ies6* cells behaved as reported and quickly duplicated their genome (Figure 31 B). However, complete removal of *htz1*, or the expression of the *htz1 (K-Q)* plasmid, had no effect on the wildtype level of ploidy (Figure 31 A). Furthermore, the *ies6, htz1* double mutant expressing the *htz1 (K-Q)* had no effect on the ploidy phenotype observed in *ies6* null cells (Figure 31 B).

The lack of an abnormal ploidy phenotype in the *htz1 (K-Q)* suggests there is no significance of H2A.Z acetylation for chromosome segregation pathways that influence the maintenance of correct cellular ploidy. In addition, the observation that *ies6* cells expressing the acetylation mimic do not show a rate of ploidy different from the *ies6* null, would suggest that increasing H2A.Z acetylation does not contribute to the maintenance of correct cellular ploidy in these cells.

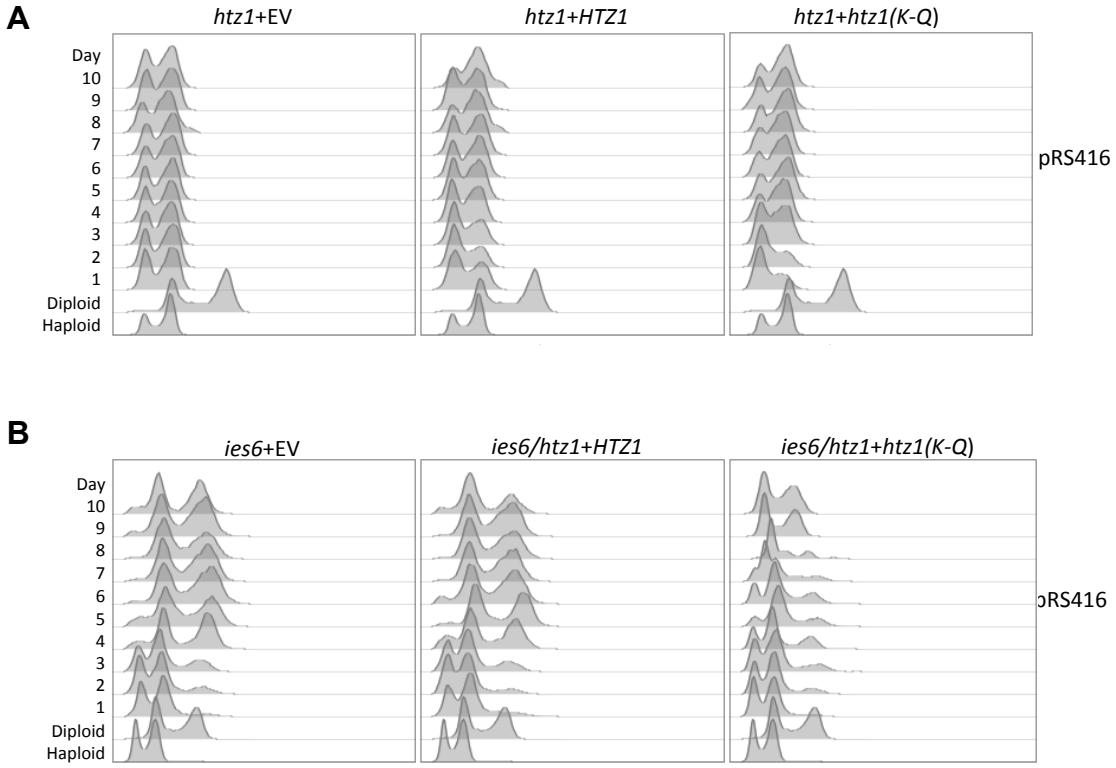

Figure 31: Expression of the *htz1 (K-Q)* acetylation mimic has no effect on ploidy, regardless of *ies6* deletion.

A. Sporulation of a *ies6/IES6, htz1/HTZ1* heterozygous diploid (JDY968) transformed with either the pRS416 empty vector, pRS416-*HTZ1* or pRS416-*htz1(K-Q)* generated *htz1*, *htz1 +HTZ1* and *htz1 +htz1(K-Q)* cells . FACS analysis demonstrated that deletion of *htz1*, or the presence of the *htz1(K-Q)* acetylation mimic, has no influence on cellular ploidy.

B. Sporulation of a *ies6/IES6, htz1/HTZ1* heterozygous diploid (JDY968) transformed with either the pRS416 empty vector, pRS416-*HTZ1* or pRS416-*htz1(K-Q)* generated *ies6*, *ies6*, *htz1 +HTZ1* and *ies6*, *htz1 +htz1(K-Q)* cells . FACS demonstrated that expression of the *htz1(K-Q)* acetylation mimic within an *ies6* null has no influence on *ies6* ploidy.

3.3.2 Expression of unacetylatable H2A.Z accelerates the *ies6* dependent polyploid phenotype.

Given the observation that *htz1 (K-Q)* had no effect on ploidy when expressed alone or in conjunction with the *ies6* deletion. Next, an acetylation deficient mutant was analysed to examine its influence on cellular ploidy.

The loss of acetylation observed in the *htz1 (K-R)*, which contains arginine substitutions at K3, 8,10 and 14 and acts as an acetyl-mutant (Yu et al., 2013). This mutant has previously been shown to increase HU sensitivity in an *ino80* null (Papamichos-Chronakis et al., 2011), and the *htz1 (K-R)* mutant alone has detrimental effects on cohesin and chromosome stability (Sharma et al., 2013). Given these previous findings, it was probable that *htz1 (K-R)* mutant may influence cellular ploidy, however, it had no effect and the DNA content remained consistent with wildtype haploids throughout the experiment (Figure 32 A). In contrast, *ies6* null cells expressing the *htz1 (K-R)* acetyl-mutant showed a rapid increase in the rate at which they became polyploid compared to the *ies6* null (Figure 32 B). Cells in this population were already displaying a DNA content consistent with a diploid cell after 1 day in culture, compared to 3 days for the *ies6* null cells.

The acceleration of the aberrant ploidy increase in *ies6* null cells lacking H2A.Z acetylation suggests that H2A.Z acetylation status is important for the roles of *ies6* and *ino80* in H2A.Z incorporation, which is consistent with previous data (Chambers et al. 2012). However, the loss of the acetylation alone having no effect

on ploidy would suggest that H2A.Z acetylation does not directly influence factors that are important for the maintenance of cellular ploidy, at least not in the presence of an intact INO80 complex containing both *ies6* and *ino80*.

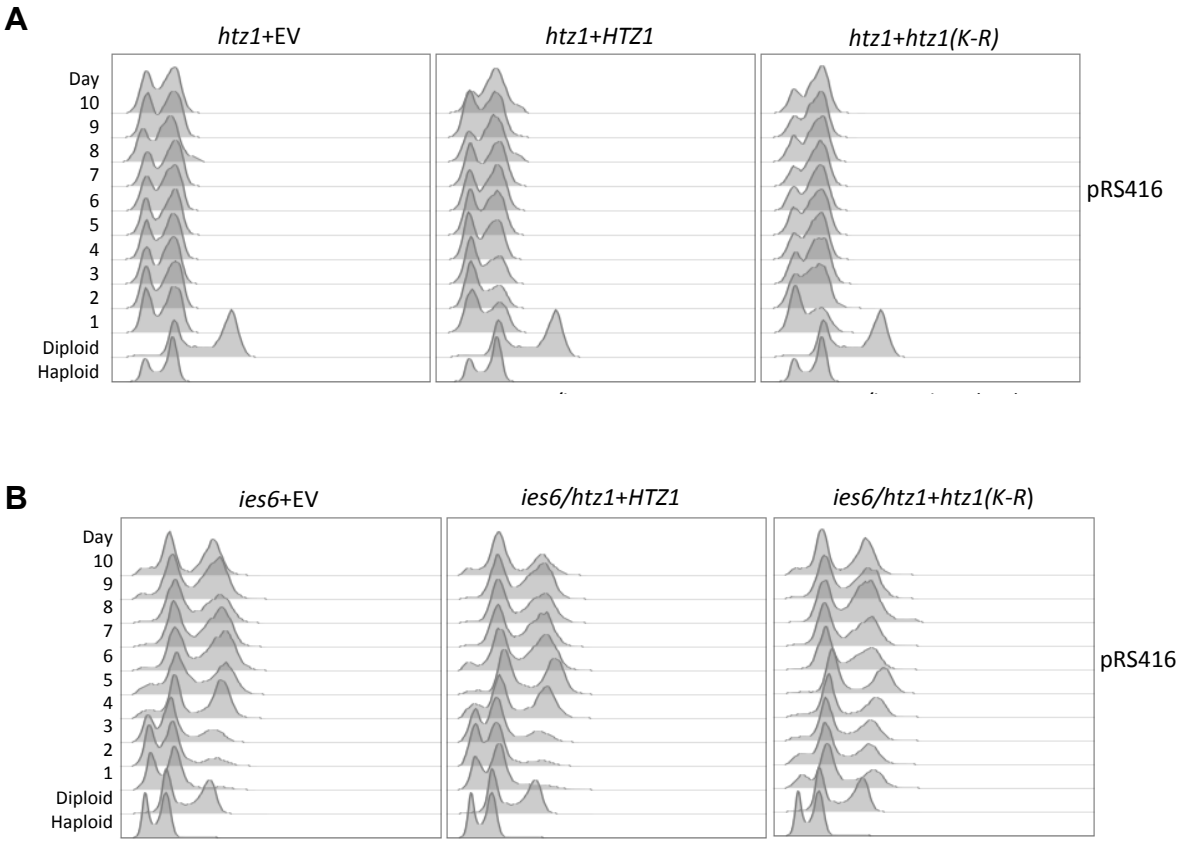

Figure 32: Cells expressing unacetylateable *htz1 (K-R)* accelerate the *ies6* polyploid phenotype.

A. Sporulation of a *ies6/IES6, htz1/HTZ1* heterozygous diploid (JDY968) transformed with either the pRS416 empty vector, pRS416-*HTZ1* or pRS416-*htz1(K-R)* generated *htz1*, *htz1 +HTZ1* and *htz1 +htz1(K-R)* cells . FACS analysis demonstrated that loss of acetylation alone has no effect on the rate at which *ies6* cells become polyploid.

B. Sporulation of a *ies6/IES6, htz1/HTZ1* heterozygous diploid (JDY968) transformed with either the pRS416 empty vector, pRS416-*HTZ1* or pRS416-*htz1(K-R)* generated *ies6*, *ies6*, *htz1 +HTZ1* and *ies6*, *htz1 +htz1(K-R)* cells . FACS demonstrated that removal of H2A.Z acetylation accelerates the *ies6* polyploidy phenotype.

3.3.3 *htz1 (K-R)* overexpression further exacerbates the influence of H2A.Z acetylation loss on *ies6* ploidy.

In addition to single copy expression, both the *htz1 (K-Q)* and *htz1 (K-R)* mutants were overexpressed to observe any further negative effects of H2A.Z acetylation status expressed above wildtype levels of H2A.Z.

The *htz1 (K-R)* alone did not change cellular ploidy (Figure 33 A), however, consistent with one previous study (Chambers et al. 2012), which observed that H2A.Z overexpression caused exacerbation of the *ies6* null ploidy phenotype, overexpression of H2A.Z in the *ies6* null caused an exacerbation of the increase in ploidy phenotype (Figure 33 B). Interestingly, the overexpression of the *htz1 (K-R)* acetyl-mutant exacerbated the increase in ploidy compared to both the *ies6* null alone and the *ies6* null overexpressing H2A.Z (Figure 33 B). These observations suggest that overexpression of H2A.Z has a negative effect on the role of Ies6 in maintaining centromere structure, which is elevated further upon the overexpression of the acetylation mutant.

The dramatic exacerbation of the *ies6* increase in ploidy phenotype in the presence of overexpressed and unacetylatable H2A.Z suggests the acetylation of H2A.Z is important for the role of Ies6 in maintaining H2A.Z levels at centromeres, which contributes to centromere structure.

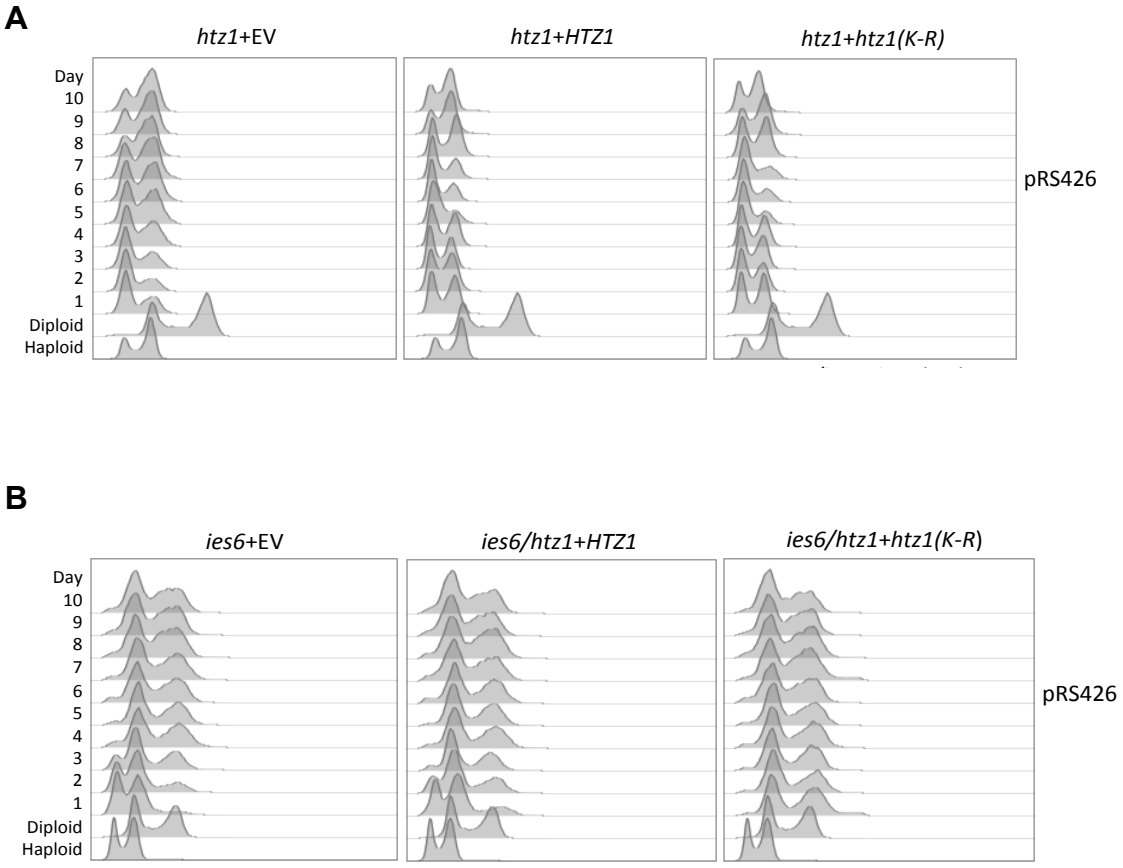

Figure 33: Overexpression of H2A.Z or the unacetylateable form of H2A.Z further accelerate the *ies6* polyploid phenotype.

A. Sporulation of a *ies6/IES6, htz1/HTZ1* heterozygous diploid (JDY968) transformed with either the pRS426 empty vector, pRS416-*HTZ1* or pRS426-*htz1(K-R)* generated *htz1*, *htz1 +HTZ1* and *htz1 +htz1(K-R)* cells. FACS analysis demonstrated that overexpression of unacetylatable H2A.Z alone has no influence on wildtype ploidy.

B. Sporulation of a *ies6/IES6, htz1/HTZ1* heterozygous diploid (JDY968) transformed with either the pRS416 empty vector, pRS416-*HTZ1* or pRS416-*htz1(K-R)* generated *ies6*, *ies6*, *htz1 +HTZ1* and *ies6*, *htz1 +htz1(K-R)* cells . FACS demonstrated that both H2A.Z and unacetylatable H2A.Z exacerbate the *ies6* increase in ploidy phenotype.

Table 8: Summary of results from Htz1 acetylation experiments. The combination of *ies6* with *htz1 (K-R)* overexpression caused the greatest acceleration to a polyploid population.

Mutant	Expression Single copy (pRS416) Overexpressed (pRS426)	Rate of polyploidy appearance
htz1 + EV	Single copy	-
	Overexpressed	-
htz1 + HTZ1	Single copy	-
	Overexpressed	-
htz1 + htz1 (K-R)	Single copy	-
	Overexpressed	-
htz1 + htz1 (K-Q)	Single copy	-
	Overexpressed	-
ies6 + EV	Single copy	+
	Overexpressed	+
ies6 + IES6	Single copy	-
	Overexpressed	-
ies6, htz1 + EV	Single copy	+
	Overexpressed	+
ies6, htz1 + HTZ1	Single copy	+
	Overexpressed	++
ies6, htz1 + htz1 (K-R)	Single copy	+
	Overexpressed	+++
ies6, htz1 + htz1 (K-Q)	Single copy	+
	Overexpressed	+

Haploid (-)
Polyploid after 72 hrs (+)
Polyploid after 48 hrs (++)
Polyploid after 24 hrs (+++)

3.3.4 *ies6*, *htz1 (K-R)* cells are hypersensitive to DNA damaging agents.

A previous study demonstrated *ino80* null cells were increasingly sensitive to HU in the presence of the unacetylatable form of H2A.Z, *htz1 (K-R)* (Papamichos-Chronakis et al. 2011). Given that *ies6* mimic *ino80* for all basic phenotype, including HU sensitivity (Chambers et al. 2012), in addition to the dramatic exacerbation of *ies6* increase in ploidy upon the removal of H2A.Z acetylation, the *htz1* mutants were screened for drug sensitivity to HU, MMS and benomyl.

The *ino80* and *ies6* deletions both exhibit sensitivity at approximately 15 mM HU and cell death at 20 mM (Papamichos-Chronakis et al. 2011; Chambers et al. 2012), however, the concentrations required to observe sensitivities in the *ies6* null cells expressing the *htz1 (K-R)* mutant were much lower, despite sufficient growth on the no drug plate (Figure 34 B). Sensitivity to benomyl and MMS was also significantly greater than either the *ino80* and *ies6* deletions, with *ies6* null cells expressing the *htz1 (K-R)* mutant being sensitive to 5 μg/ml benomyl and 0.005% MMS (Figure 34 B).

Comparatively, 15 μg/ml benomyl and 0.01% MMS are lethal doses to *ino80* and *ies6* null cells. However, as expected, the HU, benomyl or MMS sensitivities of *ies6* null cells expressing the *htz1 (K-Q)* acetylation mimic were unchanged compared to the *ies6* null alone. The increased hypersensitivity of *ies6* null cells when H2A.Z cannot be acetylated is consistent with previous observations that unacetylated and unregulated incorporation of H2A.Z increases HU sensitivity (Papamichos-Chronakis et al. 2011). Equal sensitivity to both benomyl and MMS,

above the level of the *ies6* null, indicate that the lack of H2A.Z acetylation may be influencing both replication and chromosome segregation functions of Ies6.

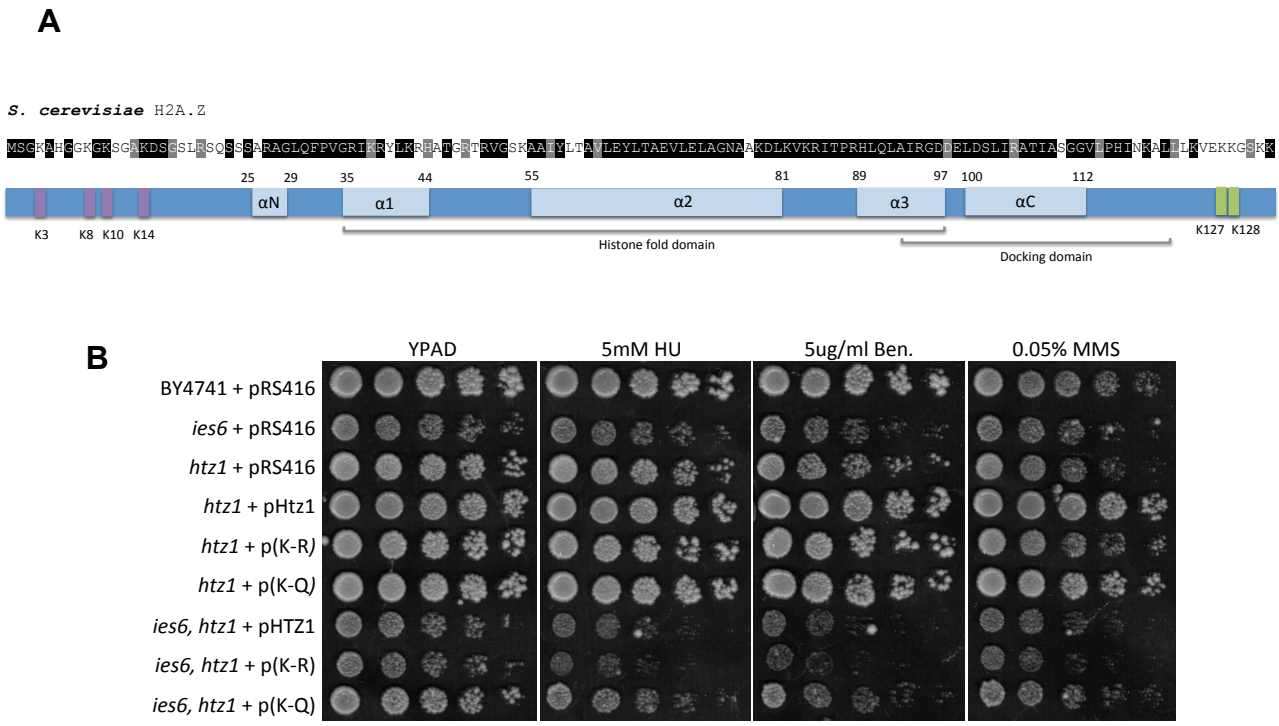

Figure 34: *ies6, htz1 (K-R)* cells are hypersensitive to DNA damaging agents.

A. Sequence of H2A.Z from *S. cerevisiae,* shaded for conservation to *H. sapiens,* and a schematic of H2A.Z from *S. cerevisiae* depicting the acetylated lysine residues in the N-terminal tail, alpha helices: N, 1, 2, 3, and C, which fold into the histone fold domain and the docking domain, and unbiquitinated lysines in the C-terminus.

B. Spores generate from the previous FACS analysis, expressing either *HTZ1*, *htz1 (K-R)* or *htz1 (K-Q)* in the single copy plasmid pRS416, were grown to mid-log and plated from a 10x dilution series. Plates were incubated at 30°C for 3 days.

3.3.5 H2A.Z K14 acetylation is maintained throughout the cell cycle.

Levels of H2A.Z acetylation, especially at K14, increase in the presence of benomyl (Mehta et al., 2010). However, it is unknown how H2A.Z acetylation levels may fluctuate throughout cell cycle. Determining levels of H2A.Z acetylation across the cell cycle would allow us to understand H2A.Z function, for example, if it were to be elevated during S-phase that may indicate it is required during replication. In order to address this question, chromatin was purified from wildtype BY4741 cells by chromatin fractionation. Chromatin fractionation enables the various components of the cell to be separated and analysed separately for DNA content, such as the cytoplasm and the chromatin. In order to investigate the levels of H2A.Z acetylation in these cellular components, the purified DNA from each extract was compared to the whole cell extract by western blot and probed for the presence of the most abundant acetylation mark, K14 (Figure 35 A).

The results demonstrated that H2A.Z remains bound to the chromatin consistently throughout the cell cycle, with no change between the signals for K15 acetylation on H2A.Z between the whole cell lysate, supernatant and chromatin in asynchronous cells, or cells in G1, S or G2 (Figure 35 A). For a better comparison of the levels of K14 acetylation across each stage of the cell cycle, extracts from asynchronous cells, G1, S or G2 from the same chromatin fractionation were examined adjacent on a second western blot (Figure 35 B). However, there was still no apparent difference between the levels of H2A.Z K14 acetylation at different stages of the cell cycle. The consistency of H2A.Z K14 acetylation in

wildtype cells demonstrates that H2A.Z acetylation is present on chromatin and is unaffected by the cell cycle stage.

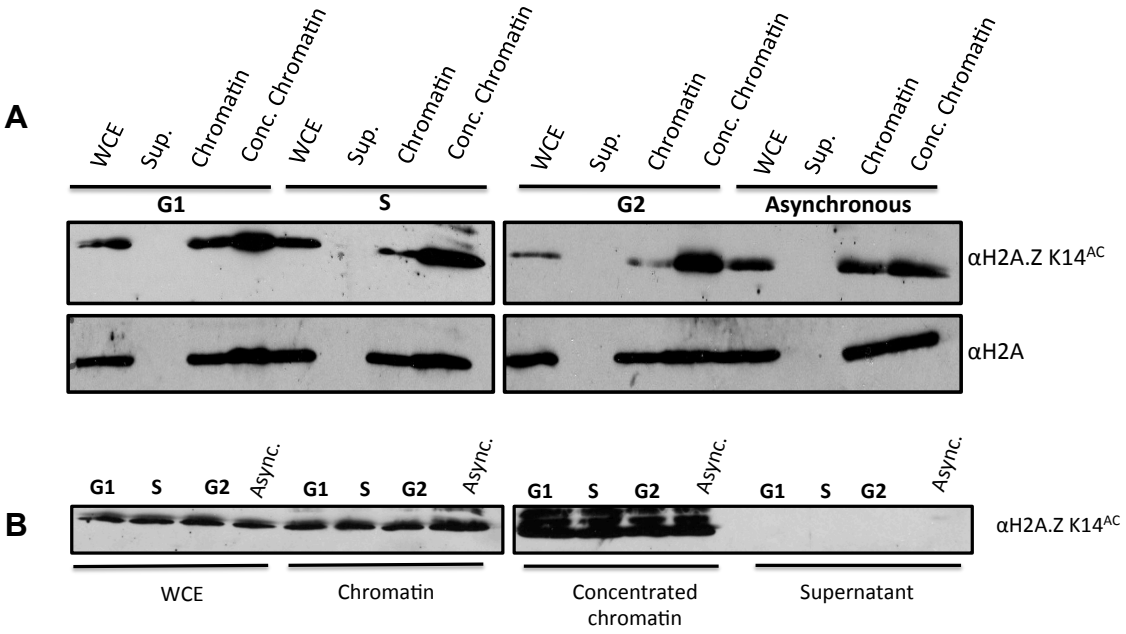

Figure 35: H2A.Z K14 acetylation remains constant throughout the cell cycle in wildtype cells.

A. Acetylation of H2A.Z K14 is chromatin bound. Wildtype cells (JDY921), arrested in G1, were released and samples were taken as the cells progressed through G1, S and G2. The whole cell extract, supernatant, chromatin and a 10x concentrated chromatin sample from one cell cycle phase were run collectively on an SDS page gel and analysed by western blotting. Blots were probed for H2A.Z K14 acetylation (top panel) and H2A as a loading control (bottom panel).

B. Chromatin bound H2A.Z K14 acetylation is consistent throughout the cell cycle. As above and probed for H2A.Z K14.

3.3.6 H2A.Z K14 acetylation remains chromatin bound throughout the cell cycle in *ies6* null cells.

Though there was no change in H2A.Z K14 acetylation levels throughout the cell cycle in wildtype cells, given the striking effect of unacetylated H2A.Z on *ies6* increase in ploidy phenotype, it was logical to assume that levels of H2A.Z acetylation may be reduced in the *ies6* null. This would help to support the hypothesis that Ies6 may be contributing to H2A.Z incorporation through H2A.Z acetylation. However, chromatin fractionations from *ies6* null cell synchronised in G1, S or G2 showed no difference between the H2A.Z K14 acetylation levels for the whole cell lysate, supernatant, or chromatin samples (Figure 36 A). Furthermore, the levels H2A.Z K14 remained consistent in the asynchronous, G1, S, and G2 samples when analysed adjacent for better quantification (Figure 36 B).

The lack of an increase or decrease in the H2A.Z acetylation levels compared to wildtype indicates that *ies6* deletion does not influence H2A.Z acetylation levels at K14, but this does not eliminate changes in acetylation at the other three residues. However, as K14 is the most abundantly acetylated, it would be reasonable to assume that any overall changes H2A.Z acetylation would be visible at this residue. Furthermore, it would suggest that H2A.Z acetylation is not a critical factor in determining the removal of H2A.Z by the INO80 complex.

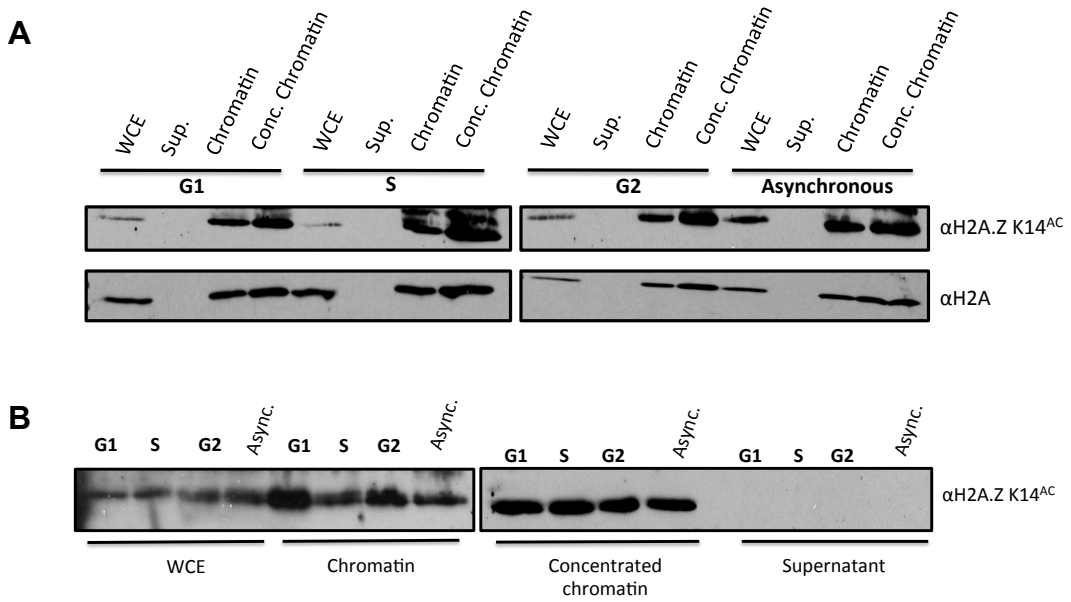

Figure 36: H2A.Z K14 acetylation is chromatin associated in *ies6* null cells and remains consistent throughout the cell cycle.

A. Levels of H2A.Z K14 acetylation are chromatin bound in *ies6* null cells. *ies6* null cells (JDY854), arrested in G1, were released and samples were taken as the cells progressed through G1, S and G2. The whole cell extract, supernatant, chromatin and a 10x concentrated chromatin sample from one cell cycle phase were run collectively on an SDS page gel and analysed by western blotting. Blots were probed for H2A.Z K14 acetylation (top panel) and H2A as a loading control (bottom panel).

B. H2A.Z acetylation at K14 in *ies6* null cells remains consistent throughout the cell cycle. As above but probed for H2A.Z K14.

4 Discussion

4.1 Single residue mutations do not disrupt Ies6 function

Using genetic and biochemical analysis, this study has further characterised previously defined regions within the Ies6 protein. This includes the further investigation of regions proposed to contact the INO80 subunits Arp5 and Rvb2 (Tosi et al. 2013), and the putative YL1_C DNA binding domain (Fenwick, 2010).

Considering the lack of structural information regarding Ies6, but the clear requirement for Ies6 within the INO80 complex (Chambers et al. 2012; Tosi et al. 2013; Watanabe et al. 2015), it was hypothesised that newly defined regions of Ies6 containing the potential sites of Arp5-Ies6 and Rvb2-Ies6 binding would be important for Ies6 function within the complex. In addition, the residues within the YL1_C domain were thought to be required for Ies6 DNA binding function. The subsequent mutation of conserved residues within these sites was predicted to result in Ies6 dysfunction. However, all the mutated alleles of *ies6* created during this study, harbouring only a single point mutation on one conserved residue, had no effect on Ies6 function.

Despite the small size of Ies6 and the highly conserved nature of the Ies6 protein, none of the 14 conserved residues mutated in this study affected sensitivity to the inhibitory drugs: HU, MMS or benomyl. Given the importance of the Ies6-Arp5 module for the functions of the INO80 complex (Watanabe et al., 2015), and it's *in vitro* DNA binding function in *S. cerevisiae* (Tosi et al., 2013), it was expected that a disruption to these conserved residues may be sufficient to cause a change in phenotype. Similarly, the importance of Rvb1 and Rvb2 for

INO80 chromatin remodelling (Jónsson et al., 2004), and the YL1_C domain being the putative DNA binding region, meant loss of Ies6 function was expected when *ies6* alleles harbouring a point mutation within these regions were screened for drug sensitivity. However, no single residue change within the putative Arp5 binding region, Rvb2 binding region or the YL1_C domain affected protein expression (Figure 10 and 14), drug sensitivity (Figure 8 and 9), or growth (Figure 11). The absence of a significant change from the wildtype could indicate that these residues, though conserved, are not important for the contact of Ies6 with Arp5, Ruvb2, or DNA binding.

Further mutation of the *IES6* gene enabled the characterisation of a double point mutant, *ies6 (K114E, Y125A)*, which was sufficient to cause a quantifiable phenotype (Figure 11 and 12). The *ies6 (K114E, Y125A)* mutant contained one substitution at K114 (within the potential Arp5 and Rvb2 interacting region, and the YL1_C domain) and another at Y125 (within the YL1_C domain). Expression of this allele caused a growth defect and a HU sensitivity that was intermediate of the *ies6* null and wildtype (Figure 9 and 11 B). However, it is important to note that only a substitution for glutamine at K114, in conjunction with alanine at Y125, caused HU sensitivity (Figure 12 B). This effect may be attributed to the change in amino acid charge, or a group of amino acids, that may be influencing the overall protein function. In this substitution, the side chains of amino acid 114 have changed from positively charged (lysine) to negatively charged (glutamic acid). This lysine residue sits within a conserved pair of lysines (K113 and K114; Figure 7 A), which may possibly function as a positively charged group. This alteration in charge, in addition to the removal of the available OH group (tyrosine-alanine) at

reside 125, could be potentially be contributing factors to the disruption of Ies6 function.

The alteration of charge, and the loss of the OH side chain, may also have influenced the fold of Ies6. As there is currently no structural information available for Ies6, the native fold of the Ies6 protein, and the fold of the YL1_C domain, is unknown. It could be that K114 and Y125, both being within the YL1_C domain, are important for contacts with specific substrates created during replication, as there is evidence to suggest Ies6 has a preference for Y-fork structures over dsDNA (Fenwick, 2010). However, the *ies6 (K114E, Y125A)* mutant was able to bind dsDNA (Figure 17 C), so a capacity to bind Y-forks would be unlikely.

Recent work has demonstrated that the loss of Ies6 from the INO80 complex retains nucleosome binding, but inactivates nucleosome sliding and H2A.Z dimer exchange (Watanabe et al., 2015). Potentially, the *ies6 (K114E, Y125A)* mutant is important for these chromatin remodelling functions of Ies6 within the INO80 complex. Both these remodelling functions would assist in the progression of DNA replication and could provide a mechanism for INO80-mediated replication stress removal (Falbo et al., 2009; Papamichos-Chronakis and Peterson, 2008; Shimada et al., 2008). However, analysis of nucleosome sliding and H2A.Z dimer exchange in an INO80 complex containing the Ies6 (K114E, Y125A) protein would be required to test this hypothesis.

The finding that residue charge, as well as the accumulation of mutations is required to disrupt Ies6 DNA binding, corroborates previous findings (Fenwick, 2010). Here, a quadruple mutant, with mutations at unconserved residues chosen for their charge, abolished *in vitro* DNA binding activity (Fenwick, 2010). However, in this instance the *ies6 (K114E, Y125A)* mutant did not inhibit DNA binding

(Figure 17 C). This suggests Ies6 is able to tolerate a certain number of mutations before functions become compromised, potentially having a better tolerance for mutations which do not have a dramatic effect on charge (Figure 7).

Furthermore, it is clear that the *ies6 (K114E, Y125A)* mutant protein is still functional on some level, as sensitivity was only observed to HU and not bneomly or MMS (Figure 11 B). In addition, additive effects were seen when the *ies6 (K114E, Y125A)* mutant was expressed in combination with *rad50* deletion, but not *cin8* or *sas3* (Table 7). This suggests that these mutations within Ies6 are affecting only Ies6 functions in DNA replication or repair, and suggests a potential separation of function between Ies6 in replication/repair and chromosome segregation. However, to confirm a separation of function in the *ies6 (K114E, Y125A)*, *rad50* these sensitivities would require further quantification.

4.2 The YL1_C domain is crucial for Ies6 DNA binding

Biochemical analysis of the *ies6 (K114E, Y125A)* mutant demonstrated those mutations were insufficient to abolish DNA binding (Figure 17 C). However, when the Ies6 protein is truncated to contain only the N-terminus or C-terminus (Figure 20 A), the N-terminus alone (without the YL1_C domain) is insufficient to bind DNA (Figure 20 B). Unlike previous studies, which have speculated about the DNA binding capacity of the YL1_C domain (Fenwick, 2010; Tosi et al. 2013; Chen et al. 2013), this work demonstrates Ies6 DNA binding capacity is dependent on the C-terminus, which contains the YL1_C domain (Figure 20 B). Confirmation of the DNA binding capacity of the YL1_C will allow future studies to further disrupt the

C-terminus to investigate the minimum YL1_C sequence required to maintain the DNA binding of the Ies6 protein.

However, there is still much to be understood about Ies6 DNA binding, its function and the contribution of other subunits. For example, previous research demonstrated DNA binding was only possible when Ies6 was in complex with Arp5 (Tosi et al. 2013), and further studies have documented the importance of the Arp5-Ies6 module for maintaining the stability of both proteins within the complex (Watanabe et al., 2015). Previous work would suggest Arp5 interacts with Ies6 approximately between S49 and K114 in *S. cerevisiae* (Tosi et al., 2013; Figure 5). The truncation Ies6 (1-76 aa), which abolished DNA binding (Figure 20 B), may have significantly disrupted this interaction, in addition to removing the YL1_C domain and Rub2 interacting region. It would be advantageous to check for Arp5 interaction within these truncated proteins through affinity purification to see if Ies6 in complex with Arp5 has a stronger affinity for DNA than full length Ies6 or the truncated C-terminus alone.

4.3 H2A.Z acetylation status influences the Ies6 ploidy increase

Prior to this study no connections had been established between any accessory subunit of the INO80 complex and H2A.Z acetylation. Only the catalytic component, Ino80, had been shown to genetically interact with the loss of acetylation, causing increased HU sensitivity when an *ino80* null was combined with the *htz1 (K-R)* acetylation mutant (Papamichos-Chronakis et al., 2011). In this study, removal of H2A.Z acetylation clearly demonstrated there was an underlying dependence on

H2A.Z acetylation to delay the occurrence of polyploid cells in an *ies6* null (Figure 28 B). The exacerbation of the appearance of polyploid cells was then elevated further with the overexpression of the unacetylatable form of H2A.Z (Figure 28 B). This demonstrates the presence of a significant relationship between Ies6 and H2A.Z acetylation.

One explanation for this effect could be that H2A.Z acetylation status exacerbates *ies6* chromosome segregation defects due to the increased levels of H2A.Z at the centromere. A previous study has demonstrated that the loss of *ies6* or *ino80* causes increased H2A.Z at *S. cerevisiae* centromeres, which causes altered chromatin structure and susceptibility to MNase digestion (Chambers et al. 2012). This hypothesis could be examined by quantifying H2A.Z acetylation levels at the centromere in wildtype and *ies6* null cells using an antibody specific to K14 acetylation. This would determine the importance of H2A.Z acetylation for the role of Ies6 in the removal of H2A.Z. In addition, indirect end labelling and southern blotting (Chambers et al. 2012) could be used to measure the susceptibility of *ies6, htz1 (K-R)* chromatin to MNase digestion. This would establish whether removal of H2A.Z acetylation is specifically influencing centromere defects in the *ies6* null.

Another explaination for the excelerated poidy pheontype in *ies6, htz1 (K-R)* mutants comes form the role of H2A.Z actylation in sister chromatid cohesion, which has been demonstrated in both *S. ceravisiae* (Sharma et al., 2013) and *S. pombe* (Kim et al., 2009). This raises the possibility that the exacerbation of *ies6* ploidy is due to an additive effect on factors influencing chromosome segregation. Potentially, the loss of *ies6* is causing an increased level of H2A.Z at the centromere, thus chromosome segregation defects, while removal of H2A.Z acetylation is causing sister chromatid cohesion defects, and together these

manifest as an accelerated progression to a higher ploidy status. This hypothesis could be examined by measuring the levels of sister chromatid separation in *ies6, htz1 (K-R)* and *ies6, htz1 (K-Q)* mutants by inserting a GFP marker at the URA3 locus (Sharma et al., 2013). However, the assay would have to be conducted on newly derived *ies6, htz1 (K-R)* and *ies6, htz1 (K-Q)* spores due to the occurrence of polyploidy. This analysis would allow comparisons between the *htz1 (K-R)* mutant alone and a newly derived *ies6* null, to establish whether *ies6* chromosome segregation defects are having an additive effect those already observed upon the loss of H2A.Z acetylation. This hypothesis could be complicated by a previous study, which has suggested the INO80 complex influences sister chromatid separation defects after the deletion of *ARP8* (Ogiwara et al., 2007).

However, this does not rule out that the exacerbation of the *ies6* ploidy is a result of cohesion defects caused by the loss of H2A.Z acetylation. The removal of H2A.Z acetylation alone did not cause ploidy defects (Figure 32 A), when defects in sister chromatid separation are known to manifest in these cells (Sharma et al., 2013). Though, this defect in sister chromatid cohesion may not be sufficient to manifest as polyploidy, when combined with genes susceptible to ploidy changes, like *ies6* deletion, this additional defect amounts to an acceleration of the polyploid phenotype.

Given what was previously demonstrated about Ino80 and H2A.Z acetylation mutant (Papamichos-Chronakis et al., 2011), and the Ies6 and Ino80 influence on H2A.Z incorporation at centromeres (Chambers et al. 2012) the dependence of Ies6 or Ino80 on acetylation for the removal of H2A.Z was tested. As acetylation of H2A.Z is required for SWR1-dependent incorporation of H2A.Z (Watanabe et al., 2013), though, it is unknown how H2A.Z acetylation effects

INO80-dependent removal of H2A.Z in *S. cerevisiae* (Papamichos-Chronakis et al., 2011). By observing H2A.Z actylation levels throughout the cell cycle in both wildtype and *ies6* null cells, it was demonstrated that *ies6* deletion did not influence the levels of H2A.Z actylation (Figure 34 A and B). Furthermore, H2A.Z acetylation in *ies6* null cells was concistent with wildtype levels throughout the cell cycle (Figure 35 A and B). Confirmation that H2A.Z actylation levels were did not fluctuate in an Ies6-dependent mannor suggests that Ies6 is not directly involved in the removal of H2A.Z. However, this interpretation would conflict with recent eveidence, which suggests *in vitro* H2A.Z dimer exchange is reduced upon the reomaval of Ies6 from the INO80 complex (Watanabe et al., 2015). Further examination of Ies6 histone binding would be required to establish binding to either H2A or H2A.Z and determine the function of Ies6 in INO80-dependent H2A.Z removal.

5 Structural mechanisms of phosphorylation-dependent recruitment of Tel2 to Hsp90 by Pih1

5.1 Introduction

Rvb1 and Rvb2 are components of the INO80 chromatin remodelling complex, and essential ATP-dependent DNA helicases in *S. cerevisiae* (Gribun et al., 2008; Jónsson et al., 2001). They are found within many multi-protein complexes, including SWR1 and the R2TP complex (Krogan et al., 2003; Zhao et al., 2005). During the course of this project these proteins were investigated within the R2TP complex.

In *Homo sapiens* the R2TP complex is implicated in the assembly and stability of vast numbers of proteins and multi-protein complexes, including the proposed assembly of Rvb1 and Rvb2 into the INO80 complex (Zhao et al. 2005). As purifications of INO80 complex components from *pih1* or *tah1* deletion strains containing TAP-tagged Ies2 showed an elevated level of both Rvb1 and Rvb2 (Zhao et al. 2005). Additional complexes influenced by R2TP and Hsp90 function are: RNA polymerase 2, small nucleolar ribonucleoproteins (snoRNPs) (Kakihara and Houry, 2012), and phosphatidylinositol-3-kinase-like kinases (PIKKs), including mTOR and SMG1 (Horejsí et al., 2010; Takai et al., 2010). In both *Homo sapiens* and *S. cerevisiae*, the R2TP complex consists of Rvb1, Rvb2, Tah1 and Pih1 (Zhao et al. 2005) (Figure 37 A).

Pih1 is a small scaffold protein of the R2TP complex, it links the Rvb1 and Rvb2 subunits, and the TTT (Tel2-Tti1-Tti2) complex, which are all implicated in

the activation of PIKKs (Kakihara and Houry, 2012) in conjunction with the Hsp90 molecular chaperone. The involvement of all these subunits depends on an interaction between the C-terminus of Pih1 and Tah1 in *S. cerevisiae* (Jiménez et al., 2012) (Figure 37 A). Pih1 binds to Rvb1 and Rvb2 constitutively (Paci et al., 2012) but the exact binding sites remain unknown. However, its interaction with the TTT complex is know to be governed by the casein kinase 2 (CK2) dependent phosphorlaytion of Tel2 and the N-terminus of Pih1 (Horejsí et al., 2010).

The function of R2TP complex is related to its interaction with the Hsp90 molecular chaperone. Hsp90 specifically binds to substrate proteins with a near-native fold towards the end of their maturation process. Its substrates include many signalling kinases and hormone receptors in eukaryotes (Pearl and Prodromou, 2000). In *S. cerevisiae*, the R2TP is recruited to Hsp90 through the simultaneous binding of its TRP domain to the MEEVD domain of Hsp90 and the N-terminus of Pih1 (Eckert et al., 2010; Jiménez et al., 2012).

Though new biological functions are being discovered for the R2TP complex, very little is understood about the mechanisms behind these processes (Kakihara and Houry, 2012). Deletion of *pih1* in *S. cerevisiae* causes a temperature sensitivity and a slow growth (Zhao et al. 2005), which has been attributed to the loss of the N-terminus, as truncation mutants, missing the $pih1^{(\Delta 1\text{-}230)}$ or $pih1^{(\Delta 1\text{-}230)}$, share both these phonotypes (Paci et al., 2012). Interestingly, the C-terminus of Pih1, responsible for Tah1 and Hsp90 binding, is dispensable for these phenotypes (Paci et al., 2012). This would suggest interactions within the N-terminus, potentially Rvb1 and Rvb2 binding sites, are significant for Pih1 function.

Given the importance of Pih1 as a scaffold for the R2TP complex, characterisation of this protein is vital to understand the mechanisms of R2TP function. This work structurally examines Pih1 and reveals how the R2TP complex connects with Hsp90, the TTT complex and contributes to PIKK activation.

5.2 Results

5.2.1 Biochemical analysis of the Pih1-Tel2 interaction

Experiments investigating the mechanistic relationship between Tel2 and the R2TP in mice showed a strong interaction being between purified mouse Pih1 (PIHD1) and a phosphorylated Tel2 peptide (Horejsí et al., 2010). Isothermal titration calorimetry (ITC) experiments were performed by our collaborators (Pal et al., 2014) this technique is used to establish the the stoichiomety of bindinging between two peptides or purified proteins. The results of ITC demonstrated significant affinity of a Tel2 phospho-peptide for N-terminal peptides of Pih1 from *Mus musculus*, mPih1(47-179aa), and *S. cerevisiae* yPih1(29-184aa) (Figure 37 C) (Pal et al., 2014). This affinity for the Tel2 peptide was only observed in the presence of CK2 phosphorylation (Pal et al., 2014).

Following confirmation of an interaction between the N-terminus of mouse Pih1 and phosphorylated Tel2 peptide, our collaborators determined the structure of the mPih1(47-179aa) N-terminus in complex with the CK2 phosphorylated Tel2 peptide (Figure 37 B). The co-crystal clearly showed the phosphorylated serine (pS492) within an acid patch clearly visible in the apo-structure of the mPih1(47-179aa) bound to the Tel2 phosphopeptide (Figure 37 B). The interaction between Pih1 and Tel2 was clearly supported by hydrogen bonding between the side chains of K57, K64, and K113 within Pih1 and the phopho and carboxyl groups of pS492, A491, and A493 of Tel2 (Figure 37 B).

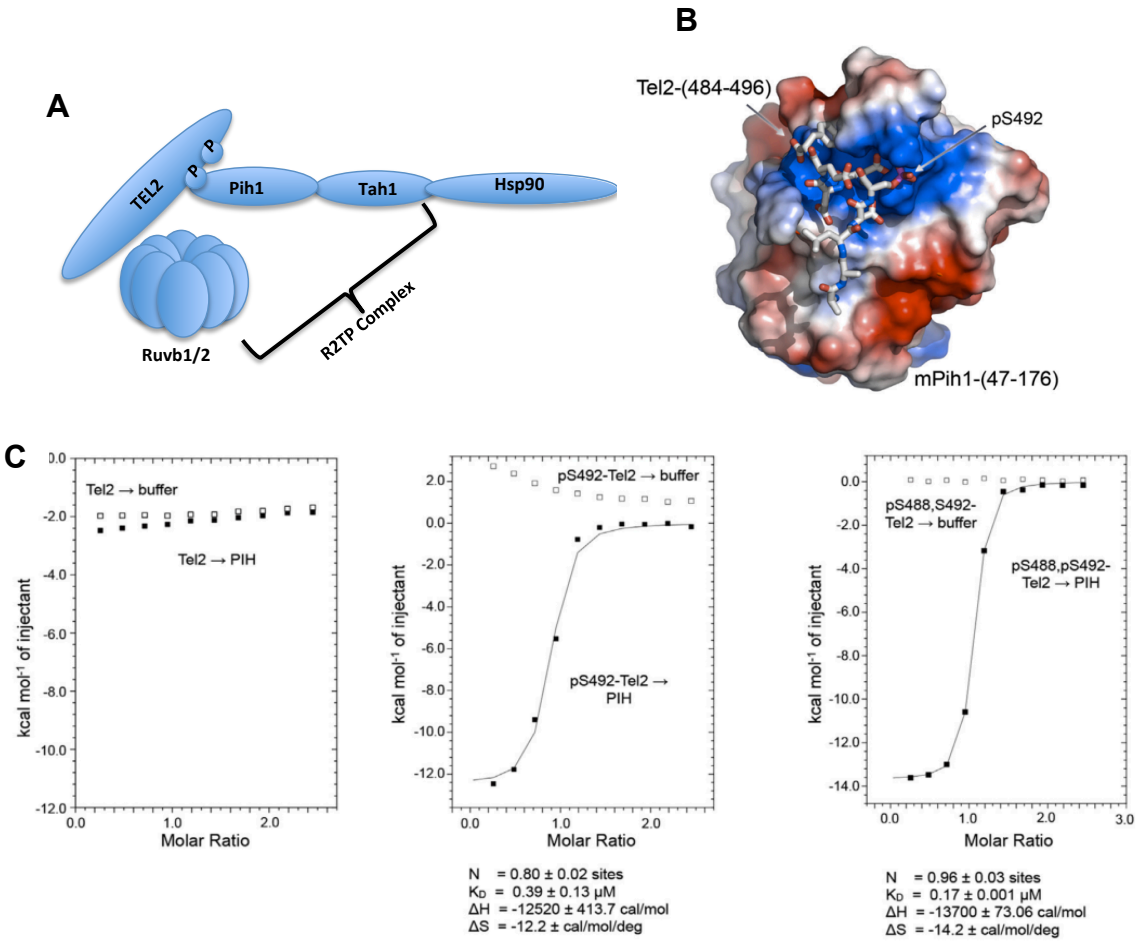

Figure 37: Pih1 is a component of the R2TP complex, and Mouse Pih1(47-176) binds to a Tel2 phospopeptide.

- **A.** Schematic of the R2TP composed of Ruvb1/Ruvb2, Tah1 and Pih1. The complex interacts with protein chaperone, Hsp90, via the c-terminus of Tah1
- **B.** Model of the co-crystal structure of mPih1(47-176) bound to a phosphorylated Tel2 peptide (Pal et al., 2014).
- **C.** ITC binding curves of Tel2 peptides containing phosphorylation on putative CK2 phosphorylation sites implicated in mediating interaction with Pih1 (Pal et al., 2014).

5.2.2 Specific lysine residues are critical to the Pih1-Tel2 interaction

Lysine residues K57, K64, and K113 of mPih1(47-179aa) were seen to mediate the interaction between the Tel2 phosphopeptide containing phosphorylation on S492 by co-crystal (Figure 38 B). All three residues are highly conserved from *H. sapiens* to *S. cerevisiae* (Figure 38 A).

Using ITC, the affinities of mutant forms of the Pih1 N-terminus were measured by our collaborators. When either K57 or K64 were mutated to glutamic acid affinity for the Tel2 S492 phosphopeptide was completely abolished (Figure 38 C). As a control, residue K153, on the opposite side of the Pih1 fragment was mutated to glutamic acid. As expected this had an affinity comparable to wildtype Pih1 as it did not impair the Pih1-Tel2 interaction (Figure 38 C). Given the conservation and importance of these Pih1 lysines for mediating the Pih1-Tel2 interaction, I investigated their functions in *S. cerevisiae*.

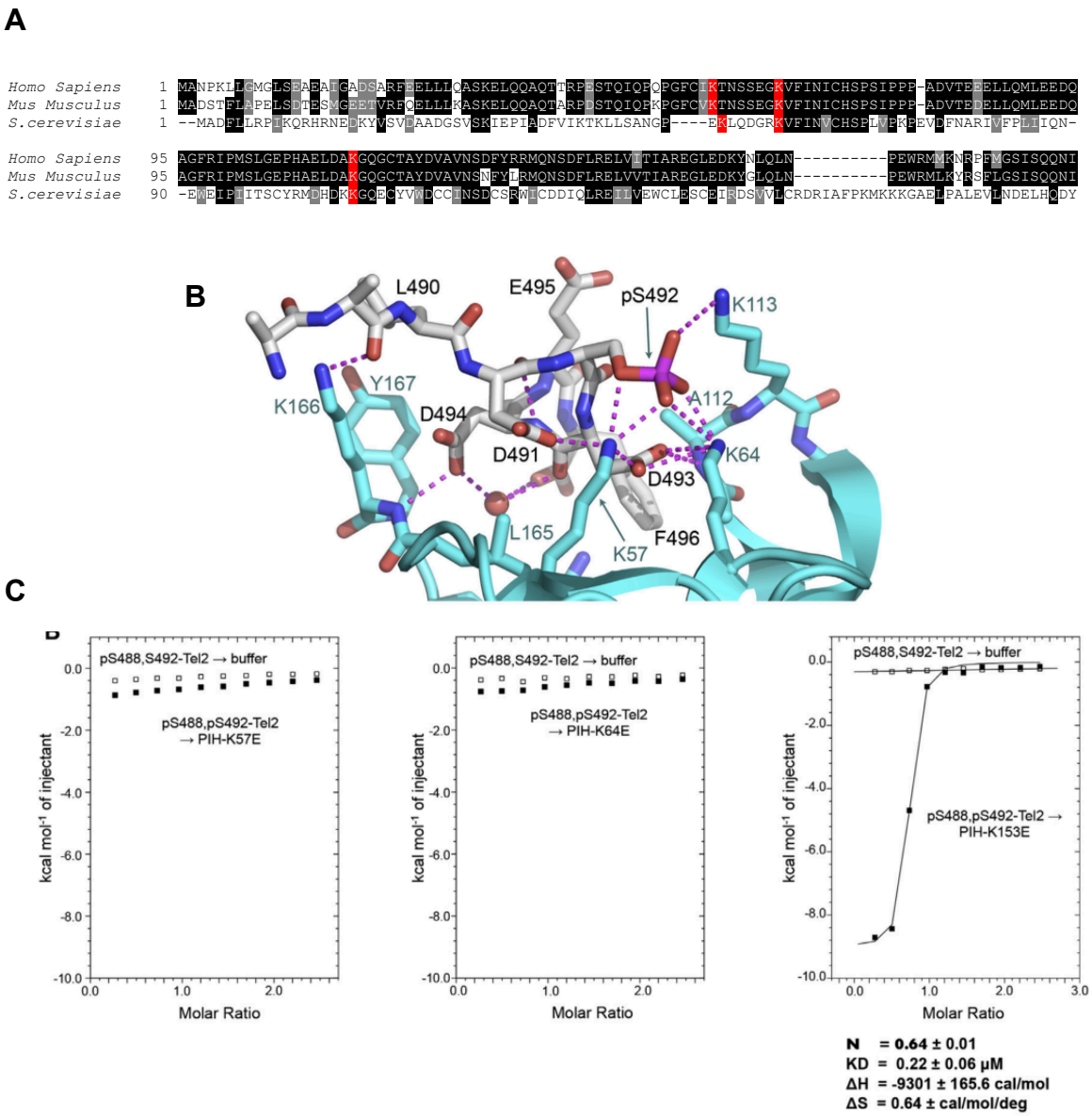

Figure 38: The lysine residues identified in mouse Pih1 are highly conserved.

A. Alignment of *S. cerevisiae* Pih1 with *Homo sapiens* and *Mus musculus* shows the highly conserved nature of the residues known to be interacting with phosphorylated Tel2.

B. Residues K57 and K64 in mPih1 and the phosphorylated Ser 492 of Tel2 mediate interactions between mPih1 and the Tel2 phosphopeptide (Pal et al., 2014).

C. ITC demonstrates, mutations residues K57 (left) or K64 (center) within Pih1 abolishes Tel2-phosphopeptide binding. The charge reversal of a conserved residue K153, not implicated in Tel2 binding, does not have affinity for the Tel2 phosphopeptide (right) (Pal et al., 2014).

5.2.3 The Pih1-Tel2 interaction is significant for Pih1 function *in vivo*.

Two of the residues that were found to be important for maintaining the Pih1-Tel2 interaction were selected for mutagenesis. These residues were K58 and K160 in *S. cerevisiae*, equivalent to K64 and K166 in *Mus musculus*. The residues were selected because of their importance for the Pih1-Tel2 interaction based on the previous structural and ITC data (Figure 38 B and Figure 39 C). Of the two residues selected, K58 had been implicated in direct interaction with the phosphorylated S492, and K160 with a side chain of the Tel2 phosphopeptide (Figure 39 B).

Previous studies in *S. cerevisiae* had shown that *pih1* deletion strains are sensitive high temperatures, and in addition have a slow growth phenotype (Zhao et al. 2005). This defect was shown to be dependent on the loss of the N-terminus, with the C-terminus of the protein being dispensable for temperature sensitivity and growth (Paci et al., 2012). The *pih1* deletion strain was used to compare our Tel2 mutants, *pih1 (K58E)* and *pih1 (K106E)*.

Interestingly, there was no phenotype in the *pih1 (K58E)* or *pih1 (K106E)* mutants, which were comparable to wildtype for growth (Figure 39 A) and temperature sensitivity (Figure 39 B). Knowing the sensitivity of the *pih1* deletion is related to the function of the N-terminus, the C-terminus of the protein was removed to mimic the mPih1(47-179aa) fragment used in the ITC and subsequent protein crystallography.

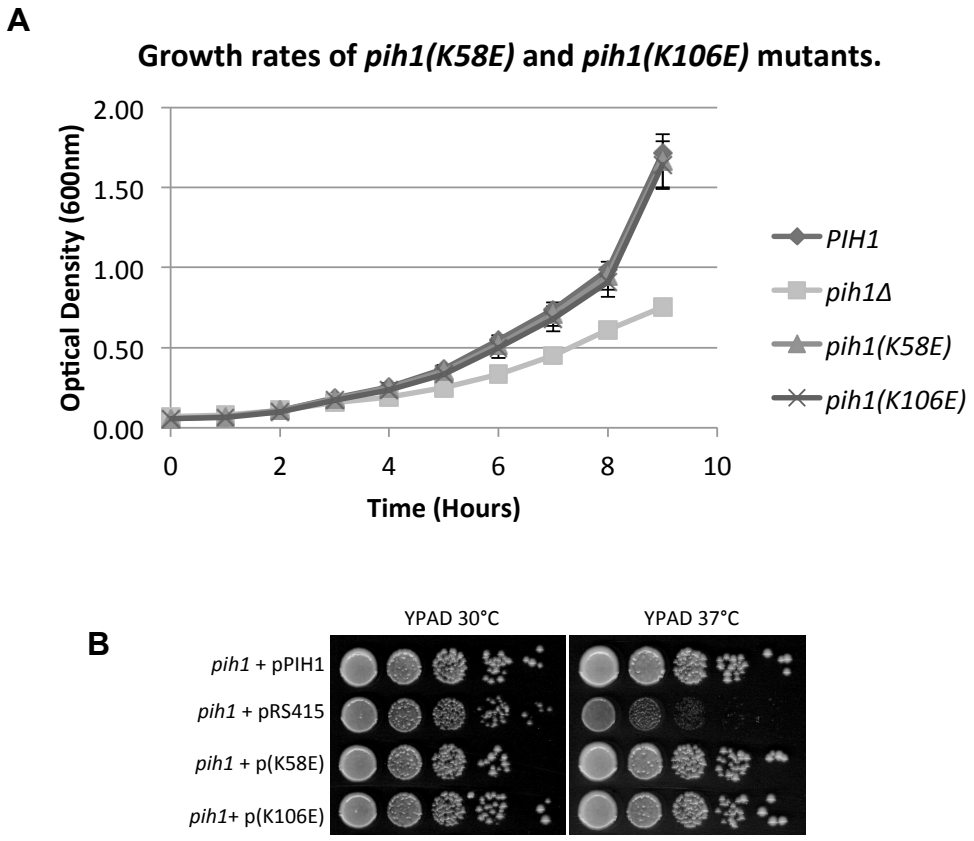

Figure 39: Abolition of the Pih1-Tel2 interaction with *pih1 (K58E)* and *pih1 (K106E)* does not effect growth defect and temperature sensitivity.

A. The optical density (260 nM) of *pih1* (JDY1029) cells transformed with either a pRS415 empty vector, *PIH1*, *pih1 (K58E)* or *pih1 (K106E)* expressing plasmid was measured periodically over 10 hours at 30°C. Error bars represent standard deviation of triplicates.

B. Transformants used to assay growth were plated onto YPAD and drug containing medium, from 10x serial dilutions of mid-log cultures, and grown at 30°C or 37°C for 3 days.

Based on previous studies (Paci et al., 2012), a truncation was produced through the introduction of a stop codon at position E167 to create *pih1 (1-167aa)*. This results in the expression of a truncated form of the Pih1 protein containing only the N-terminus. Subsequent expression of *pih1 (1-167aa)* within the *pih1* deletion strain was comparable to wildtype for growth and temperature sensitivity (Figure 40 A and C).

This is consistent with previous observations, that the Tah1-Hsp90 interaction is dispensable, so we next wanted to examine the effect of mutations that disrupt the Pih1-Tel2 interaction. Using site-directed mutagenesis, K58E or K106E mutations were introduced and the resulting plasmids were transformed into the *pih1* deletion strain. Interestingly, both growth and temperature sensitivity were defective in both the *pih1 (K58E)(1-167aa)* and the *pih1 (K160E)(1-167aa)* (Figure 35 A and C). In both strains growth and temperature sensitivity was comparable to the complete *pih1* null. (Figure 40 A and C).

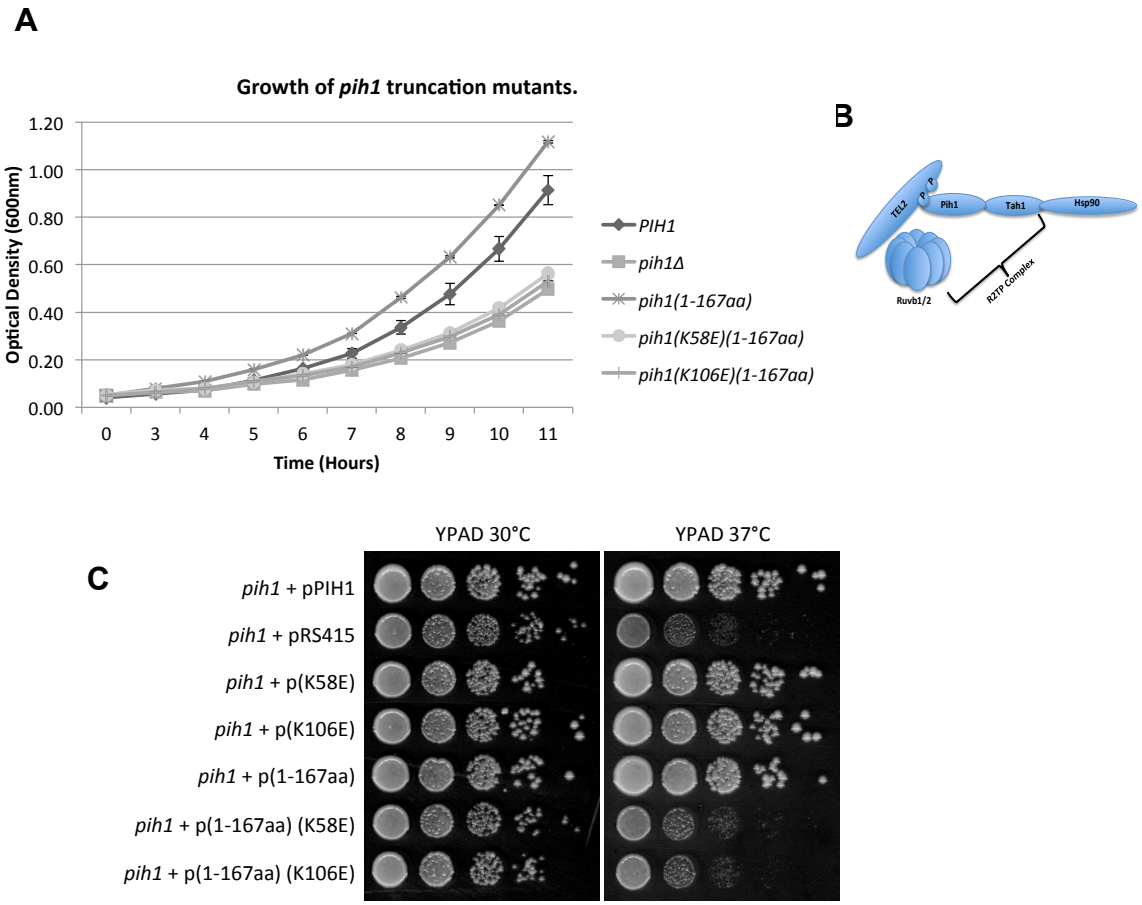

Figure 40: Truncated *pih1(K58E)*$^{(1\text{-}167aa)}$ and *pih1(K106E)*$^{(1\text{-}167aa)}$ cause growth defects and temperature sensitivity comparable to a *pih1* null.

A. The optical density (260 nM) of *pih1* null cells (JDY1029) transformed with either a pRS415 empty vector, *PIH1*, *pih1(K58E)*, *pih1(K106E)*, *pih1 (1-167 aa)*, *pih1 (1-167aa, K58E)*, *pih1(1-167aa, K106E)*, expressing plasmid was measured periodically over 10 hours at 30°C. Error bars represent standard deviation.

B. Schematic of the R2TP composed of Ruvb1/Ruvb2, Tah1 and Pih1. The complex interacts with protein chaperone, Hsp90, via the c-terminus of Tah1

C. Transformants used to assay growth were plated onto YPAD and drug containing medium, from 10x serial dilutions of mid-log cultures, and grown at 30°C or 37°C for 3 days.

5.3 Discussion

The R2TP complex, through interactions with Hsp90, is important for RNA polymerase 2, small nucleolar ribonucleoproteins (snoRNPs) synthesis (Kakihara and Houry, 2012), and for the maturation of phosphatidylinositol-3-kinase-like kinases (PIKKs), including mTOR and SMG1 (Horejsí et al., 2010; Takai et al., 2010). The scaffold protein Pih1 mediates the interaction of the R2TP complex with PIKKs. The CS C-terminal domain of Pih1 interacts with the TRP domain of Tah1, recruiting Hsp90 through its MEEVD domain. However, links between the R2TP complex and Tel2 were unknown.

This study has clearly demonstrated a previously unknown interaction between the N-terminus of the Pih1 scaffold and the Tel2 protein of the TTT complex. An interaction that is dependent on the phosphorylation of CK2 site S492 in Tel2, and lysine residues K58 and K64 of mPhi1, found within a basic pocket of Pih1 crystallised from *Mus musculus* (Figure 38 C). Furthermore, additional residues within the basic pocket were shown to be important for the Tel2 interaction, through interactions with side chains, including K116 (Figure 38 B). Determining the basis of this interaction has helped reveal the importance of the Pih1 N-terminus that was previously unknown and suggests a mechanism for the Hsp90-mediated function of the R2TP complex in the maturation and stabilisation of PIKKS.

Furthermore, removal of both the phospho-specific interaction with Tel2, and dissociation of Tah1-Hsp90 from the R2TP complex, was required to mimic a

pih1 deletion in *S. cerevisiae* (Figure 40 A and C). This result corroborates previous work highlighting the importance of the N-terminus of Pih1 (Paci et al., 2012). However, new importance was placed on residues within the N-terminus, which are now known to be critical for the phospo-dependent interaction of Tel2, when Hsp90 has been removed from the R2TP complex. The dependency on the Pih1-Tel2 interaction upon the loss of Hsp90 highlights the complexity of the interaction between R2TP, Hsp90 and the TTT complex, and suggest there are compensatory pathways available should important pathways, such as the R2TP-Hsp90 interaction become lost. In addition, these findings would suggest that the Rvb1/Rvb2-Pih1 interaction is redundant for Pih1 functions, as the removal of Tah1-Hsp90 and the phospo-Tel2 interaction caused a defect identical to the *pih1* deletion.

References

Adam, M., Robert, F., and Larochelle, M. (2001). H2A . Z Is Required for Global Chromatin Integrity and for Recruitment of RNA Polymerase II under Specific Conditions H2A . Z Is Required for Global Chromatin Integrity and for Recruitment of RNA Polymerase II under Specific Conditions. Mol. Cell. Biol. *21*, 6270–6279.

Aguilera, A., and Gómez-González, B. (2008). Genome instability: a mechanistic view of its causes and consequences. Nat. Rev. Genet. *9*, 204–217.

Alcasabas, a a, Osborn, a J., Bachant, J., Hu, F., Werler, P.J., Bousset, K., Furuya, K., Diffley, J.F., Carr, a M., and Elledge, S.J. (2001). Mrc1 transduces signals of DNA replication stress to activate Rad53. Nat. Cell Biol. *3*, 958–965.

Alexander, S., and Rieder, C. (1991). Chromosome motion during attachment to the vertebrate spindle: initial saltatory-like behavior of chromosomes and quantitative analysis of force production by nascent kinetochore fibers. J. Cell Biol. *113*, 805–815.

Altaf, M., Auger, A., Monnet-Saksouk, J., Brodeur, J., Piquet, S., Cramet, M., Bouchard, N., Lacoste, N., Utley, R.T., Gaudreau, L., et al. (2010). NuA4-dependent acetylation of nucleosomal histones H4 and H2A directly stimulates incorporation of H2A.Z by the SWR1 complex. J. Biol. Chem. *285*, 15966–15977.

Ambrosio, C.D., Schmidt, C.K., Katou, Y., Kelly, G., Itoh, T., Shirahige, K., and Uhlmann, F. (2008). Identification of cis -acting sites for condensin loading onto budding yeast chromosomes. 2215–2227.

Arents, G., and Moudrianakis, E.N. (1995). The histone fold: a ubiquitous architectural motif utilized in DNA compaction and protein dimerization. Proc. Natl. Acad. Sci. U. S. A. *92*, 11170–11174.

Arents, G., Burlingame, R.W., Wang, B.C., Love, W.E., and Moudrianakis, E.N. (1991). The nucleosomal core histone octamer at 3.1 A resolution: a tripartite protein assembly and a left-handed superhelix. Proc. Natl. Acad. Sci. U. S. A. *88*, 10148–10152.

Van Attikum, H., Fritsch, O., Hohn, B., Gasser, S.M., Ansermet, Q.E., and Geneva, C.- (2004). Recruitment of the INO80 Complex by H2A Phosphorylation Links ATP-Dependent Chromatin Remodeling with DNA Double-Strand Break Repair NCCR Frontiers in Genetics Program. *119*, 777–788.

Van Attikum, H., Fritsch, O., and Gasser, S.M. (2007). Distinct roles for SWR1 and INO80 chromatin remodeling complexes at chromosomal double-strand breaks. EMBO J. *26*, 4113–4125.

Azvolinsky, A., Giresi, P.G., Lieb, J.D., and Zakian, V. a. (2009). Highly Transcribed RNA Polymerase II Genes Are Impediments to Replication Fork Progression in Saccharomyces cerevisiae. Mol. Cell *34*, 722–734.

Bando, M., Katou, Y., Komata, M., Tanaka, H., Itoh, T., Sutani, T., and Shirahige, K. (2009). Csm3, Tof1, and Mrc1 form a heterotrimeric mediator complex that associates with DNA replication forks. J. Biol. Chem. *284*, 34355–34365.

Baptista, T., Graça, I., Sousa, E.J., Oliveira, A.I., and Natália, R. (2013). Regulation of histone H2A . Z expression is mediated by sirtuin 1 in prostate cancer ABSTRACT : *4*.

Bennett, G., Papamichos-Chronakis, M., and Peterson, C.L. (2013). DNA repair choice defines a common pathway for recruitment of chromatin regulators. Nat. Commun. *4*, 2084.

Biggar, S.R., and Crabtree, G.R. (1999). Continuous and widespread roles for the Swi-Snf complex in transcription. EMBO J. *18*, 2254–2264.

Bilousova, G., Marusyk, A., Porter, C.C., Cardiff, R.D., and DeGregori, J. (2005). Impaired DNA replication within progenitor cell pools promotes leukemogenesis. PLoS Biol. *3*, 1–13.

Bošković, A., Bender, A., Gall, L., Ziegler-Birling, C., Beaujean, N., and Torres-Padilla, M.E. (2012). Analysis of active chromatin modifications in early mammalian embryos reveals uncoupling of H2A.Z acetylation and H3K36 trimethylation from embryonic genome activation. Epigenetics *7*, 747–757.

Boyer, L. a., and Peterson, C.L. (2000). Actin-related proteins (Arps): Conformational switches for chromatin-remodeling machines? BioEssays *22*, 666–672.

Brownlee, P.M., Chambers, A.L., Cloney, R., Bianchi, A., and Downs, J. a. (2014). BAF180 Promotes Cohesion and Prevents Genome Instability and Aneuploidy. Cell Rep. *6*, 973–981.

Bruce, K., Myers, F. a., Mantouvalou, E., Lefevre, P., Greaves, I., Bonifer, C., Tremethick, D.J., Thorne, A.W., and Crane-Robinson, C. (2005). The replacement histone H2A.Z in a hyperacetylated form is a feature of active genes in the chicken. Nucleic Acids Res. *33*, 5633–5639.

Burrell, R. a, McGranahan, N., Bartek, J., and Swanton, C. (2013). The causes and consequences of genetic heterogeneity in cancer evolution. Nature *501*, 338–345.

Cai, Y., Jin, J., Tomomori-Sato, C., Sato, S., Sorokina, I., Parmely, T.J., Conaway, R.C., and Conaway, J.W. (2003). Identification of New Subunits of the Multiprotein Mammalian TRRAP/TIP60-containing Histone Acetyltransferase Complex. J. Biol. Chem. *278*, 42733–42736.

Cai, Y., Jin, J., Florens, L., Swanson, S.K., Kusch, T., Li, B., Workman, J.L., Washburn, M.P., Conaway, R.C., and Conaway, J.W. (2005). The mammalian YL1 protein is a shared subunit of the TRRAP/TIP60 histone acetyltransferase and SRCAP complexes. J. Biol. Chem. *280*, 13665–13670.

Cai, Y., Jin, J., Yao, T., Gottschalk, A.J., Swanson, S.K., Wu, S., Shi, Y., Washburn, M.P., Florens, L., Conaway, R.C., et al. (2007). YY1 functions with INO80 to activate transcription. Nat. Struct. Mol. Biol. *14*, 872–874.

Cairns, B.R., Lorch, Y., Li, Y., Zhang, M., Lacomis, L., Erdjument-Bromage, H., Tempst, P., Du, J., Laurent, B., and Kornberg, R.D. (1996). RSC, an essential, abundant chromatin-remodeling complex. Cell *87*, 1249–1260.

Carr, A.M., Dorrington, S.M., Hindley, J., Phear, G. a, Aves, S.J., and Nurse, P. (1994). Analysis of a histone H2A variant from fission yeast: evidence for a role in chromosome stability. Mol. Gen. Genet. *245*, 628–635.

Carter, S.L., Cibulskis, K., Helman, E., McKenna, A., Shen, H., Zack, T., Laird, P.W., Onofrio, R.C., Winckler, W., Weir, B. a, et al. (2012). Absolute quantification of somatic DNA alterations in human cancer. Nat. Biotechnol. *30*, 413–421.

Chai, B., Huang, J., Cairns, B.R., and Laurent, B.C. (2005). Distinct roles for the RSC and Swi / Snf ATP-dependent chromatin remodelers in DNA double-strand break repair. Genes Dev. *19*, 1656–1661.

Chambers, A.L., and Downs, J. a. (2012). The RSC and INO80 chromatin-remodeling complexes in DNA double-strand break repair (Elsevier Inc.).

Chambers, A.L., Ormerod, G., Durley, S.C., Sing, T.L., Brown, G.W., Kent, N. a, and Downs, J. a (2012a). The INO80 chromatin remodeling complex prevents polyploidy and maintains normal chromatin structure at centromeres. Genes Dev. *26*, 2590–2603.

Chambers, A.L., Brownlee, P.M., Durley, S.C., Beacham, T., Kent, N. a., and Downs, J. a. (2012b). The two different isoforms of the RSC chromatin remodeling complex play distinct roles in DNA damage responses. PLoS One *7*, 1–11.

Chen, L., Cai, Y., Jin, J., Florens, L., Swanson, S.K., Washburn, M.P., Conaway, J.W., and Conaway, R.C. (2011). Subunit organization of the human INO80 chromatin remodeling complex: an evolutionarily conserved core complex catalyzes ATP-dependent nucleosome remodeling. J. Biol. Chem. *286*, 11283–11289.

Chen, L., Conaway, R.C., and Conaway, J.W. (2013). Multiple modes of regulation of the human Ino80 SNF2 ATPase by subunits of the INO80 chromatin-remodeling complex. Proc. Natl. Acad. Sci. U. S. A. *110*, 20497–20502.

Chen, R.H., Waters, J.C., Salmon, E.D., and Murray, a W. (1996). Association of spindle assembly checkpoint component XMAD2 with unattached kinetochores. Science (80-.). *274*, 242–246.

Chi, Y.H., and Jeang, K.T. (2007). Aneuploidy and cancer. J. Cell. Biochem. *102*, 531–538.

Chiba, H., Muramatsu, M., Nomoto, a, and Kato, H. (1994). Two human homologues of Saccharomyces cerevisiae SWI2/SNF2 and Drosophila brahma are transcriptional coactivators cooperating with the estrogen receptor and the retinoic acid receptor. Nucleic Acids Res. *22*, 1815–1820.

Choi, J., Heo, K., and An, W. (2009). Cooperative action of TIP48 and TIP49 in H2A.Z exchange catalyzed by acetylation of nucleosomal H2A. Nucleic Acids Res. *37*, 5993–6007.

Cimini, D., Howell, B., Maddox, P., Khodjakov, A., Degrassi, F., and Salmon, E.D. (2001). Merotelic kinetochore orientation is a major mechanism of aneuploidy in mitotic mammalian tissue cells. J. Cell Biol. *152*, 517–527.

Cimini, D., Moree, B., Canman, J.C., and Salmon, E.D. (2003). Merotelic kinetochore orientation occurs frequently during early mitosis in mammalian tissue cells and error correction is achieved by two different mechanisms. J. Cell Sci. *116*, 4213–4225.

Ciosk, R., Zachariae, W., Michaelis, C., Shevchenko, A., Mann, M., and Nasmyth, K. (1998). An ESP1/PDS1 complex regulates loss of sister chromatid cohesion at the metaphase to anaphase transition in yeast. Cell *93*, 1067–1076.

Clapier, C.R., and Cairns, B.R. (2009). The biology of chromatin remodeling complexes. Annu. Rev. Biochem. *78*, 273–304.

Clarke, L., and Carbon, J. (1980). Isolation of yeast centromere and construction of functional small circular chromosomes. Nature *287*, 504–509.

Clarke, L., and Carbon, J. (1983). Genomic substitutions of centromeres in Saccharomyces cerevisiae. Nature *305*, 23–28.

Clarkson, M.J., Wells, J.R., Gibson, F., Saint, R., and Tremethick, D.J. (1999). Regions of variant histone His2AvD required for Drosophila development. Nature *399*, 694–697.

Cohen-Fix, O., Peters, J.-M., Kirschner, M.W., and Koshland, D. (1996). Anaphase initiation in Saccharomyces cerevisiae is cobtrolled by the APC-dependent degradation of the anaphase inhibtitor Psd1p. Genes Dev *10*, 3081–3093.

Connelly, C., and Hieter, P. (1996). Budding yeast SKP1 encodes an evolutionarily conserved kinetochore protein required for cell cycle progression. Cell *86*, 275–285.

Corona, D.F. V, and Tamkun, J.W. (2004). Multiple roles for ISWI in transcription, chromosome organization and DNA replication. Biochim. Biophys. Acta - Gene Struct. Expr. *1677*, 113–119.

Czaja, W., Bespalov, V.A., Hinz, J.M., and Smerdon, M.J. (2010a). Proficient repair in chromatin remodeling defective ino80 mutants of Saccharomyces cerevisiae highlights replication defects as the main contributor to DNA damage sensitivity. DNA Repair (Amst). *9*, 976–984.

Czaja, W., Bespalov, V. a., Hinz, J.M., and Smerdon, M.J. (2010b). Proficient repair in chromatin remodeling defective ino80 mutants of Saccharomyces cerevisiae highlights replication defects as the main contributor to DNA damage sensitivity. DNA Repair (Amst). *9*, 976–984.

Daal, A. Van, and Elgin, S.C.R. (1992). A Histone Variant , H2AvD , is Essential in Drosophila melanogaster. *3*, 593–602.

Daniel, J. a., Keyes, B.E., Ng, Y.P.Y., Freeman, C.O., and Burke, D.J. (2006). Diverse functions of spindle assembly checkpoint genes in Saccharomyces cerevisiae. Genetics *172*, 53–65.

Darlington, C.D. (1942). Chromosome Chemistry and Gene Action. Nature *149*, 66–69.

Deindl, S., Hwang, W.L., Hota, S.K., Blosser, T.R., Prasad, P., Bartholomew, B., and Zhuang, X. (2013). ISWI remodelers slide nucleosomes with coordinated multi-base-pair entry steps and single-base-pair exit steps. Cell *152*, 442–452.

Delmas, V., Stokes, D.G., and Perry, R.P. (1993). A mammalian DNA-binding protein that contains a chromodomain and an SNF2/SWI2-like helicase domain. Proc. Natl. Acad. Sci. U. S. A. *90*, 2414–2418.

Dhalluin, C., Carlson, J.E., Zeng, L., He, C., Aggarwal, a K., and Zhou, M.M. (1999). Structure and ligand of a histone acetyltransferase bromodomain. Nature *399*, 491–496.

Dominski, Z., and Marzluff, W.F. (1999). Formation of the 3' end of histone mRNA. Gene *239*, 1–4.

Downs, J. a, Lowndes, N.F., and Jackson, S.P. (2000). A role for Saccharomyces cerevisiae histone H2A in DNA repair. Nature *408*, 1001–1004.

Downs, J.A., Allard, S., Jobin-Robitaille, O., Javaheri, A., Auger, A., Bouchard, N., Kron, S.J., Jackson, S.P., and Côté, J. (2004). Binding of chromatin-modifying activities to phosphorylated histone H2A at DNA damage sites. Mol. Cell *16*, 979–990.

Doyon, Y., Selleck, W., Lane, W.S., Tan, S., and Côté, J. (2004). Structural and functional conservation of the NuA4 histone acetyltransferase complex from yeast to humans. Mol. Cell. Biol. *24*, 1884–1896.

Durkin, S.G., Ragland, R.L., Arlt, M.F., Mulle, J.G., Warren, S.T., and Glover, T.W. (2008). Replication stress induces tumor-like microdeletions in FHIT/FRA3B. Proc. Natl. Acad. Sci. U. S. A. *105*, 246–251.

Ebbert, R., Birkmann, a, and Schüller, H.J. (1999). The product of the SNF2/SWI2 paralogue INO80 of Saccharomyces cerevisiae required for efficient expression of various yeast structural genes is part of a high-molecular-weight protein complex. Mol. Microbiol. *32*, 741–751.

Eckert, K., Saliou, J.-M., Monlezun, L., Vigouroux, A., Atmane, N., Caillat, C., Quevillon-Chéruel, S., Madiona, K., Nicaise, M., Lazereg, S., et al. (2010). The Pih1-Tah1 cochaperone complex inhibits Hsp90 molecular chaperone ATPase activity. J. Biol. Chem. *285*, 31304–31312.

Faast, R., Thonglairoam, V., Schulz, T.C., Beall, J., Wells, J.R., Taylor, H., Matthaei, K., Rathjen, P.D., Tremethick, D.J., and Lyons, I. (2001). Histone variant H2A.Z is required for early mammalian development. Curr. Biol. *11*, 1183–1187.

Falbo, K.B., Alabert, C., Katou, Y., Wu, S., Han, J., Wehr, T., Xiao, J., He, X., Zhang, Z., Shi, Y., et al. (2009). Involvement of a chromatin remodeling complex in damage tolerance during DNA replication. Nat. Struct. Mol. Biol. *16*, 1167–1172.

Feijoo, C., Hall-Jackson, C., Wu, R., Jenkins, D., Leitch, J., Gilbert, D.M., and Smythe, C. (2001). Activation of mammalian Chk1 during DNA replication arrest: A role for Chk1 in the intra-S phase checkpoint monitoring replication origin firing. J. Cell Biol. *154*, 913–923.

Fenwick, G. (2010). The Role of the Ino80 Chromatin Remodelling Complex Subunit Ies6 in Maintaining Genome Stability.

Filion, G.J., van Bemmel, J.G., Braunschweig, U., Talhout, W., Kind, J., Ward, L.D., Brugman, W., de Castro, I.J., Kerkhoven, R.M., Bussemaker, H.J., et al. (2010). Systematic Protein Location Mapping Reveals Five Principal Chromatin Types in Drosophila Cells. Cell *143*, 212–224.

Fitzgerald-Hayes, M., Clarke, L., and Carbon, J. (1982). Nucleotide sequence comparisons and functional analysis of yeast centromere DNAs. Cell *29*, 235–244.

Flanagan, J.F., Mi, L.-Z., Chruszcz, M., Cymborowski, M., Clines, K.L., Kim, Y., Minor, W., Rastinejad, F., and Khorasanizadeh, S. (2005). Double chromodomains cooperate to recognize the methylated histone H3 tail. Nature *438*, 1181–1185.

Fraga, M.F., Ballestar, E., Villar-Garea, A., Boix-Chornet, M., Espada, J., Schotta, G., Bonaldi, T., Haydon, C., Ropero, S., Petrie, K., et al. (2005). Loss of acetylation at Lys16 and trimethylation at Lys20 of histone H4 is a common hallmark of human cancer. Nat. Genet. *37*, 391–400.

Freeman, L., Aragon-Alcaide, L., and Strunnikov, A. (2000). The condensin complex governs chromosome condensation and mitotic transmission of rDNA. J. Cell Biol. *149*, 811–824.

Gaillard, H., García-Muse, T., and Aguilera, A. (2015). Replication stress and cancer. Nat. Rev. Cancer *15*, 276–289.

Gévry, N., Ho, M.C., Laflamme, L., Livingston, D.M., and Gaudreau, L. (2007). p21 transcription is regulated by differential localization of histone H2A.Z. Genes Dev. *21*, 1869–1881.

Gick, O., Krämer, a, Keller, W., and Birnstiel, M.L. (1986). Generation of histone mRNA 3' ends by endonucleolytic cleavage of the pre-mRNA in a snRNP-dependent in vitro reaction. EMBO J. *5*, 1319–1326.

Gillett, E.S., Espelin, C.W., and Sorger, P.K. (2004). Spindle checkpoint proteins and chromosome-microtubule attachment in budding yeast. J. Cell Biol. *164*, 535–546.

Goh, P.-Y., and Kilmartin, J. V (1986). NDC10: A Gene Involved in Chromosome Segregation in Saccharomyces cerevisiae. J. Gen. Microbiol. *35*, 503–512.

Gordon, D.J., Resio, B., and Pellman, D. (2012). Causes and consequences of aneuploidy in cancer. Nat. Rev. Genet. *13*, 189–203.

Gospodinov, A., Vaissiere, T., Krastev, D.B., Legube, G., Anachkova, B., and Herceg, Z. (2011). Mammalian Ino80 mediates double-strand break repair through its role in DNA end strand resection. Mol. Cell. Biol. *31*, 4735–4745.

Greaves, I.K., Rangasamy, D., Ridgway, P., and Tremethick, D.J. (2007). H2A.Z contributes to the unique 3D structure of the centromere. Proc. Natl. Acad. Sci. U. S. A. *104*, 525–530.

Gribun, A., Cheung, K.L.Y., Huen, J., Ortega, J., and Houry, W.A. (2008). Yeast Rvb1 and Rvb2 are ATP-dependent DNA helicases that form a heterohexameric complex. J. Mol. Biol. *376*, 1320–1333.

Guacci, V., Koshland, D.E., and Strunnikov, A. V (1997). A direct link between sister chromatid cohesion and chromosome condensation revealed through the analysis of MCD1 in S. cerevisiae. Cell *91*, 47–57.

Haber, J.E., and Garvik, B. (1977). A new gene affecting the efficiency of mating-type interconversions in homothallic strains of Saccharomyces cerevisiae. Genetics *87*, 33–50.

Haering, C.H., Löwe, J., Hochwagen, A., and Nasmyth, K. (2002). Molecular architecture of SMC proteins and the yeast cohesin complex. Mol. Cell *9*, 773–788.

Harata, M., Oma, Y., Mizuno, S., Jiang, Y.W., Stillman, D.J., and Wintersberger, U. (1999). The nuclear actin-related protein of Saccharomyces cerevisiae, Act3p/Arp4, interacts with core histones. Mol. Biol. Cell *10*, 2595–2605.

Hardwick, K.G., Weiss, E., Luca, F.C., Winey, M., and Murray, a W. (1996). Activation of the budding yeast spindle assembly checkpoint without mitotic spindle disruption. Science (80-.). *273*, 953–956.

Harris, M.E., Böhni, R., Schneiderman, M.H., Ramamurthy, L., Schümperli, D., and Marzluff, W.F. (1991). Regulation of histone mRNA in the unperturbed cell cycle: evidence suggesting control at two posttranscriptional steps. Mol. Cell. Biol. *11*, 2416–2424.

Hartlepp, K.F., Fernández-Tornero, C., Eberharter, A., Grüne, T., Müller, C.W., and Becker, P.B. (2005). The histone fold subunits of Drosophila CHRAC facilitate nucleosome sliding through dynamic DNA interactions. Mol. Cell. Biol. *25*, 9886–9896.

Hassold, T., and Hunt, P. (2001). To err (meiotically) is human: the genesis of human aneuploidy. Nat. Rev. Genet. *2*, 280–291.

Hatch, L., Bonner, M., and Gene, H.H. a Z. (1990). The Human Histone H2A.Z Gene: Sequence and regulation. J. Biol. Chem. *265*, 15211–15218.

Hauf, S., Waizenegger, I.C., and Peters, J.M. (2001). Cohesin cleavage by separase required for anaphase and cytokinesis in human cells. Science *293*, 1320–1323.

Hauk, G., McKnight, J.N., Nodelman, I.M., and Bowman, G.D. (2010). The Chromodomains of the Chd1 Chromatin Remodeler Regulate DNA Access to the ATPase Motor. Mol. Cell *39*, 711–723.

Heitz, E. (1928). Das Heterochromatin der Moose. Jahrb Wiss Bot. *69*, 762–818.

Hieter, P., Pridmore, D., Hegemann, J.H., Thomas, M., Davis, R.W., and Philippsen, P. (1985). Functional selection and analysis of yeast centromeric DNA. Cell *42*, 913–921.

Hirano, T. (2002). The ABCs of SMC proteins: Two-armed ATPases for chromosome condensation, cohesion, and repair. Genes Dev. *16*, 399–414.

Hirano, T. (2005). Condensins: Organizing and segregating the genome. Curr. Biol. *15*, 265–275.

Hoege, C., Pfander, B., Moldovan, G.-L., Pyrowolakis, G., and Jentsch, S. (2002). RAD6-dependent DNA repair is linked to modification of PCNA by ubiquitin and SUMO. Nature *419*, 135–141.

Hong, J., Feng, H., Wang, F., Ranjan, A., Chen, J., Jiang, J., Ghirlando, R., Xiao, T.S., Wu, C., and Bai, Y. (2014). The Catalytic Subunit of the SWR1 Remodeler Is a Histone Chaperone for the H2A.Z-H2B Dimer. Mol. Cell *53*, 498–505.

Van Hooser, a a, Ouspenski, I.I., Gregson, H.C., Starr, D. a, Yen, T.J., Goldberg, M.L., Yokomori, K., Earnshaw, W.C., Sullivan, K.F., and Brinkley, B.R. (2001). Specification of kinetochore-forming chromatin by the histone H3 variant CENP-A. J. Cell Sci. *114*, 3529–3542.

Horejsí, Z., Takai, H., Adelman, C. a, Collis, S.J., Flynn, H., Maslen, S., Skehel, J.M., de Lange, T., and Boulton, S.J. (2010). CK2 phospho-dependent binding of R2TP complex to TEL2 is essential for mTOR and SMG1 stability. Mol. Cell *39*, 839–850.

Horikawa, I., Tanaka, H., Yuasa, Y., Suzuki, M., and Oshimura, M. (1995). Molecular cloning of a novel human cDNA on chromosome 1q21 and its mouse homolog encoding a nuclear protein with DNA-binding ability. Biochem. Biophys. Res. Commun. *208*, 999–1007.

Hou, H., Wang, Y., Kallgren, S.P., Thompson, J., Yates, J.R., and Jia, S. (2010). Histone variant H2A.Z regulates centromere silencing and chromosome segregation in fission yeast. J. Biol. Chem. *285*, 1909–1918.

Howman, E. V, Fowler, K.J., Newson, a J., Redward, S., MacDonald, a C., Kalitsis, P., and Choo, K.H. (2000). Early disruption of centromeric chromatin organization in centromere protein A (Cenpa) null mice. Proc. Natl. Acad. Sci. U. S. A. *97*, 1148–1153.

Hoyt, M. a, Totis, L., and Roberts, B.T. (1991). S. cerevisiae genes required for cell cycle arrest in response to loss of microtubule function. Cell *66*, 507–517.

Hoyt, M.A., He, L., Loo, K.K., and Saunders, W.S. (1992). Kinesin-related Gene Products Required for Mitotic Spindle Assembly. J. Cell Biol. *118*, 109–120.

Hua, S., Kallen, C.B., Dhar, R., Baquero, M.T., Mason, C.E., Russell, B. a, Shah, P.K., Liu, J., Khramtsov, A., Tretiakova, M.S., et al. (2008). Genomic analysis of estrogen cascade reveals histone variant H2A.Z associated with breast cancer progression. Mol. Syst. Biol. *4*, 188.

Huang, C.E., Milutinovich, M., and Koshland, D. (2005). Rings, bracelet or snaps: fashionable alternatives for Smc complexes. Philos. Trans. R. Soc. Lond. B. Biol. Sci. *360*, 537–542.

Hur, S.-K., Park, E.-J., Han, J.-E., Kim, Y.-A., Kim, J.-D., Kang, D., and Kwon, J. (2010). Roles of human INO80 chromatin remodeling enzyme in DNA replication and chromosome segregation suppress genome instability. Cell. Mol. Life Sci. *67*, 2283–2296.

Hwang, L.H., Lau, L.F., Smith, D.L., Mistrot, C. a, Hardwick, K.G., Hwang, E.S., Amon, A., and Murray, a W. (1998). Budding yeast Cdc20: a target of the spindle checkpoint. Science (80-.). *279*, 1041–1044.

Ito, T., Levenstein, M.E., Fyodorov, D. V., Kutach, A.K., Kobayashi, R., and Kadonaga, J.T. (1999). ACF consists of two subunits, Acf1 and ISWI, that function cooperatively in the ATP-dependent catalysis of chromatin assembly. Genes Dev. *13*, 1529–1539.

Jeanmougin, F., Wurtz, J.M., Le Douarin, B., Chambon, P., and Losson, R. (1997). The bromodomain revisited. Trends Biochem. Sci. *22*, 151–153.

Jensen, D.E., Proctor, M., Marquis, S.T., Gardner, H.P., Ha, S.I., Chodosh, L. a, Ishov, a M., Tommerup, N., Vissing, H., Sekido, Y., et al. (1998). BAP1: a novel ubiquitin hydrolase which binds to the BRCA1 RING finger and enhances BRCA1-mediated cell growth suppression. Oncogene *16*, 1097–1112.

Jha, S., and Dutta, A. (2009). RVB1/RVB2: running rings around molecular biology. Mol. Cell *34*, 521–533.

Jha, S., Shibata, E., and Dutta, A. (2008). Human Rvb1/Tip49 is required for the histone acetyltransferase activity of Tip60/NuA4 and for the downregulation of phosphorylation on H2AX after DNA damage. Mol. Cell. Biol. *28*, 2690–2700.

Jiménez, B., Ugwu, F., Zhao, R., Ortí, L., Makhnevych, T., Pineda-Lucena, A., and Houry, W. a (2012). Structure of minimal tetratricopeptide repeat domain protein Tah1 reveals mechanism of its interaction with Pih1 and Hsp90. J. Biol. Chem. *287*, 5698–5709.

Jin, J., Cai, Y., Yao, T., Gottschalk, A.J., Florens, L., Swanson, S.K., Gutiérrez, J.L., Coleman, M.K., Workman, J.L., Mushegian, A., et al. (2005). A mammalian chromatin remodeling complex with similarities to the yeast INO80 complex. J. Biol. Chem. *280*, 41207–41212.

Johnston, H., Kneer, J., Chackalaparampil, I., Yaciuk, P., and Chrivia, J. (1999). Identification of a novel SNF2/SWI2 protein family member, SRCAP, which interacts with CREB-binding protein. J. Biol. Chem. *274*, 16370–16376.

Jónsson, Z.O., Dhar, S.K., Narlikar, G.J., Auty, R., Wagle, N., Pellman, D., Pratt, R.E., Kingston, R., and Dutta, A. (2001). Rvb1p and Rvb2p are essential components of a chromatin remodeling complex that regulates transcription of over 5% of yeast genes. J. Biol. Chem. *276*, 16279–16288.

Jónsson, Z.O., Jha, S., Wohlschlegel, J. a., and Dutta, A. (2004). Rvb1p/Rvb2p recruit Arp5p and assemble a functional Ino80 chromatin remodeling complex. Mol. Cell *16*, 465–477.

Kabsch, W., Mannherz, H.G., Suck, D., Pai, E.F., and Holmes, K.C. (1990). Atomic structure of the actin:DNase I complex. Nature *347*, 37–44.

Kakarougkas, A., Ismail, A., Chambers, A., Riballo, E., Herbert, A., Künzel, J., Löbrich, M., Jeggo, P., and Downs, J. (2013). Requirement for PBAF in Transcriptional Repression and Repair at DNA Breaks in Actively Transcribed Regions of Chromatin. Mol. Cell 723–732.

Kakihara, Y., and Houry, W. a (2012). The R2TP complex: discovery and functions. Biochim. Biophys. Acta *1823*, 101–107.

Kapoor, P., and Shen, X. (2014). Mechanisms of nuclear actin in chromatin-remodeling complexes. Trends Cell Biol. *24*, 238–246.

Kapoor, P., Chen, M., Winkler, D.D., Luger, K., and Shen, X. (2013). Evidence for monomeric actin function in INO80 chromatin remodeling. Nat. Struct. Mol. Biol. *20*, 426–432.

Kashiwaba, S., Kitahashi, K., Watanabe, T., Onoda, F., Ohtsu, M., and Murakami, Y. (2010). The mammalian INO80 complex is recruited to DNA damage sites in an ARP8 dependent manner. Biochem. Biophys. Res. Commun. *402*, 619–625.

Kato, D., Waki, M., Umezawa, M., Aoki, Y., Utsugi, T., Ohtsu, M., and Murakami, Y. (2012). Phosphorylation of human INO80 is involved in DNA damage tolerance. Biochem. Biophys. Res. Commun. *417*, 433–438.

Katou, Y., Kanoh, Y., Bando, M., Noguchi, H., Tanaka, H., Ashikari, T., Sugimoto, K., and Shirahige, K. (2003). S-phase checkpoint proteins Tof1 and Mrc1 form a stable replication-pausing complex. Nature *424*, 1078–1083.

Keogh, M.-C., Mennella, T. a, Sawa, C., Berthelet, S., Krogan, N.J., Wolek, A., Podolny, V., Carpenter, L.R., Greenblatt, J.F., Baetz, K., et al. (2006). The Saccharomyces cerevisiae histone H2A variant Htz1 is acetylated by NuA4. Genes Dev. *20*, 660–665.

Khachaturov, V., Xiao, G.-Q., Kinoshita, Y., Unger, P.D., and Burstein, D.E. (2014). Histone H1.5, a novel prostatic cancer marker: an immunohistochemical study. Hum. Pathol. *45*, 2115–2119.

Khavari, P.A., Peterson, C.L., Tamkun, J.W., Mendel, D.B., and Crabtree, G.R. (1993). BRG1 contains a conserved domain of the SWI2/SNF2 family necessary for normal mitotic growth and transcription. Nature *366*, 170–174.

Kim, H.-S., Vanoosthuyse, V., Fillingham, J., Roguev, A., Watt, S., Kislinger, T., Treyer, A., Carpenter, L.R., Bennett, C.S., Emili, A., et al. (2009). An acetylated form of histone H2A.Z regulates chromosome architecture in Schizosaccharomyces pombe. Nat. Struct. Mol. Biol. *16*, 1286–1293.

Kim, K., Punj, V., Choi, J., Heo, K., Kim, J.-M., Laird, P.W., and An, W. (2013). Gene dysregulation by histone variant H2A.Z in bladder cancer. Epigenetics Chromatin *6*, 34.

Kimura, K., Hirano, M., Kobayashi, R., and Hirano, T. (1998). Phosphorylation and activation of 13S condensin by Cdc2 in vitro. Science (80-.). *282*, 487–490.

Kitayama, K., Kamo, M., Oma, Y., Matsuda, R., Uchida, T., Ikura, T., Tashiro, S., Ohyama, T., Winsor, B., and Harata, M. (2009). The human actin-related protein hArp5: Nucleo-cytoplasmic shuttling and involvement in DNA repair. Exp. Cell Res. *315*, 206–217.

Kobor, M.S., Venkatasubrahmanyam, S., Meneghini, M.D., Gin, J.W., Jennings, J.L., Link, A.J., Madhani, H.D., and Rine, J. (2004). A protein complex containing the conserved Swi2/Snf2-related ATPase Swr1p deposits histone variant H2A.Z into euchromatin. PLoS Biol. *2*, E131.

Koç, A., Wheeler, L.J., Mathews, C.K., and Merrill, G.F. (2004). Hydroxyurea Arrests DNA Replication by a Mechanism that Preserves Basal dNTP Pools. J. Biol. Chem. *279*, 223–230.

Krogan, N.J., Keogh, M.-C., Datta, N., Sawa, C., Ryan, O.W., Ding, H., Haw, R.A., Pootoolal, J., Tong, A., Canadien, V., et al. (2003). A Snf2 Family ATPase Complex Required for Recruitment of the Histone H2A Variant Htz1. Mol. Cell *12*, 1565–1576.

Krokan, H., Wist, E., and Krokan, R.H. (1981). Aphidicolin inhibits DNA synthesis by DNA polymerase alpha and isolated nuclei by a similar mechanism. Nucleic Acids Res. *9*, 4709–4719.

Kulaeva, O.I., Hsieh, F.-K., and Studitsky, V.M. (2010). RNA polymerase complexes cooperate to relieve the nucleosomal barrier and evict histones. Proc. Natl. Acad. Sci. U. S. A. *107*, 11325–11330.

Kuo, M.H., Zhou, J., Jambeck, P., Churchill, M.E., and Allis, C.D. (1998). Histone acetyltransferase activity of yeast Gcn5p is required for the activation of target genes in vivo. Genes Dev. *12*, 627–639.

Kurdistani, S.K., Tavazoie, S., and Grunstein, M. (2004). Mapping global histone acetylation patterns to gene expression. Cell *117*, 721–733.

Laflamme, L., Svotelis, A., and Hardy, S. (2009). Histone H2A . Z is essential for estrogen receptor signaling. 1522–1533.

Lavoie, B.D., Hogan, E., and Koshland, D. (2004). In vivo requirements for rDNA chromosome condensation reveal two cell-cycle-regulated pathways for mitotic chromosome folding. Genes Dev. *18*, 76–87.

Lechner, J., and Carbon, J. (1991). A 240 kd multisubunit protein complex, CBF3, is a major component of the budding yeast centromere. Cell *64*, 717–725.

Lecona, E., and Fernández-Capetillo, O. (2014). Replication stress and cancer: It takes two to tango. Exp. Cell Res. *329*, 26–34.

Lee, H., Lee, S., Hur, S., Seo, J., and Kwon, J. (2014). Stabilization and targeting of INO80 to repliction forks by BAP1 during normal DNA synthesis. Nat. Commun. *5*, 1–14.

Lehmann, A.R., Niimi, A., Ogi, T., Brown, S., Sabbioneda, S., Wing, J.F., Kannouche, P.L., and Green, C.M. (2007). Translesion synthesis: Y-family polymerases and the polymerase switch. DNA Repair (Amst). *6*, 891–899.

Leitner, A., Walzthoeni, T., and Aebersold, R. (2013). Lysine-specific chemical cross-linking of protein complexes and identification of cross-linking sites using LC-MS/MS and the xQuest/xProphet software pipeline. Nat. Protoc. *9*, 120–137.

Lengronne, A., McIntyre, J., Katou, Y., Kanoh, Y., Hopfner, K.P., Shirahige, K., and Uhlmann, F. (2006). Establishment of Sister Chromatid Cohesion at the S. cerevisiae Replication Fork. Mol. Cell *23*, 787–799.

Li, R., and Murray, a W. (1991). Feedback control of mitosis in budding yeast [published erratum appears in Cell 1994 Oct 21;79(2):following 388]. Cell *66*, 519–531.

Li, B., Pattenden, S.G., Lee, D., Gutiérrez, J., Chen, J., Seidel, C., Gerton, J., and Workman, J.L. (2005). Preferential occupancy of histone variant H2AZ at inactive promoters influences local histone modifications and chromatin remodeling. Proc. Natl. Acad. Sci. U. S. A. *102*, 18385–18390.

Li, M., Luo, J., Brooks, C.L., and Gu, W. (2002). Acetylation of p53 inhibits its ubiquitination by Mdm2. J. Biol. Chem. *277*, 50607–50611.

Lin, H., De Carvalho, P., Kho, D., Tai, C.Y., Pierre, P., Fink, G.R., and Pellman, D. (2001). Polyploids require Bik1 for kinetochore-microtubule attachment. J. Cell Biol. *155*, 1173–1184.

Lin, Y.Y., Qi, Y., Lu, J.Y., Pan, X., Yuan, D.S., Zhao, Y., Bader, J.S., and Boeke, J.D. (2008). A comprehensive synthetic genetic interaction network governing yeast histone acetylation and deacetylation. Genes Dev. *22*, 2062–2074.

Lindahl, T. (1993). Instability and decay of the primary structure of DNA. Nature *362*, 709–715.

London, N., and Biggins, S. (2014). Signalling dynamics in the spindle checkpoint response. Nat. Rev. Mol. Cell Biol. *15*, 736–748.

López-Perrote, A., Alatwi, H.E., Torreira, E., Ismail, A., Ayora, S., Downs, J. a., and Llorca, O. (2014). Structure of Yin Yang 1 oligomers that cooperate with RuvBL1-RuvBL2 ATPases. J. Biol. Chem. *289*, 22614–22629.

Louzalen, N., Moreau, J., and Méchali, M. (1996). H2A.ZI, a new variant histone expressed during Xenopus early development exhibits several distinct features from the core histone H2A. Nucleic Acids Res. *24*, 3947–3952.

Löwe, J., Cordell, S.C., and van den Ent, F. (2001). Crystal structure of the SMC head domain: an ABC ATPase with 900 residues antiparallel coiled-coil inserted. J. Mol. Biol. *306*, 25–35.

Luger, K., Mäder, A.W., Richmond, R.K., Sargent, D.F., and Richmond, T.J. (1997). Crystal structure of the nucleosome core particle at 2.8 A resolution. Nature *389*, 251–260.

Lundin, C., North, M., Erixon, K., Walters, K., Jenssen, D., Goldman, A.S.H., and Helleday, T. (2005). Methyl methanesulfonate (MMS) produces heat-labile DNA damage but no detectable in vivo DNA double-strand breaks. Nucleic Acids Res. *33*, 3799–3811.

Mannironi, C., Bonner, W.M., and Hatch, C.L. (1989). H2A.X. a histone isoprotein with a conserved C-terminal sequence, is encoded by a novel mRNA with both DNA replication type and polyA 3' processing signals. Nucleic Acids Res. *17*, 9113–9126.

Mao, Z., Pan, L., Wang, W., Sun, J., Shan, S., Dong, Q., Liang, X., Dai, L., Ding, X., Chen, S., et al. (2014). Anp32e, a higher eukaryotic histone chaperone directs preferential recognition for H2A.Z. Cell Res. *24*, 389–399.

Marfella, C.G. a, and Imbalzano, A.N. (2007). The Chd family of chromatin remodelers. Mutat. Res. - Fundam. Mol. Mech. Mutagen. *618*, 30–40.

Marzluff, W.F., Gongidi, P., Woods, K.R., Jin, J., and Maltais, L.J. (2002). The human and mouse replication-dependent histone genes. Genomics *80*, 487–498.

Masliah-Planchon, J., Bièche, I., Guinebretière, J.-M., Bourdeaut, F., and Delattre, O. (2014). SWI/SNF Chromatin Remodeling and Human Malignancies. Annu. Rev. Pathol.

Mehta, M., Braberg, H., Wang, S., Lozsa, A., Shales, M., Solache, A., Krogan, N.J., and Keogh, M.-C. (2010). Individual lysine acetylations on the N terminus of Saccharomyces cerevisiae H2A.Z are highly but not differentially regulated. J. Biol. Chem. *285*, 39855–39865.

Meneghini, M.D., Wu, M., and Madhani, H.D. (2003). Conserved histone variant H2A.Z protects euchromatin from the ectopic spread of silent heterochromatin. Cell *112*, 725–736.

Merrick, C.J., Jackson, D., and Diffley, J.F.X. (2004). Visualization of altered replication dynamics after DNA damage in human cells. J. Biol. Chem. *279*, 20067–20075.

Michaelis, C., Ciosk, R., and Nasmyth, K. (1997). Cohesins: Chromosomal proteins that prevent premature separation of sister chromatids. Cell *91*, 35–45.

Millar, C.B., Kurdistani, S.K., and Grunstein, M. (2004). Acetylation of yeast histone H4 lysine 16: A switch for protein interactions in heterochromatin and euchromatin. Cold Spring Harb. Symp. Quant. Biol. *69*, 193–200.

Millar, C.B., Xu, F., Zhang, K., and Grunstein, M. (2006). Acetylation of H2AZ Lys 14 is associated with genome-wide gene activity in yeast. Genes Dev. *20*, 711–722.

Milutinovich, M., and Koshland, D.E. (2003). SMC Complexes — Wrapped Up in Controversy. Science (80-.). 1101–1102.

Miranda, J.L., Wulf, P. De, Sorger, P.K., and Harrison, S.C. (2005). The yeast DASH complex forms closed rings on microtubules. Nat. Struct. & Mol. Biol. *12*, 138–143.

Mirkin, E. V, and Mirkin, S.M. (2007). Replication fork stalling at natural impediments. Microbiol. Mol. Biol. Rev. *71*, 13–35.

Mizuguchi, G., Shen, X., Landry, J., Wu, W.-H., Sen, S., and Wu, C. (2004). ATP-driven exchange of histone H2AZ variant catalyzed by SWR1 chromatin remodeling complex. Science *303*, 343–348.

Moldovan, G.L., Pfander, B., and Jentsch, S. (2006). PCNA Controls Establishment of Sister Chromatid Cohesion during S Phase. Mol. Cell *23*, 723–732.

Morrison, A.J., Highland, J., Krogan, N.J., Arbel-Eden, A., Greenblatt, J.F., Haber, J.E., and Shen, X. (2004). INO80 and gamma-H2AX interaction links ATP-dependent chromatin remodeling to DNA damage repair. Cell *119*, 767–775.

Morrison, A.J., Kim, J.-A., Person, M.D., Highland, J., Xiao, J., Wehr, T.S., Hensley, S., Bao, Y., Shen, J., Collins, S.R., et al. (2007). Mec1/Tel1 phosphorylation of the INO80 chromatin remodeling complex influences DNA damage checkpoint responses. Cell *130*, 499–511.

Muchardt, C., and Yaniv, M. (1993). A human homologue of Saccharomyces cerevisiae SNF2/SWI2 and Drosophila brm genes potentiates transcriptional activation by the glucocorticoid receptor. EMBO J. *12*, 4279–4290.

Nagaoka, S.I., Hassold, T.J., and Hunt, P. a. (2012). Human aneuploidy: mechanisms and new insights into an age-old problem. Nat. Rev. Genet. *13*, 493–504.

Nedelcheva, M.N., Roguev, A., Dolapchiev, L.B., Shevchenko, A., Taskov, H.B., Shevchenko, A., Stewart, a. F., and Stoynov, S.S. (2005). Uncoupling of unwinding from DNA synthesis implies regulation of MCM helicase by Tof1/Mrc1/Csm3 checkpoint complex. J. Mol. Biol. *347*, 509–521.

Neigeborn, L., and Carlson, M. (1984). Genes affecting the regulation of SUC2 gene expression by glucose repression in Saccharomyces cerevisiae. Genetics *108*, 845–858.

Ng, R., and Carbon, J. (1987). Mutational and in vitro protein-binding studies on centromere DNA from Saccharomyces cerevisiae. Mol. Cell. Biol. *7*, 4522–4534.

Niimi, A., Chambers, A.L., Downs, J. a, and Lehmann, A.R. (2012). A role for chromatin remodellers in replication of damaged DNA. Nucleic Acids Res. *40*, 7393–7403.

Obri, A., Ouararhni, K., Papin, C., Diebold, M.-L., Padmanabhan, K., Marek, M., Stoll, I., Roy, L., Reilly, P.T., Mak, T.W., et al. (2014). ANP32E is a histone chaperone that removes H2A.Z from chromatin. Nature *505*, 648–653.

Ogiwara, H., Enomoto, T., and Seki, M. (2007). The INO80 chromatin remodeling complex functions in sister chromatid cohesion. Cell Cycle *6*, 1090–1095.

Ogiyama, Y., Ohno, Y., Kubota, Y., and Ishii, K. (2013). Epigenetically induced paucity of histone H2A.Z stabilizes fission-yeast ectopic centromeres. Nat. Struct. Mol. Biol. *20*, 1397–1406.

Olins, a L., and Olins, D.E. (1974). Spheroid chromatin units (v bodies). Science *183*, 330–332.

Onn, I., Aono, N., Hirano, M., and Hirano, T. (2007). Reconstitution and subunit geometry of human condensin complexes. EMBO J. *26*, 1024–1034.

Oum, J.-H., Seong, C., Kwon, Y., Ji, J.-H., Sid, A., Ramakrishnan, S., Ira, G., Malkova, A., Sung, P., Lee, S.E., et al. (2011). RSC Facilitates Rad59-Dependent Homologous Recombination between Sister Chromatids by Promoting Cohesin Loading at DNA Double-Strand Breaks. Mol. Cell. Biol. *31*, 3924–3937.

Ouspenski, I.I., Cabello, O. a, and Brinkley, B.R. (2000). Chromosome condensation factor Brn1p is required for chromatid separation in mitosis. Mol. Biol. Cell *11*, 1305–1313.

Paci, A., Liu, X.H., Huang, H., Lim, A., Houry, W. a, and Zhao, R. (2012). The stability of the small nucleolar ribonucleoprotein (snoRNP) assembly protein Pih1 in Saccharomyces cerevisiae is modulated by its C terminus. J. Biol. Chem. *287*, 43205–43214.

Pal, M., Morgan, M., Phelps, S.E.L., Roe, S.M., Parry-morris, S., Downs, J.A., Polier, S., Pearl, L.H., and Prodromou, C. (2014). Structural Basis for Phosphorylation-Dependent Recruitment of Tel2 to Hsp90 by Pih1. Struct. Des. *22*, 805–818.

Pan, X., Yuan, D.S., Xiang, D., Wang, X., Sookhai-Mahadeo, S., Bader, J.S., Hieter, P., Spencer, F., and Boeke, J.D. (2004). A robust toolkit for functional profiling of the yeast genome. Mol. Cell *16*, 487–496.

Pandey, N.B., Chodchoy, N., Liu, T.J., and Marzluff, W.F. (1990). Introns in histone genes alter the distribution of 3' ends. Nucleic Acids Res. *18*, 3161–3170.

Pantazis, P., and Bonner, W. (1966). Quantitative determination of histone modification. H2A acetylation and phosphorylation. J. Biol. Chem. *17*, 1–7.

Papamichos-Chronakis, M., and Peterson, C.L. (2008). The Ino80 chromatin-remodeling enzyme regulates replisome function and stability. Nat. Struct. Mol. Biol. *15*, 338–345.

Papamichos-Chronakis, M., Watanabe, S., Rando, O.J., and Peterson, C.L. (2011). Global regulation of H2A.Z localization by the INO80 chromatin-remodeling enzyme is essential for genome integrity. Cell *144*, 200–213.

Park, E., Hur, S., Lee, H., Lee, S., and Kwon, J. (2011). The human Ino80 binds to microtubule via the E-hook of tubulin : Implications for the role in spindle assembly. Biochem. Biophys. Res. Commun. *416*, 416–420.

Paro, R., and Hogness, D.S. (1991). The Polycomb protein shares a homologous domain with a heterochromatin-associated protein of Drosophila. Proc. Natl. Acad. Sci. U. S. A. *88*, 263–267.

Patterson, D. (2009). Molecular genetic analysis of Down syndrome. Hum. Genet. *126*, 195–214.

Pearl, L.H., and Prodromou, C. (2000). Structure and in vivo function of Hsp90. Curr. Opin. Struct. Biol. *10*, 46–51.

Peterson, C.L., and Herskowitz, I. (1992). Characterization of the yeast SWI1, SWI2, and SWI3 genes, which encode a global activator of transcription. Cell *68*, 573–583.

Pinsky, B. a, Kung, C., Shokat, K.M., and Biggins, S. (2006). The Ipl1-Aurora protein kinase activates the spindle checkpoint by creating unattached kinetochores. Nat. Cell Biol. *8*, 78–83.

Poirier, M.G., Eroglu, S., and Marko, J.F. (2002). Mutation of YCS4, a Budding Yeast Condensin Subunit, Affects Mitotic and Nonmitotic Chromosome Behavior. Mol. Biol. Cell *13*, 2170–2179.

Puri, T., Wendler, P., Sigala, B., Saibil, H., and Tsaneva, I.R. (2007). Dodecameric structure and ATPase activity of the human TIP48/TIP49 complex. J. Mol. Biol. *366*, 179–192.

Qiu, X.B., Lin, Y.L., Thome, K.C., Pian, P., Schlegel, B.P., Weremowicz, S., Parvin, J.D., and Dutta, A. (1998). An eukaryotic RuvB-like protein (RUVBL1) essential for growth. J. Biol. Chem. *273*, 27786–27793.

Quinlan, R. a, Pogson, C.I., and Gull, K. (1980). The influence of the microtubule inhibitor, methyl benzimidazol-2-yl-carbamate (MBC) on nuclear division and the cell cycle in Saccharomyces cerevisiae. J. Cell Sci. *46*, 341–352.

Robbins, E., and Borun, T.W. (1967). The cytoplasmic synthesis of histones in hela cells and its temporal relationship to DNA replication. Proc. Natl. Acad. Sci. U. S. A. *57*, 409–416.

Roof, D.M., Meluh, P.B., and Rose, M.D. (1992). Kinesin-related proteins required for assembly of the mitotic spindle. J. Cell Biol. *118*, 95–108.

Santisteban, M.S., Kalashnikova, T., and Smith, M.M. (2000). Histone H2A.Z regulats transcription and is partially redundant with nucleosome remodeling complexes. Cell *103*, 411–422.

Santocanale, C., and Diffley, J.F. (1998). A Mec1- and Rad53-dependent checkpoint controls late-firing origins of DNA replication. Nature *395*, 615–618.

Schueler, M.G., Higgins, a W., Rudd, M.K., Gustashaw, K., and Willard, H.F. (2001). Genomic and genetic definition of a functional human centromere. Science (80-.). *294*, 109–115.

Schwartzentruber, J., Korshunov, A., Liu, X.-Y., Jones, D.T.W., Pfaff, E., Jacob, K., Sturm, D., Fontebasso, A.M., Quang, D.-A.K., Tönjes, M., et al. (2012). Driver mutations in histone H3.3 and chromatin remodelling genes in paediatric glioblastoma. Nature *482*, 226–231.

Seligson, D.B., Horvath, S., Shi, T., Yu, H., Tze, S., Grunstein, M., and Kurdistani, S.K. (2005). Global histone modification patterns predict risk of prostate cancer recurrence. Nature *435*, 1262–1266.

Selmecki, A.M., Maruvka, Y.E., Richmond, P. a, Guillet, M., Shoresh, N., Sorenson, A.L., De, S., Kishony, R., Michor, F., Dowell, R., et al. (2015). Polyploidy can drive rapid adaptation in yeast. Nature *519*, 349–352.

Sharma, U., Stefanova, D., and Holmes, S.G. (2013). Histone variant H2A.Z functions in sister chromatid cohesion in Saccharomyces cerevisiae. Mol. Cell. Biol. *33*, 3473–3481.

Shen, X., Mizuguchi, G., Hamiche, A., and Wu, C. (2000). A chromatin remodelling complex involved in transcription and DNA processing. Nature *406*, 541–544.

Shen, X., Ranallo, R., Choi, E., and Wu, C. (2003). Involvement of actin-related proteins in ATP-dependent chromatin remodeling. Mol. Cell *12*, 147–155.

Shibata, Y., and Nishiwaki, K. (2014). Maintenance of cell fates through acetylated histone and the histone variant H2A.z in. 1–5.

Shim, E.Y., Ma, J., Oum, J., Yanez, Y., and Lee, S.E. (2005). The Yeast Chromatin Remodeler RSC Complex Facilitates End Joining Repair of DNA Double-Strand Breaks The Yeast Chromatin Remodeler RSC Complex Facilitates End Joining Repair of DNA Double-Strand Breaks. Mol. Cell. Biol. *25*, 3934–3944.

Shim, E.Y., Hong, S.J., Oum, J.-H., Yanez, Y., Zhang, Y., and Lee, S.E. (2007). RSC mobilizes nucleosomes to improve accessibility of repair machinery to the damaged chromatin. Mol. Cell. Biol. *27*, 1602–1613.

Shimada, K., Oma, Y., Schleker, T., Kugou, K., Ohta, K., Harata, M., and Gasser, S.M. (2006). Supplemental Data Ino80 Chromatin Remodeling Complex Promotes Recovery of Stalled Replication Forks.

Shimada, K., Oma, Y., Schleker, T., Kugou, K., Ohta, K., Harata, M., and Gasser, S.M. (2008). Ino80 chromatin remodeling complex promotes recovery of stalled replication forks. Curr. Biol. *18*, 566–575.

Shirahige, K., Hori, Y., Shiraishi, K., Yamashita, M., Takahashi, K., Obuse, C., Tsurimoto, T., and Yoshikawa, H. (1998). Regulation of DNA-replication origins during cell-cycle progression. Nature *395*, 618–621.

Shogren-Knaak, M., Ishii, H., Sun, J.-M., Pazin, M.J., Davie, J.R., and Peterson, C.L. (2006). Histone H4-K16 acetylation controls chromatin structure and protein interactions. Science *311*, 844–847.

Sims, R.J., Chen, C.F., Santos-Rosa, H., Kouzarides, T., Patel, S.S., and Reinberg, D. (2005). Human but not yeast CHD1 binds directly and selectively to histone H3 methylated at lysine 4 via its tandem chromodomains. J. Biol. Chem. *280*, 41789–41792.

Sinha, M., Watanabe, S., Johnson, A., Moazed, D., and Peterson, C.L. (2009). Recombinational Repair within Heterochromatin Requires ATP-Dependent Chromatin Remodeling. Cell *138*, 1109–1121.

Smith, C.M., Gafken, P.R., Zhang, Z., Gottschling, D.E., Smith, J.B., and Smith, D.L. (2003). Mass spectrometric quantification of acetylation at specific lysines within the amino-terminal tail of histone H4. Anal. Biochem. *316*, 23–33.

Spencer, F., and Hieter, P. (1992). Centromere DNA mutations induce a mitotic delay in Saccharomyces cerevisiae. Proc. Natl. Acad. Sci. U. S. A. *89*, 8908–8912.

St-Pierre, J., Douziech, M., Bazile, F., Pascariu, M., Bonneil, É., Sauvé, V., Ratsima, H., and D'Amours, D. (2009). Polo Kinase Regulates Mitotic Chromosome Condensation by Hyperactivation of Condensin DNA Supercoiling Activity. Mol. Cell *34*, 416–426.

Stern, B.M., and Murray, A.W. (2001). Lack of tension at kinetochores activates the spindle checkpoint in budding yeast. Curr. Biol. *11*, 1462–1467.

Stoler, S., Keith, K.C., Curnick, K.E., and Fitzgerald-Hayes, M. (1995). A mutation in CSE4, an essential gene encoding a novel chromatin-associated protein in yeast, causes chromosome nondisjunction and cell cycle arrest at mitosis. Genes Dev. *9*, 573–586.

Strunnikov, a. V., Hogan, E., and Koshland, D. (1995). SMC2, a Saccharomyces cerevisiae gene essential for chromosome segregation and condensation, defines a subgroup within the SMC family. Genes Dev. *9*, 587–599.

Stucki, M., Clapperton, J. a., Mohammad, D., Yaffe, M.B., Smerdon, S.J., and Jackson, S.P. (2005). MDC1 directly binds phosphorylated histone H2AX to regulate cellular responses to DNA double-strand breaks. Cell *123*, 1213–1226.

Sudarsanam, P., Iyer, V.R., Brown, P.O., and Winston, F. (2000). Whole-genome expression analysis of snf/swi mutants of Saccharomyces cerevisiae. Proc. Natl. Acad. Sci. U. S. A. *97*, 3364–3369.

Sullivan, K.F., Hechenberger, M., and Masri, K. (1994). Human CENP-A Contains a Histone H3 Related Histone Fold Domain That Is Required for Targeting to the Centromere. Cell *127*, 581–592.

Sunada, R., Görzer, I., Oma, Y., Yoshida, T., Suka, N., Wintersberger, U., and Harata, M. (2005). The nuclear actin-related protein Act3p/Arp4p is involved in the dynamics of chromatin-modulating complexes. Yeast *22*, 753–768.

Suto, R.K., Clarkson, M.J., Tremethick, D.J., and Luger, K. (2000). Crystal structure of a nucleosome core particle containing the variant histone H2A.Z. Nat. Struct. Biol. *7*, 1121–1124.

Svotelis, A., Gévry, N., Grondin, G., and Gaudreau, L. (2014). H2A.Z overexpression promotes cellular proliferation of breast cancer cells. Cell Cycle *9*, 364–370.

Symington, L.S. (2002). Role of RAD52 epistasis group genes in homologous recombination and double-strand break repair. Microbiol. Mol. Biol. Rev. *66*, 630–670, table of contents.

Szerlong, H., Hinata, K., Viswanathan, R., Erdjument-bromage, H., Tempst, P., and Cairns, B.R. (2010). The HSA domain binds nuclear actin-related proteins to regulate chromatin-remodeling ATPases. Nat. Struct. Mol. Biol. *15*, 469–476.

Takai, H., Xie, Y., de Lange, T., and Pavletich, N.P. (2010). Tel2 structure and function in the Hsp90-dependent maturation of mTOR and ATR complexes. Genes Dev. *24*, 2019–2030.

Talbert, P.B., and Henikoff, S. (2010). Histone variants--ancient wrap artists of the epigenome. Nat. Rev. Mol. Cell Biol. *11*, 264–275.

Tamkun, J.W., Deuring, R., Scott, M.P., Kissinger, M., Pattatucci, a M., Kaufman, T.C., and Kennison, J. a (1992). brahma: a regulator of Drosophila homeotic genes structurally related to the yeast transcriptional activator SNF2/SWI2. Cell *68*, 561–572.

Tanaka, T.U., Rachidi, N., Janke, C., Pereira, G., Galova, M., Schiebel, E., Stark, M.J.R., and Nasmyth, K. (2002). Evidence that the Ipl1-Sli15 (Aurora Kinase-INCENP) complex promotes chromosome bi-orientation by altering kinetochore-spindle pole connections. Cell *108*, 317–329.

Tapia-Alveal, C., Lin, S.-J., Yeoh, A., Jabado, O.J., and O'Connell, M.J. (2014). H2A.Z-dependent regulation of cohesin dynamics on chromosome arms. Mol. Cell. Biol. *34*, 2092–2104.

Torreira, E., Jha, S., López-Blanco, J.R., Arias-Palomo, E., Chacón, P., Cañas, C., Ayora, S., Dutta, A., and Llorca, O. (2008). Architecture of the pontin/reptin complex, essential in the assembly of several macromolecular complexes. Cell *16*, 1511–1520.

Torres, E.M., Sokolsky, T., Tucker, C.M., Chan, L.Y., Boselli, M., Dunham, M.J., and Amon, A. (2007). Effects of aneuploidy on cellular physiology and cell division in haploid yeast. Science *317*, 916–924.

Tosi, A., Haas, C., Herzog, F., Gilmozzi, A., Berninghausen, O., Ungewickell, C., Gerhold, C.B., Lakomek, K., Aebersold, R., Beckmann, R., et al. (2013). Structure and Subunit Topology of the INO80 Chromatin Remodeler and Its Nucleosome Complex. Cell *154*, 1207–1219.

Toyotaka Ishibashi, Deanna Dryhurst, Kristie L. Rose, Jeffrey Shabanowitz, D.F.H. and J.A. (2009). Acetylation of Vertebrate H2A.Z and Its Effect on the Structure of the Nucleosome. Biochemistry *48*, 5007–5017.

Tse, C., Sera, T., Wolffe, a P., and Hansen, J.C. (1998). Disruption of higher-order folding by core histone acetylation dramatically enhances transcription of nucleosomal arrays by RNA polymerase III. Mol. Cell. Biol. *18*, 4629–4638.

Tsukuda, T., Fleming, A.B., Nickoloff, J. a, and Osley, M.A. (2005). Chromatin remodelling at a DNA double-strand break site in Saccharomyces cerevisiae. Nature *438*, 379–383.

Udugama, M., Sabri, A., and Bartholomew, B. (2011). The INO80 ATP-dependent chromatin remodeling complex is a nucleosome spacing factor. Mol. Cell. Biol. *31*, 662–673.

Uhlmann, F., Lottspeich, F., and Nasmyth, K. (1999). Sister-chromatid separation at anaphase onset is promoted by cleavage of the cohesin subunit Scc1. Nature *400*, 37–42.

Ulrich, H.D. (2007). Conservation of DNA damage tolerance pathways from yeast to humans. Biochem. Soc. Trans. *35*, 1334–1337.

Uzunova, S., Zarkov, A., Ivanova, A., Stoynov, S., and Nedelcheva-Veleva, M. (2014). The subunits of the S-phase checkpoint complex Mrc1/Tof1/Csm3: dynamics and interdependence. Cell Div. *9*, 4.

Valdés-Mora, F., Song, J.Z., Statham, A.L., Strbenac, D., Robinson, M.D., Nair, S.S., Patterson, K.I., Tremethick, D.J., Stirzaker, C., and Clark, S.J. (2012). Acetylation of H2A.Z is a key epigenetic modification associated with gene deregulation and epigenetic remodeling in cancer. Genome Res. *22*, 307–321.

Vassileva, I., Yanakieva, I., Peycheva, M., Gospodinov, A., and Anachkova, B. (2014). The mammalian INO80 chromatin remodeling complex is required for replication stress recovery. Nucleic Acids Res. *42*, 1–13.

Verdaasdonk, J.S., and Bloom, K. (2011). Centromeres: unique chromatin structures that drive chromosome segregation. Nat. Rev. Mol. Cell Biol. *12*, 320–332.

Vincent, J. a, Kwong, T.J., and Tsukiyama, T. (2008). ATP-dependent chromatin remodeling shapes the DNA replication landscape. Nat. Struct. Mol. Biol. *15*, 477–484.

Visintin, R., Prinz, S., and Amon, A. (1997). CDC20 and CDH1: a family of substrate-specific activators of APC-dependent proteolysis. Science (80-.). *278*, 460–463.

Van Vugt, J.J.F. a, Ranes, M., Campsteijn, C., and Logie, C. (2007). The ins and outs of ATP-dependent chromatin remodeling in budding yeast: Biophysical and proteomic perspectives. Biochim. Biophys. Acta - Gene Struct. Expr. *1769*, 153–171.

Wang, L., Du, Y., Ward, J.M., Shimbo, T., Lackford, B., Zheng, X., Miao, Y.L., Zhou, B., Han, L., Fargo, D.C., et al. (2014). INO80 facilitates pluripotency gene activation in embryonic stem cell self-renewal, reprogramming, and blastocyst development. Cell Stem Cell *14*, 575–591.

Wang, Z.F., Whitfield, M.L., Ingledue, T.C., Dominski, Z., and Marzluff, W.F. (1996). The protein that binds the 3' end of histone mRNA: A novel RNA-binding protein required for histone pre-mRNA processing. Genes Dev. *10*, 3028–3040.

Watanabe, S., and Peterson, C.L. (2010). The INO80 family of chromatin-remodeling enzymes: regulators of histone variant dynamics. Cold Spring Harb. Symp. Quant. Biol. *75*, 35–42.

Watanabe, S., Radman-Livaja, M., Rando, O.J., and Peterson, C.L. (2013). A histone acetylation switch regulates H2A.Z deposition by the SWR-C remodeling enzyme. Science *340*, 195–199.

Watanabe, S., Tan, D., Lakshminarasimhan, M., Washburn, M.P., Erica Hong, E.-J., Walz, T., and Peterson, C.L. (2015). Structural analyses of the chromatin remodelling enzymes INO80-C and SWR-C. Nat. Commun. *6*, 7108.

Wells, W. a E. (1996). The spindle-assembly checkpoint: Aiming for a perfect mitosis, every time. Trends Cell Biol. *6*, 228–234.

West, S.C. (1996). The RuvABC proteins and Holliday junction processing in Escherichia coli. J. Bacteriol. *178*.

Williams, B.R., Prabhu, V.R., Hunter, K.E., Glazier, C.M., Whittaker, C. a, Housman, D.E., and Amon, A. (2008). Aneuploidy Affects Proliferation and Spontaneous Immortalization. October *322*, 703–710.

Wilson, B.G., and Roberts, C.W. (2011). SWI/SNF nucleosome remodellers and cancer. Nat. Rev. Cancer *11*, 481–492.

Wood, A.J., Severson, A.F., and Meyer, B.J. (2010). Condensin and cohesin complexity: the expanding repertoire of functions. Nat. Rev. Genet. *11*, 391–404.

Wood, L.D., Parsons, D.W., Jones, S., Lin, J., Sjöblom, T., Leary, R.J., Shen, D., Boca, S.M., Barber, T., Ptak, J., et al. (2007). The genomic landscapes of human breast and colorectal cancers. Science *318*, 1108–1113.

Woodage, T., Basrai, M. a, Baxevanis, a D., Hieter, P., and Collins, F.S. (1997). Characterization of the CHD family of proteins. Proc. Natl. Acad. Sci. U. S. A. *94*, 11472–11477.

Wratting, D., Thistlethwaite, A., Harris, M., Zeef, L. a H., and Millar, C.B. (2012). A conserved function for the H2A.Z C-terminus. J. Biol. Chem. *1*.

Wu, S., Shi, Y., Mulligan, P., Gay, F., Landry, J., Liu, H., Lu, J., Qi, H.H., Wang, W., Nickoloff, J. a, et al. (2007). A YY1-INO80 complex regulates genomic stability through homologous recombination-based repair. Nat. Struct. Mol. Biol. *14*, 1165–1172.

Wu, W.-H., Alami, S., Luk, E., Wu, C.-H., Sen, S., Mizuguchi, G., Wei, D., and Wu, C. (2005). Swc2 is a widely conserved H2AZ-binding module essential for ATP-dependent histone exchange. Nat. Struct. Mol. Biol. *12*, 1064–1071.

De Wulf, P., McAinsh, A.D., and Sorger, P.K. (2003). Hierarchical assembly of the budding yeast kinetochore from multiple subcomplexes. Genes Dev. *17*, 2902–2921.

Xue, Y., Wong, J., Moreno, G.T., Young, M.K., Côté, J., and Wang, W. (1998). NURD, a novel complex with both ATP-dependent chromatin-remodeling and histone deacetylase activities. Mol. Cell *2*, 851–861.

Yamada, K., Frouws, T.D., Angst, B., Fitzgerald, D.J., DeLuca, C., Schimmele, K., Sargent, D.F., and Richmond, T.J. (2011). Structure and mechanism of the chromatin remodelling factor ISW1a. Nature *472*, 448–453.

Yamamoto, T. (1997). Novel Substrate Specificity of the Histone Acetyltransferase Activity of HIV-1-Tat Interactive. Biochemistry 30595–30598.

Yu, Y., Deng, Y., Reed, S.H., Millar, C.B., and Waters, R. (2013). Histone variant Htz1 promotes histone H3 acetylation to enhance nucleotide excision repair in Htz1 nucleosomes. Nucleic Acids Res. *41*, 9006–9019.

Zack, T.I., Schumacher, S.E., Carter, S.L., Cherniack, A.D., Saksena, G., Tabak, B., Lawrence, M.S., Zhang, C.-Z., Wala, J., Mermel, C.H., et al. (2013). Pan-cancer patterns of somatic copy number alteration. Nat. Genet. *45*, 1134–1140.

Zhang, H., Roberts, D.N., and Cairns, B.R. (2005). Genome-wide dynamics of Htz1, a histone H2A variant that poises repressed/basal promoters for activation through histone loss. Cell *123*, 219–231.

Zhang, Y., LeRoy, G., Seelig, H.P., Lane, W.S., and Reinberg, D. (1998). The dermatomyositis-specific autoantigen Mi2 is a component of a complex containing histone deacetylase and nucleosome remodeling activities. Cell *95*, 279–289.

Zhang, Y., Ng, H.H., Erdjument-Bromage, H., Tempst, P., Bird, A., and Reinberg, D. (1999). Analysis of the NuRD subunits reveals a histone deacetylase core complex and a connection with DNA methylation. Genes Dev. *13*, 1924–1935.

Zhao, R., Davey, M., Hsu, Y.-C., Kaplanek, P., Tong, A., Parsons, A.B., Krogan, N., Cagney, G., Mai, D., Greenblatt, J., et al. (2005). Navigating the chaperone network: an integrative map of physical and genetic interactions mediated by the hsp90 chaperone. Cell *120*, 715–727.

Zhou, Z., Feng, H., Zhou, B.-R., Ghirlando, R., Hu, K., Zwolak, A., Miller Jenkins, L.M., Xiao, H., Tjandra, N., Wu, C., et al. (2011). Structural basis for recognition of centromere histone variant CenH3 by the chaperone Scm3. Nature *472*, 234–237.

Zlatanova, J., and Thakar, A. (2008). H2A.Z: view from the top. Structure *16*, 166–179.

Appendix

Abbreviations

ChIP	Chromatin immunoprecipitation
CPT	Camptothecin
C-terminus	Carboxyl terminus
D. melanogastor	*Drosophila melanogastor*
DDR	DNA damage response
D-loop	Displacement loop
DMSO	Dimethyl sulfoxide
EM	Electron microscopy
FACS	Fluorescently activated cell sorting
FLAG	Polypeptide protein tag (DYKDDDDK)
HR	Homologous recombination
HRP	Horseradish peroxidase
HU	hydroxyurea
IPTG	isopropyl β-D-1-thiogalactopyranoside
IR	Ionising radiation
LB	Broth Luria Bertani broth
MBP	Maltose binding protein
MCS	Multiple cloning site
MMS	Methyl methane sulphonate
MNase	Micrococcal nuclease
MW	Molecular weight
NHEJ	Non-homologous end joining
N-terminus	Amino terminus
ORC	Origin recognition complex
ORF	Open reading frame
PCNA	Proliferating cell nuclear antigen
PCR	Polymerase chain reaction
PEG	Polyethylene glycol
PIKK	Phosphatidylinositol kinase-related kinase
PMSF	Phenylmethyl sulphonyl fluoride
RNase	Ribonuclease

RPA	Replication protein A
rpm	Revolutions per minute
RSC	Remodels the structure of chromatin
S. cerevisiae	*Saccharomyces cerevisiae*
S. pombe	*Schizosaccharomyces pombe*
SC	Synthetic complete
SD	Synthetic drop-out
SDS	Sodium dodecyl sulphate
SDS-PAGE	Sodium dodecyl sulphate polyacrylamide
SGD	Saccharomyces genome database
SWI/SNF	Switch mating type/sucrose non-fermenting
TCA	trichloroacetic acid
TEMED	N,N,N',N'-tetramethyl-ethylenediamine
Tris	2-amino-2hydroxymethyl-propane-1,3-diol
UV	Ultraviolet
w/v	Weight per unit volume
X-GAL	5-bromo-4-chloro-3-indoyl-β-D-galactopyranoside
YPAD	Yeast extract, peptone, adenine, dextrose

Index of tables

Index of figures